UNIVERSIDADE ESTADUAL PAULISTA
"JÚLIO DE MESQUITA FILHO"
Câmpus de Ilha Solteira - SP

WILLIAN RICARDO BISPO MURBAK NUNES

A New Dynamic Model Applied to Electrically Stimulated Lower Limbs and Switched Control Design Subject to Actuator Saturation and Non-Ideal Conditions

Ilha Solteira
2019

WILLIAN RICARDO BISPO MURBAK NUNES

A New Dynamic Model Applied to Electrically Stimulated Lower Limbs and Switched Control Design Subject to Actuator Saturation and Non-Ideal Conditions

Thesis submitted to the Faculdade de Engenharia de Ilha Solteira - UNESP in conformity with the requirements for the degree of PhD in Electrical Engineering.
Field of Expertise: Automation.

Prof. Dr. Aparecido Augusto de Carvalho
Advisor

Ilha Solteira
2019

FICHA CATALOGRÁFICA
Desenvolvido pelo Serviço Técnico de Biblioteca e Documentação

N972n

Nunes, Willian Ricardo Bispo Murbak.
A new dynamic model applied to electrically stimulated lower limbs and switched control design subject to actuator saturation and non-ideal conditions / Willian Ricardo Bispo Murbak Nunes. -- Ilha Solteira: [s.n.], 2019
126 f. : il.

Tese (doutorado) - Universidade Estadual Paulista. Faculdade de Engenharia de Ilha Solteira. Área de conhecimento: Automação, 2019

Orientador: Aparecido Augusto de Carvalho
Inclui bibliografia

1. Estimulação elétrica. 2. Paraplégicos. 3. Modelos Fuzzy Takagi-Sugeno. 4. Desigualdades matriciais Lineares. 5. Controle chaveado.

Raiane da Silva Santos
Raiane da Silva Santos
Supervisora Técnica de Seção
Seção Técnica de Referência, Atendimento ao usuário e Documentação
Diretoria Técnica de Biblioteca e Documentação
CRB/8 - 9999

UNIVERSIDADE ESTADUAL PAULISTA

Câmpus de Ilha Solteira

CERTIFICADO DE APROVAÇÃO

TÍTULO DA TESE: A New Dynamic Model Applied to Electrically Stimulated Lower Limbs and Switched Control Design Subject to Actuator Saturation and Non-Ideal Conditions

AUTOR: WILLIAN RICARDO BISPO MURBAK NUNES

ORIENTADOR: APARECIDO AUGUSTO DE CARVALHO

Aprovado como parte das exigências para obtenção do Título de Doutor em ENGENHARIA ELÉTRICA, área: Automação pela Comissão Examinadora:

Prof. Dr. APARECIDO AUGUSTO DE CARVALHO
Departamento de Engenharia Elétrica / Faculdade de Engenharia de Ilha Solteira

Prof. Dr. MARCELO CARVALHO MINHOTO TEIXEIRA
Departamento de Engenharia Elétrica / Faculdade de Engenharia de Ilha Solteira

Prof. Dr. MARCELO AUGUSTO ASSUNÇÃO SANCHES
Departamento de Engenharia Elétrica / Faculdade de Engenharia de Ilha Solteira

Prof. Dr. ALBERTO CLIQUET JUNIOR
Departamento de Ortopedia e Traumatologia / Universidade Estadual de Campinas - UNICAMP

Diogo Ramalho de Oliveira
Prof. Dr. DIOGO RAMALHO DE OLIVEIRA
IFMS - Câmpus de Três Lagoas / Instituto Federal de Educação, Ciência e Tecnologia de Mato Grosso do Sul

Ilha Solteira, 04 de julho de 2019

À minha família, em especial aos meus pais Wilson, Gisele e Maria (in memoriam),
ao meu irmão Wallisson, por todo amor, apoio,
confiança e incentivo nos momentos difíceis.

I dedicate to my family.
Grateful for all support, confidence and encouragement in difficult moments.

ACKNOWLEDGEMENTS

First, I must say that I am grateful to the God that I believe. He is invisible to human eyes, but I can hear and feel this presence all the time. To the God who gave me life, health, and security. I may not deserve it, but He is merciful to me. Even though I fail, He forgives me and loves me. What love is that? It's the true love that God has for everyone, including you dear reader. I am grateful to God for all the blessings and opportunities he gave me, including this important study. Are there times when I think of giving up? Yeah, but He gave me strength and courage to overcome the challenges during this journey. I am not worthy of anything, all honor and glory belongs to Him. Difficult moments are inevitable, but God grants us victory to persevere and to continue in the daily toil and life challenges. Praise, adoration, and thanksgiving to the one true God.

I am also grateful to my family. In my opinion, the family must be together at moments of joy and sadness. Some people do not value their family. However, family is a splendid divine plan, in which you can find enough strength to overcome turbulence moments. Family support has been fundamental to my journey. I want to thank my parents for teaching me the most valuable principles of life.

I must thank my professors who are exceptional and a source of inspiration for my career. They always helped me with their excellence scientific knowledge and showed me immeasurable personal value. My advisor Prof. Dr. Aparecido Augusto de Carvalho, thank you so much for your trust, for your loyalty, for the advice and honor in the guidance of this work. It has been an inspiration not only for showing your scientific vision and originality, but also for sharing your valuable knowledge through wisdom, kindness, charity, and humanity with others. I have no words describe it and express my gratitude. Also to Prof. Dr. Marcelo Carvalho Minhoto Teixeira, an incredible and brilliant researcher. His contagious laughter, words of encouragement and altruistic attitudes make him a very special person to every one of us. I am immensely grateful for his collaboration in the examining boards, his suggestions in the papers, and incentives to conduct the research.

To the professors who aroused my interest in the magnificent control area. To Prof. Dr. Edvaldo Assunção for the rich opportunity to exchange experiences and for sharing his vast knowledge of robust control, always having an unmatched didactics in his classes. To Prof. Dr. Rodrigo Cardim, an example of a gentle and humble person, which teaches with excellence its extensive knowledge about TS fuzzy via LMIs.

Time reserves us new bonds of friendship. Friends who are willing to help others without pride or personal boasting. I am really happy to meet new friends. My gratitude to Prof. Dr. Ricardo G. Teodoro (IFPR) and to Prof. Dr. Uiliam N. L. T. Alves (IFPR), who contributed a lot in this study.

Thank you all the colleagues at the Federal University of Technology - Paraná (UTFPR) (COELT-AP, DIRPPG-AP, and COGERH-AP) for supporting this study.

To the Prof. Dr. Marcelo A. A. Sanches (UNESP) and all other researchers who brilliantly contributed to the research of electrical stimulation in the laboratory.

To the professors at the Londrina State University (UEL). Prof. Dr. Márcio Covacic and Prof. Dr. Ruberlei Gaino by the indication and initial follow-up. To Prof. Dr. Eddy Kruger (UEL/UTFPR) and all members of the Neural Engineering and Rehabilitation Laboratory (LENeR) for all the tips in the biomedical area.

To all the colleagues at the laboratories LIEB, LPC and LENeR... we shared great moments together, especially Rafael, Héber, Fabian, Jorge, Ricardo Taoni, Andressa, Maurício, Paulo Broniera, Anderson, Gustavo, and Marco.

To my roommates, who opened their doors and welcomed me. Luiz Henrique, João Carlos Pelicer Jr., João Gabriel, Manuel, Igor and Heitor, I was pleased to meet you. To Jaci Rosa de Carvalho, a warrior of inestimable value and always willing to help, without hesitation. Thank you for the friendship in the coffee moments, in the lunches, and dinners.

To all the technical and administrative servers, who always look after the UNESP maintenance and operation.

This study was financed in part by the Coordenação de Aperfeiçoamento de Pessoal de Nível Superior - Brasil (CAPES) - Finance Code 001, and the Conselho Nacional de Desenvolvimento Científico e Tecnológico - (CNPq).

Anyway, I want to say thank you to everyone who directly or indirectly contributed to the success of this study.

“Um pouco de ciência nos afasta de Deus.
Muito, nos aproxima.”

“Little science takes you away from God but
more of it takes you to Him.”

Louis Pasteur (1822-1895)

RESUMO

A estimulação elétrica é uma técnica promissora para reabilitação motora em casos de lesão medular. A saturação do estimulador também é um requisito importante no projeto de sistemas de controle aplicados à estimulação elétrica. A negligência da saturação do atuador pode conduzir a resultados de controle indesejados, que evidencia os efeitos de fadiga muscular. Pela primeira vez é proposto um controlador chaveado sujeito à saturação para membro inferior estimulado eletricamente. O modelo dinâmico de extensão do membro inferior é não linear e incerto. O sistema descrito por modelos fuzzy Takagi-Sugeno e operando dentro de uma região de operação no espaço de estados é considerado neste trabalho. Além disto, falha do atuador, incerteza de ativação muscular, e não idealidades musculares, tais como fadiga, espasmos e tremor foram considerados em três níveis de severidade. O controle chaveado é comparado com a compensação distribuída paralela. Simulações denotam melhores resultados do controlador chaveado lidando com incertezas paramétricas da planta. Por outro lado, um desafio dos sistemas de controle para estimulação elétrica funcional é monitorar a dinâmica do torque em contrações musculares. Em aplicações de contração isotônica, medir o torque é algo difícil. A novidade neste estudo é a proposta de um novo modelo não linear, cujas variáveis de estado são posição angular, velocidade angular e aceleração angular. Neste novo modelo a variável torque é substituída adequadamente pela aceleração angular. Ensaios experimentais listam os parâmetros correspondentes a 24 indivíduos (20 saudáveis e 4 paraplégicos) para o modelo linearizado usando abordagem de identificação caixa cinza.
Palavras-chave: Estimulação elétrica. Paraplégicos. Modelos fuzzy Takagi-Sugeno. Desigualdades matriciais lineares. Controle chaveado.

ABSTRACT

Electrical stimulation is a promising technique for motor rehabilitation in cases of spinal cord injury. Stimulator saturation is important in the control system designs applied to electrical stimulation. The negligence of the actuator saturation in the electrical stimulation can lead to unwanted control results, which evidences the muscular fatigue effects. For the first time a switched controller subject to actuator saturation for electrically stimulated lower limb is proposed. The dynamic limb extension model is nonlinear and uncertain. The uncertain nonlinear system described by Takagi-Sugeno fuzzy models operating within an operating region in the state space is considered in this study. In addition, fault in the actuator, muscle activation uncertainty, and muscular non-idealities, such as fatigue, spasms, and tremor were considered at three three severity levels. The switched controller is compared to parallel distributed compensation technique. Simulations denote better results of the switched controller by dealing with parametric uncertainties. On the other hand, a challenge for FES control systems is to monitor torque in muscle contractions. In isotonic contraction applications, measuring torque is difficult. The novelty in this study is the proposal of a new nonlinear model, whose state variables are angular position, angular velocity and angular acceleration. In this new model the torque variable is replaced by the angular acceleration. Experimental tests list the parameters corresponding to 24 individuals (20 healthy and 4 paraplegic) for the linearized model using gray box identification approach.

Key words: Electrical stimulation. Paraplegics. Takagi-Sugeno fuzzy models. Linear matrix inequalities. Switched control.

LIST OF FIGURES

LIST OF TABLES

LIST OF ABBREVIATIONS & ACRONYMS

BMC	BioMedCentral
CFT	Constant-Frequency Trains
DM	Direct Model
DFT	Doublet-Frequency Trains
I	Electrical Current
FC	Fatigue Compensator
FEL	Feedback Error Learning
FN	Feedforward Neural
FM	Frequency Modulation
FES	Functional Electrical Stimulation
GS	Gain Scheduling
GA	Genetic Algorithm
HOSM	High Order Sliding Mode
IOFL	Input Output Feedback Linearization
IEEE	Institute of Electrical and Electronics Engineers
IOP	Institute of Physics
IM	Inverse Model
ILC	Iterative Learning Control
LMIs	Linear Matrix Inequalities
LMPC	Lyapunov-based Model Predictive Control
LQG	Linear Quadratic Gaussian
MPC	Model Predictive Control
MRAC	Model Reference Adaptive Controller
MLP	Multilayer Perceptron
MFTDNN	Multilayered Feedforward Time Delay Neural Network
NN	Neural Network
NMES	Neuromuscular Electrical Stimulation
NMPC	Nonlinear Model Predictive Control
NI	Not Informed
OL	Open-loop
PDC	Parallel Distributed Compensation
PG	Pattern Generator
PS	Pattern Shaper
PD	Proportional Derivative

PID	Proportional Integral Derivative
PAM	Pulse Amplitude Modulation
PW	Pulse Width
PWM	Pulse Width Modulation
RBF	Radial Basis Function
RISE	Robust Integral of the Sign of the Error
RMS	Root Mean Square
RMSE	Root Mean Square Error
SSRMSE	Root Mean Square Error in the steady-state time
SMC	Sliding Mode Controller
SOF	Static Output Feedback
TS	Takagi-Sugeno
TRMSE	Root Mean Square Error in the transient time
TTRMSE	Root Mean Square Error in the total time
VFT	Variable-Frequency Trains
V	Voltage
WHO	World Healthy Organization

LIST OF SYMBOLS

$\otimes$	Kronecker product. For example, consider $\mathbf{A} = \begin{bmatrix} a_{11} & a_{12} \\ a_{21} & a_{22} \end{bmatrix}$, and $\mathbf{B} = \begin{bmatrix} b_{11} & b_{12} \\ b_{21} & b_{22} \end{bmatrix}$. Then, the Kronecker product $\mathbf{A} \otimes \mathbf{B}$ is equal to

$$\mathbf{A} \otimes \mathbf{B} = \begin{bmatrix} a_{11} & a_{12} \\ a_{21} & a_{22} \end{bmatrix} \otimes \begin{bmatrix} b_{11} & b_{12} \\ b_{21} & b_{22} \end{bmatrix} = \begin{bmatrix} a_{11} \cdot \begin{bmatrix} b_{11} & b_{12} \\ b_{21} & b_{22} \end{bmatrix} & a_{12} \cdot \begin{bmatrix} b_{11} & b_{12} \\ b_{21} & b_{22} \end{bmatrix} \\ a_{21} \cdot \begin{bmatrix} b_{11} & b_{12} \\ b_{21} & b_{22} \end{bmatrix} & a_{22} \cdot \begin{bmatrix} b_{11} & b_{12} \\ b_{21} & b_{22} \end{bmatrix} \end{bmatrix},$$

$$= \begin{bmatrix} a_{11} \cdot b_{11} & a_{11} \cdot b_{12} & a_{12} \cdot b_{11} & a_{12} \cdot b_{12} \\ a_{11} \cdot b_{21} & a_{11} \cdot b_{22} & a_{12} \cdot b_{21} & a_{12} \cdot b_{22} \\ a_{21} \cdot b_{11} & a_{21} \cdot b_{12} & a_{22} \cdot b_{11} & a_{22} \cdot b_{12} \\ a_{21} \cdot b_{21} & a_{21} \cdot b_{22} & a_{22} \cdot b_{21} & a_{22} \cdot b_{22} \end{bmatrix}.$$

$\star$	For a symmetric matrix, it denotes the symmetric blocks in relation to the main diagonal
$\mathbb{R}$	Set of real numbers
$\mathbb{R}_+$	Set of positive real numbers
$\mathbb{Z}_+$	Set of positive integers numbers
$\mathbb{Z}_+^*$	Set of non-zero positive integers numbers
$\mathbb{N}$	Set of natural numbers
$\mathbb{R}^{n_x}$	Set of vectors $n_x \times 1$ with real elements
$\mathbb{R}^{n_x \times n_u}$	Set of matrices $n_x \times n_u$ with real elements
$\overset{\rightleftharpoons}{p}$	It corresponds to $p2^{p-1}$
$\mathbf{I}_{n_u}$	Identity matrix, $n_u \times n_u$
$\mathbf{P}^T$	Transposed matrix, $\mathbf{P} \in \mathbb{R}$
$\mathbf{P} > (\geqslant) 0$	It is a symmetric matrix and defined (semidefinited) positive
$\mathbf{P} < (\leqslant) 0$	It is a symmetric matrix and defined (semidefinited) negative
$\mathbf{sl}_{p,j}$	$\mathbf{sl}_{p,j} \in \mathbb{R}^{1 \times p}$ denotes a row vector whose j-th element is 1 and the others elements are zero
$\text{co}\{v_1, \cdots, v_p\}$	It denotes $\alpha_1 v_1 + \cdots + \alpha_p v_p$, $\alpha_1, \cdots, \alpha_p \geqslant 0$ and $\alpha_1 + \cdots + \alpha_p = 1$
$\mathbb{I}_k$	Set of first non-zero positive integers $\mathbb{I}_k = \{1, 2, \cdots, k\}$, $k \in \mathbb{Z}_+^*$
$\prod$	Product operator between elements
$\arg^* \min_{i \in \mathbb{I}_{n_r}} \{x_i\}$	Lower index $j \in \mathbb{I}_{n_r}$ such that, for the set $\{x_1, \cdots, x_{n_r}\}$, $x_j = \min_{i \in \mathbb{I}_{n_r}} \{x_i\}$

CONTENTS

1 INTRODUCTION

This chapter describes the problem treated and briefly introduces the proposal, motivation, objectives and thesis outline.

1.1 Context of the problem

Spinal cord injury has a significant incidence in the world population. The lesion may result in a partial or total obstruction of the sensory and motor connections below the level of the lesion. With this, the central nervous system ceases to receive the sensory-motor signals referring to the parts of the body below the level of the lesion. Paraplegic individuals begin to live under different limitations of locomotion and changes in their daily activities. Simple activities for healthy individuals become complex and painful for paraplegics. In this sense, the use of functional electrical stimulation has the potential to restore the movement of paralyzed limbs, offering both therapeutic and functional benefits.

Results in the area of motor rehabilitation with electrical stimulation show a promising future of this technique. Different approaches by researchers have concentrated efforts in intramuscular and surface stimulation, neuro technological implants, and hybrid mechanisms aided by robotic systems to enable that paraplegic individuals walk again.

One strand of this field is the study of controllers using surface electrical stimulation. Recent works in this area of closed-loop control highlights the challenges related to muscle delay; to high frequency switching in the control signal, also called chattering; to modulation parameters; to the parametric uncertainties of the plant; strategies to compensate muscular fatigue, among others.

However, the effect of the actuator saturation is also an important requirement in the system control design applied to electrical stimulation. The negligence of the actuator saturation in electrical stimulation can lead to unwanted control results, causing a overstimulation that evidences the effects of muscular fatigue.

By the author's knowledge, for the first time, a switched controller for the lower limb is proposed considering the saturation and fault of the electric stimulation actuator and analysis under non-ideal muscular conditions (fatigue, spasm and tremor). The dynamic model of the lower limb extension is nonlinear and uncertain. An exact description by the Takagi-Sugeno fuzzy model of the plant, operating within a region of operation is considered in the control design. A comparative analysis between the switched and parallel distributed compensation controllers is presented. Due to the uncertainties of the plant, the parallel distributed compensation (PDC) performance is compromised, because it is dependent on the knowledge of membership functions. Results obtained by simulation emphasize the best performance of the switched control law in non-ideal conditions, treated as parametric uncertainties.

In this study, the idea is to design several feedback gains, being only one gain used at a time, chosen based on a switching law that depends on the state vector of the controlled system. A schema that represents the use of the switched control is shown in the Figure 1.

A challenging problem is to measure muscle torque dynamics. In general, the variable of muscle torque state is estimated through strategies from the control signal or from state observers. Therefore, measuring torque becomes a complex task, especially for isotonic contractions.

The novelty in this study refers to a new nonlinear dynamic model. The proposed model presents the state variables: angular position, velocity, and acceleration. Therefore, the torque state variable is replaced by angular acceleration, which can be measured easily by accelerometers, for example. In addition, the nonlinear plant is described by fuzzy TS models and the LMIs-based control design is presented. LMIs are convex constraints to solve optimization problems with convex objective functions. The LMI constraints can easily be solved efficiently using specific softwares. In recent years, this method has been widely used among control engineers because a wide variety of control problems can be formulated as LMIs.

1.2 Objectives

1.2.1 General

This doctoral thesis proposes application of the switched control subject to actuator saturation and a new dynamic model for electrically stimulated lower limbs.

1.2.2 Specific

- Research and investigate the state-of-the-art on closed-loop control techniques in knee joint applications using electrical stimulation.
- Perform the control system design by parallel distributed compensation and switched law via LMI's.

Figure 1 - Electrical stimulation system of the lower limbs using switched controller subject to actuator saturation.

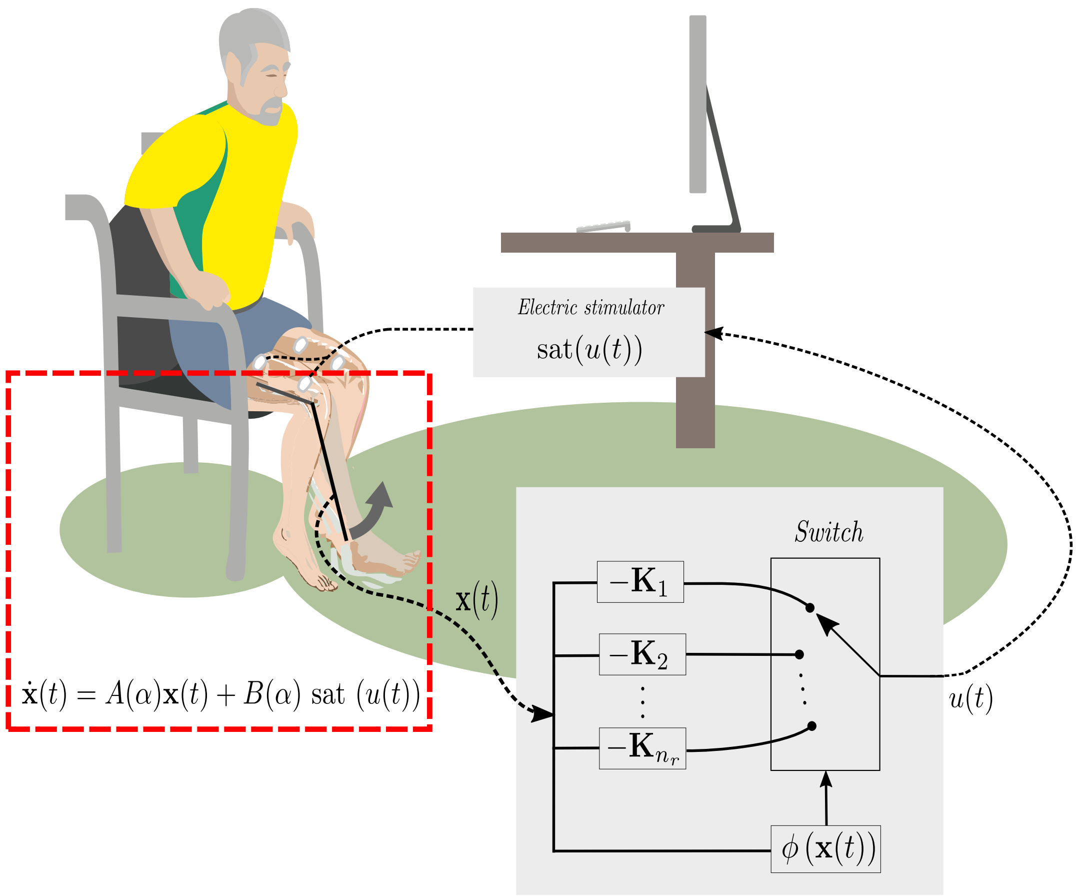

Source: From author.

- Simulate the two control techniques for different operating points of the lower limb under isometric conditions, considering healthy and paraplegic individuals.
- Analyze and compare the controlled system results by inserting saturation and fault in the actuator using torque-based model.
- Develop and test different levels to non-ideal muscle conditions (fatigue, spasms and tremor).
- To highlight the results obtained from switched control law in relation to parametric uncertainties.
- Measure and compare the RMS error between the PDC and switched controllers for the time interval corresponding to the transient and steady-state.
- Propose a new dynamic model applied to electrically stimulated lower limbs.

- Describe by TS fuzzy models and design PDC and switched control using the new proposed model.
- Perform experiments with healthy and paraplegic individuals and state-space identification of the electrically stimulated lower limb using gray-box approach.

1.3 Justification

The life expectancy of individuals with spinal cord injury is lower than the average of healthy people. In this sense, efforts have been made so that these individuals have facilitated access to physiotherapy activities for muscular strengthening using electrical stimulation with a closed-loop control system. In addition to granting therapeutic and/or functional benefits to individuals with spinal cord injury, the main objective is that these individuals are socially inserted, offering expectation and quality of life.

Arguably, rehabilitation systems using closed-loop control can improve performance and achieve desired movements with safety and reliability. However, some challenges must be overcome to allow a wide reach of this technology, among them we highlight:

- **Nonlinear musculoskeletal system and parametric uncertainties in control system design:** the great challenge of this area corresponds to the system being nonlinear and endowed with uncertain parameters make the control task more complex. More advanced control techniques have been employed in recent years. We propose a contribution to literature using a switched controller for regulation improvement under uncertain and non-ideal conditions of the lower limb.
- **Difficulty in monitoring and designing control systems based on muscular variables:** numerous mathematical models propose state variables that are difficult to measure. One contribution of this thesis is to establish an improved model based on measurable state variables of kinematics and which implicitly contemplating the lower limb muscle dynamics.
- **Model parameter variability in a larger individuals number:** the statistical analysis of parametric variability under electrical stimulation in different situations for a larger number of individuals is a gap in the literature. In this work, we investigate the parameter variability from 24 individuals considering the new model proposed.

1.4 Thesis outline

This work is organized as follows. Chapter 2 establishes the state-of-the-art on the subject of closed-loop control for electrical stimulation of lower limbs, focusing on studies of the knee joint. It presents the basic principles for understanding the area of electrical stimulation. It shows a systematic methodology for the literature review. It discusses and exposes the control techniques already investigated. It then reveals the technical characteristics of the experimental studies regarding the modulation type, stimulator and its output topology, electrode dimension, stimulation parameters, performance indexes of tracking and regulation in isometric contractions. Finally, the levels of spinal cord injury, the benefits and limitations of the FES closed-loop systems are indicated.

Chapter 3 introduces the switched controller and the regulation problem at an operating point subject to the non-ideal muscle condition (fatigue, spasms and tremor), as well as fault and saturation of the actuator. The torque-based model is evaluated for healthy and paraplegic individuals. LMIs conditions are established for the system to operate using switched control law in a region of operation and subject to symmetric saturation. The performance of the switched controller is compared to technique proposed by Gaino et al. (2017). Simulated results attest minor RMS error using switched controller applied to regulation considering non-idealities in the muscular model.

Chapter 4 emphasizes the new dynamic model for electrically stimulated lower limb. The design of the acceleration-based model is presented from a generic system of state space equations, whose states variables relate kinematics of movement and muscle torque dynamics. A description by TS fuzzy models of the nonlinear system is detailed. From this model, fuzzy controllers via PDC are designed to a region of operation considering healthy and paraplegics individuals.

Chapter 5 shows the experimental apparatus for lower limbs electrical stimulation. It then details the protocol of motor-point identification, and technical specifications of the tests. Experimental results are obtained from 24 individuals (20 healthy and 4 paraplegics) and the parameters of the state space model are listed by gray box approach.

Finally, the main conclusion of this work and some future works are in the Chapter 6.

2 CLOSED-LOOP CONTROL TECHNIQUES APPLIED TO MOTOR REHABILITATION OF THE KNEE JOINT USING ELECTRICAL STIMULATION: A SURVEY OF THE STATE-OF-THE-ART AND FUTURE PERSPECTIVES

"If you can't fly then run, if you can't run then walk, if you can't walk then crawl, but whatever you do, you have to keep moving forward."

Martin Luther King Jr

In the past decades, the FES control systems have been the target of intense research for the development of motor rehabilitation applications for individuals with spinal cord injuries. We conducted a systematic literature review of electrical stimulation of the lower limbs using the closed-loop control system in the main databases. The results highlight several research points, as well as the challenges to be overcome to use FES control systems in a large number of individuals.

2.1 Introduction

Functional electrical stimulation (FES) may be applied to restore movements in patients with reduced mobility. The neurophysiological principle is to generate potential artificial actions in motor neurons to cause muscular contraction using external electrical stimulation.

In 1757, Franklin (1757) was the first to cause involuntary contractions in paralyzed muscles using electrical signals coming from an external source. After approximately 200 years, Kantrowitz (1960) electrically stimulated the skeletal muscles of a patient with spinal cord injury to enable him to stand up. After a decade, FES systems started to be developed for lower limb applications in paraplegic patients (COOPER; BUNCH; CAMPA, 1973) and hemiplegic patients (WATERS; MCNEAL; PERRY, 1975). Initially, these systems provided limited benefits due to the on-off stimulation protocol. Over the years, some improvements have been made, such as programmable and flexible sequence stimulation, multichannel application and even feedback (closed-loop) control strategies.

In the early days, the electrical stimulation with closed-loop controllers was applied only in animals. Starting in the 1980s, electrical stimulation began to be studied more deeply in humans. As a result, the development and application of controllers have taken on a large scale along with researchers increasingly motivated to overcome challenges that limited the application of FES on a large scale.

Electrical stimulation proves to be a technique for restoring lost motor function and brings innumerable benefits to upper (SANTOS et al., 2016) and lower limbs in different clinical cases such as stroke (ERAIFEJ et al., 2017), multiple sclerosis (MILLER et al., 2017), and spinal cord injury.

With the improvement of the FES feedback system, it is believed that injured individuals can walk (WAGNER et al., 2018; HA; MURRAY; GOLDFARB, 2016), practice sports (cycling (MCDANIEL et al., 2017), rowing (ANDREWS; GIBBONS; WHEELER, 2017), swimming (WIESENER et al., 2018), among others) and pivot transfer with great efficiency (JOVIC et al., 2013; BO et al., 2019), among other applications.

Although there are several studies on controllers for lower limbs using FES, the literature lacks a systematic review elucidating the main contributions already made, showing the most relevant results found and indicating the limitations faced and the challenges still unresolved.

To our knowledge, this is the chapter conducting a systematic literature review that presents and discusses results coming from the closed-loop control system applied to electrical stimulation of lower limbs.

This chapter is organized as follows. Section 2.2 discusses some essential concepts and principles for a better understanding of the effects of electrical stimulation and its role in motor rehabilitation associated with closed-loop control systems. Section 2.3 describes the methodology used in the systematic literature review, only considering the studies on control in closed-loop of the knee joint by electrical stimulation. Section 2.4 presents the selected papers and based on them discusses strategies of identification of the model; control techniques adopted; aspects of validation (simulation or experimental); benefits, limitations, and future perspectives of FES control systems. Finally, Section 2.5 presents a conclusion of the main points presented in this chapter.

2.2 Basic principles of electrical stimulation

2.2.1 What happens when an electric stimulus is applied to the muscle?

It is very common to associate electrical stimulation with the recruitment of muscle fibers. However, some concepts should be clarified for a better understanding of muscle contraction from artificial electrical stimuli.

First, regardless of the type and size of electrode used, the electrical stimulation artificially activates the motor neurons and not the muscle fibers. This is because the activation potential threshold of motor axons is smaller than that of muscle fibers. Nerve fibers innervate the muscles. Consequently, muscle contractions result from the activation of motor neurons.

Functional electrical stimulation consists of applying a pulsed current or voltage signal to the muscular or intramuscular surface. Each pulse releases an action potential capable of depolarizing neurons above the activation threshold. The factors that determine which neuron is recruited is determined by both the amplitude, pulse width, frequency, and shape of the pulses. The intensity of electrical stimulation is associated with the energy transfer to the muscle. Thus, considering a biphasic and symmetrical constant frequency waveform, the total energy is given by the product between the amplitude and duration of the electric pulse.

The threshold value corresponding to the recruitment of a neuron varies according to the size, type and relative position of the electrode. When applying pulses of small intensity, only large neurons with a small threshold and close to the electrode are recruited. By increasing the intensity of the pulses, small neurons with a higher threshold value and more distant from the electrodes are also recruited.

When applying electrical stimuli, muscular strength increases with the number of motor units recruited. Muscle strength control can be by amplitude modulation or pulse width (so-called spatial summation) or by frequency modulation (temporal summation).

Among the limitations of frequency modulation is the saturation of muscle strength for frequencies above 30 Hz and early fatigue with increasing frequencies.

2.2.2 What is the difference between natural and artificial neural activation?

The action potential caused in the muscle using FES differs from the natural physiology of neural activation. The order of recruitment through FES is reversed. For example, suppose the goal is to achieve low muscle strength by electrical stimulation. When applying a low-intensity stimulus, large motor units are recruited, fatiguing rapidly. Keeping the same position of the electrode and parameters of stimulation constant, the same motor units are activated. This strategy deteriorates the performance of spatial summation since the same motor nerves are recruited simultaneously, while the central nervous system asynchronously triggers the action potential.

In other words, the FES recruits the motor units in synchronous mode (all at the same time), while the central nervous system performs asynchronously (alternates recruitment at each time interval). Thus, a tetanus contraction by FES requires a higher frequency (20-50Hz) while natural recruitment by the central nervous system occurs at lower frequency (6-10Hz).

2.2.3 Which fibers are recruited during electrical stimulation and what does this influence?

Fast-twitch fibers are recruited first with simultaneous mode activation. The order is different when compared to natural recruitment, in which slow-twitch fibers are recruited first. The diameter of the axons that innervate the fast-twitching fibers are larger than that of the slow-twitching fibers. Consequently, in the occurrence of an action potential, there will be a field of higher intensity in the axons of the fast-twitching fibers.

A disadvantage of this artificial recruitment process is that fast-twitch fibers tend to fatigue in a faster time than slow-twitch fibers.

2.2.4 What is the importance and purpose of modeling?

Many contributions can be obtained from a model. Primarily, it can promote the understanding and prediction of the behavior of a system. A complex phenomenon can be described by a limited number of simple concepts and by modeling each component separately. Moreover, a model can enable the evaluation of the behavior of a system in adverse situations, or that cannot be validated experimentally.

However, the understanding and prediction of a system are not necessarily associated. For example, some black-box predictive models come from statistical or measured input/output datasets. In general, black-box models do not contribute to an understanding of the system whose behavior they predict.

2.2.5 What is the difference between open-loop and closed-loop?

The application of neuroprostheses for lower limb movement is still not widely accepted at the clinical level. Most commercially available systems are of the open-loop type. Open-loop systems do not provide state feedback of the stimulated limb. Therefore it is difficult to determine the most suitable stimulation pattern.

The closed-loop has a considerable advantage over the open-loop. In situations of external disturbances (e.g., obstacles and loads) or internal disturbances (e.g., spasms and muscle fatigue) closed-loop can compensate for such events by automatically adjusting the stimulation pattern. For complex movements, the closed-loop control strategy can track trajectories, minimize disturbances, and achieve smooth movement.

Most studies in this research field focus on closed-loop systems for strength or angle control of a single joint, not considering multi-joint movements. This is because multi-joint movements such as applications for standing, going from seated to standing, and walking are more difficult to analyze.

2.2.6 What should be considered in modeling?

The dynamic model of a neurophysiological or biomechanical process can be represented by a direct (DM) or inverse (IM) model.

The DMs are used to represent the behavior of the real system, using the same assignment of input and output. The inputs in such models are for example the stimulation parameters, and the outputs are generally the torques of the joints or movements of the limbs.

Unlike DM, an IM describes the system inversely, that is, the model input is a measured or desired motion signal, and then the model predicts the stimulation pattern required to achieve the predefined motion. Alternatively, an IM can analyze the biomechanical movement and record the moment of a given joint.

The most common approach to modeling is to consider the integration of three dynamic subsystems corresponding to the movement of the segment of the body, muscle contraction and muscular activation using electrical stimuli. The figure shows the association between the three subsystems for motion control by electrical stimulation. The dynamics of the body segment consider the kinematics around the joint, the muscle moment arms as a function of the angle and the anthropometry of limbs (mass, geometry, and moment of inertia). Muscle contraction dynamics describes mechanical contraction, tendon and muscle relaxation, compound length and velocity-dependent strength relationships along with muscle activation. The muscle activation dynamics subsystem describes the temporal and spatial summation effect of muscle strength. This subsystem describes the behavior of action potentials, neuromuscular transmission and the process of electrochemical-mechanical activation within muscle fibers, such as calcium dynamics.

Figure 2 - Schematic representation of the dynamic subsystems that compose a extension neuroprothesis model using electrical stimulation.

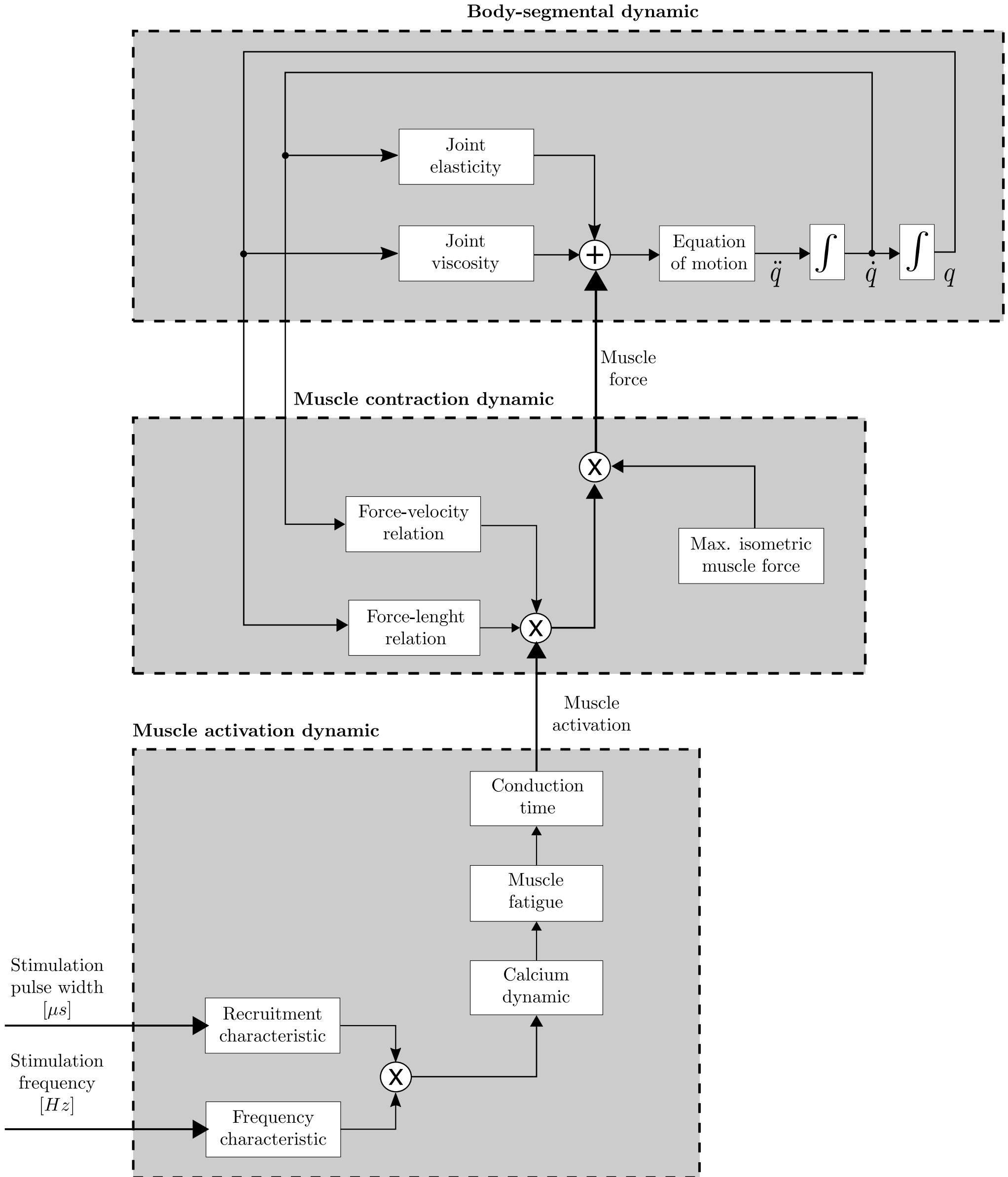

Source: From author.

The dynamic model of the body segment can be more sophisticated depending on the complexity considered. In general, the passive viscoelastic properties are separated from the active properties of the muscle to simplify the model. The passive elastic properties are modeled by exponential equations, and the passive viscosity property of the joint can be modeled by a linear damping function. To keep the number of parameters relatively small, the viscoelastic properties are attributed to the joints.

The dynamic muscle contraction and activation models presented in the Figure 2 are not unique. Some modeling variants are depending on the complexity of the application desired. The muscle models can be divided into microscopic and macroscopic approach. Microscopic models describe the internal processes of muscle fibers at the level of cross-bridges, based on structures such as Hill, Huxley, Hazte, and others. While macroscopic models, the muscle is represented by a component containing viscoelastic properties or by a black-box. Furthermore, it is common to consider the system macroscopically as a Hammerstein or Wiener-Hammerstein structure, where a static non-linearity (representing the recruitment curve) is followed by one or two linear dynamics (representing the rest of the muscle dynamics), respectively.

It is emphasized that although the Hammerstein structure is widely used, it is not a suitable representation for isometric conditions. Also note that such models ignore the nonlinear dynamics of the muscle, namely: temporal delay due to the speed of conduction and properties varying in time as fatigue.

2.3 Literature review methodology

The state-of-the-art was carried out in the BioMedCentral (BMC), Elsevier, Google Scholar, IEEE Xplore, Institute of Physics (IOP), PUBMED, Scopus, Springer and Web of Science databases.

Search terms were defined in three sets using the logical connective AND to connect them. The sets and their terms were as follows: ["*electrical stimulation*" OR "FES" OR "NMES"], ["*lower limb*" OR "*knee*"], ["*controller*" OR "*control*"].

The preferred language was English with search criteria restricted for knee joint control systems by electrical stimulation, i.e., leg-foot complex movements. After the search in the databases, the papers were read, and the exclusion and inclusion criteria were used.

The exclusion criteria were only to consider works addressing the closed-loop control of the knee joint by electrical stimulation. Therefore, duplicate works were excluded; dorsiflexor muscle activation systems for ankle joint; hybrid systems, that is, the use of electrical stimulus of joint way to orthoses and exoskeletons; those applied to agonist muscles and antagonists in a synchronized way to generate a functional movement in applications such as cycling, walking, lifting and sitting, seat transfer and among others. Studies addressing stimulation from intramuscular electrodes, and using animals in experiments were also excluded. With regard to the inclusion criteria, articles from citations and references were analyzed.

Figure 3 - Methodology used to state-of-the-art research.

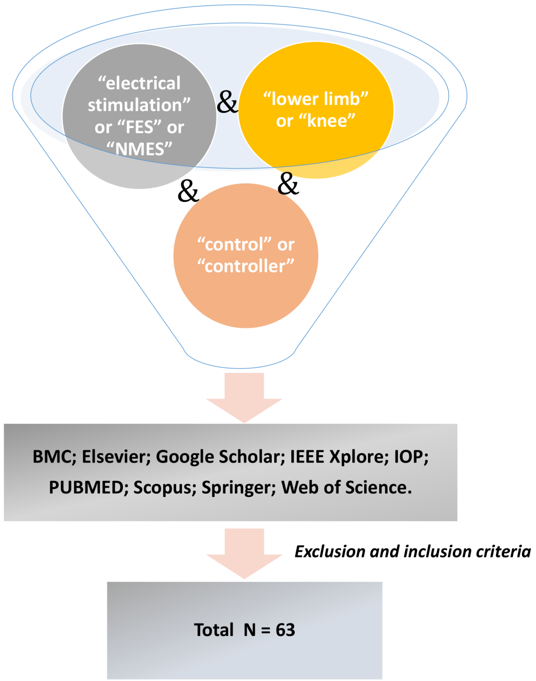

Source: From author.

2.4 Identification and control techniques for the knee joint using FES

Electrical stimulation with closed-loop control of the knee joint began in the 1990s (HATWELL et al., 1991). Over the years, studies in this area have intensified and more researchers have contributed to state-of-the-art.

Thus, the main contributions on control techniques, identification class of the dynamic model and type of validation of the system (simulation and/or experimental) are briefly presented in the Table 1.

Table 1 - General description of the studies involving electrical stimulation to control the knee joint.

Author(s)	**Control Technique(s)**	**Identification**	**Validation**
(HATWELL et al., 1991)	MRAC	Black-box	Simulation and experimental
(ABBAS et al., 1997)	Neural Network PG/PS	Black-box	Experimental
(CHANG et al., 1997)	MFTDNN, PID, neuro-PID	Black-box	Simulation and experimental
(JEZERNIK; RIENER, 1999)	SMC, PID	Black-box	Simulation
(PREVIDI; CARPANZANO; CIRILLO, 1999)	LQG, GS	Black-box	Simulation
(SCHAUER; HUNT, 2000)	LQG, GS	Black-box	Experimental
(RIESS; ABBAS, 2000)	PD, PG/PS-NN	Black-box	Simulation and experimental
(FERRARIN et al., 2001)	OL, PID, PID+feedforward, adaptive PID	Gray-box	Simulation and experimental
(SCHAUER; HOLDERBAUM; HUNT, 2002)	SMC	Gray-box	Experimental
(IANNÒ et al., 2002)	Adaptive neuro-PID + FN	Black-box	Simulation
(JEZERNIK et al., 2002)	SMC	Black-box	Simulation
(PREVIDI; CARPANZANO, 2003)	LQ, GS	Black-box	Simulation
(JEZERNIK; WASSINK; KELLER, 2004)	SMC	Black-box	Simulation and experimental
(FERRANTE et al., 2004)	PID, neuro-PID and adaptive NN	Black-box	Simulation and experimental
(SCHAUER et al., 2005)	Backstepping	Gray-box	Simulation
(MOHAMMED et al., 2005)	HOSM	Gray-box	Simulation and experimental
(AJOUDANI; ERFANIAN, 2006)	Neuro-SMC	Black-box	Experimental
(MOHAMMED; POIGNET; GUIRAUD, 2006)	MPC	Gray-box	Simulation
(PEDROCCHI et al., 2006)	EMC, PID+anti-windup, FN, PID+FN	Black-box	Simulation
(TEIXEIRA et al., 2006)	TS-PDC fuzzy	TS fuzzy	Simulation
(MOHAMMED et al., 2007)	MPC+IOFL	Gray-box	Simulation
(STEGATH et al., 2008)	RISE	Black-box	Experimental
(SHARMA et al., 2009a)	FN+Backstepping	Black-box	Simulation
(SHARMA et al., 2009b)	RISE	Black-box	Experimental
(AJOUDANI; ERFANIAN, 2009)	Neuro-SMC	Gray-box	Simulation and experimental
(LONGLONG et al., 2009)	Neuro-PID	Black-box	Experimental
(WANG et al., 2010a)	PD+FN optimum	Black-box	Simulation

Continued on next page

Table 1 – *Continued from previous page*

Author(s)	**Control Technique(s)**	**Identification**	**Validation**
(WANG et al., 2010b)	Neuro+RISE+optimum	Black-box	Simulation
(LYNCH; GRAHAM; POPOVIC, 2011a)	PID, SMC	Gray-box	Simulation
(SHARMA; GREGORY; DIXON, 2011)	PD, PD+delay	Black-box	Experimental
(IBRAHIM et al., 2011c)	FL Mamdani+GA	Black-box	Simulation and experimental
(KOIKE et al., 2011)	PD+FEL	Black-box	Simulation
(IBRAHIM et al., 2011b)	FL Mamdani+GA	Black-box	Simulation
(IBRAHIM et al., 2011a)	FL cycle-to-cycle	Black-box	Simulation
(LYNCH; GRAHAM; POPOVIC, 2011b)	PID, SMC	Gray-box	Simulation
(LYNCH, 2011)	PID, SMC, GS	Gray-box	Simulation
(CHENGWEI; QIAN, 2011)	Neuro-PID	Black-box	Simulation
(MIURA et al., 2011)	FL cycle-to-cycle	Black-box	Experimental
(MOHAMMED et al., 2012)	MPC+IOFL	Gray-box	Experimental
(SHARMA et al., 2012)	RISE+FN	Black-box	Experimental
(LYNCH; POPOVIC, 2012)	PID, GS, SMC	Gray-box	Simulation
(COVACIC et al., 2012)	SOF	Gray-box	Simulation
(WANG et al., 2013)	Optimal PD+FN	Black-box	Experimental
(BENAHMED; KERMIA; TADJINE, 2013)	PID	Gray-box	Simulation
(SANCHES et al., 2014)	PID	Gray-box	Simulation and experimental
(KARAFYLLIS et al., 2014)	Prediction of delay	Gray-box	Simulation
(OBUZ et al., 2015)	RISE delay	Black-box	Experimental
(DOWNEY et al., 2015b)	RISE asynchronous	Black-box	Experimental
(SANTOS et al., 2015)	Robust	Gray-box	Simulation
(YANG; QUEIROZ, 2016)	Adaptive	Gray-box	Simulation
(CHENG et al., 2016)	MLP	Black-box	Experimental
(GAINO et al., 2017)	TS-PDC fuzzy	TS fuzzy	Simulation
(DOWNEY et al., 2017)	Switched SMC	Black-box	Experimental
(ALIBEJI et al., 2017)	PID+DSC, PID+DC	Black-box	Experimental
(KIRSCH; ALIBEJI; SHARMA, 2017)	NMPC	Gray-box	Simulation e experimental

Continued on next page

Table 1 – *Continued from previous page*

Author(s)	Control Technique(s)	Identification	Validation
(LI et al., 2017)	RBF+SMC, GA+RBF+SMC	Gray-box	Experimental
(WU et al., 2017)	PID, PD+ILC	Black-box	Simulation
(BENAHMED; TADJINE; KERMIA, 2017)	Adaptive super twisting	Black-box	Simulation
(SHARMA et al., 2017)	PD, NN+PD, NN+PD+FC	Black-box	Experimental
(YANG; QUEIROZ, 2018)	Adaptive Robust	Gray-box	Simulation
(SUN; BAO; SHARMA, 2019)	LMPC	Black-box	Simulation
UNESP-Theses/Dissertations			
(FARIA, 2006)	TS-PDC fuzzy	TS fuzzy	Simulation
(SILVA, 2007)	TS-PDC fuzzy	TS fuzzy	Simulation
(GAINO, 2009)	TS-PDC fuzzy	TS fuzzy	Simulation
(PRADO, 2009)	PID	Gray-box	Simulation
(KOZAN, 2012)	PID	Gray-box	Simulation and experimental
(JUNQUEIRA, 2013)	PID	Gray-box	Simulation and experimental
(SANCHES, 2013)	PID, TS-PDC fuzzy	Gray-box and TS fuzzy	Simulation and experimental
(KOZAN, 2016)	LQG/LTR	Gray-box	Simulation and experimental
(TEODORO, 2018)	RSG, RSwC	Gray-box	Simulation and experimental
This study	**TS-PDC fuzzy, RSwCSS**	**Gray-box and TS fuzzy**	**Simulation and experimental**

Legend - FC: Fatigue Compensator; FN: Feedforward Neural; FEL: Feedback Error Learning; GA: Genetic Algorithm; GS: Gain Scheduling; HOSM: High Order Sliding Mode; ILC: Iterative Learning Control; IOFL: Input Output Feedback Linearization; LMPC: Lyapunov-based Model Predictive Control; LQG: Linear Quadratic Gaussian; MFTDNN: Multilayered Feedforward Time Delay Neural Network; MPC: Model Predictive Control; MRAC: Model Reference Adaptive Controller; NN:Neural Network; NMPC: Nonlinear Model Predictive Control; OL: Open-loop; PD: Proportional Derivative; PDC: Parallel Distributed Compensation; PG: Pattern Generator; PS: Pattern Shaper; PID: Proportional Integral Derivative; MLP: Multilayer Perceptron; RBF: Radial Basis Function; RISE: Robust Integral of the Sign of the Error; RSS: Robust Single-Gain Controller; RSwC: Robust Switched Controller; RSwCSS: Robust Switched Controller Subject to Saturation; SMC: Sliding Mode Controller; SOF: Static Output Feedback; TS: Takagi-Sugeno.

Source: From author.

The Figure 4 shows the 61 works from Table considering the established criteria of identification type and validation. Among them, 33 correspond to the results obtained using simulation, 19 experimentally validated and 11 using simulation and experimental verification.

Figure 4 - Numerical analysis of scientific contributions.

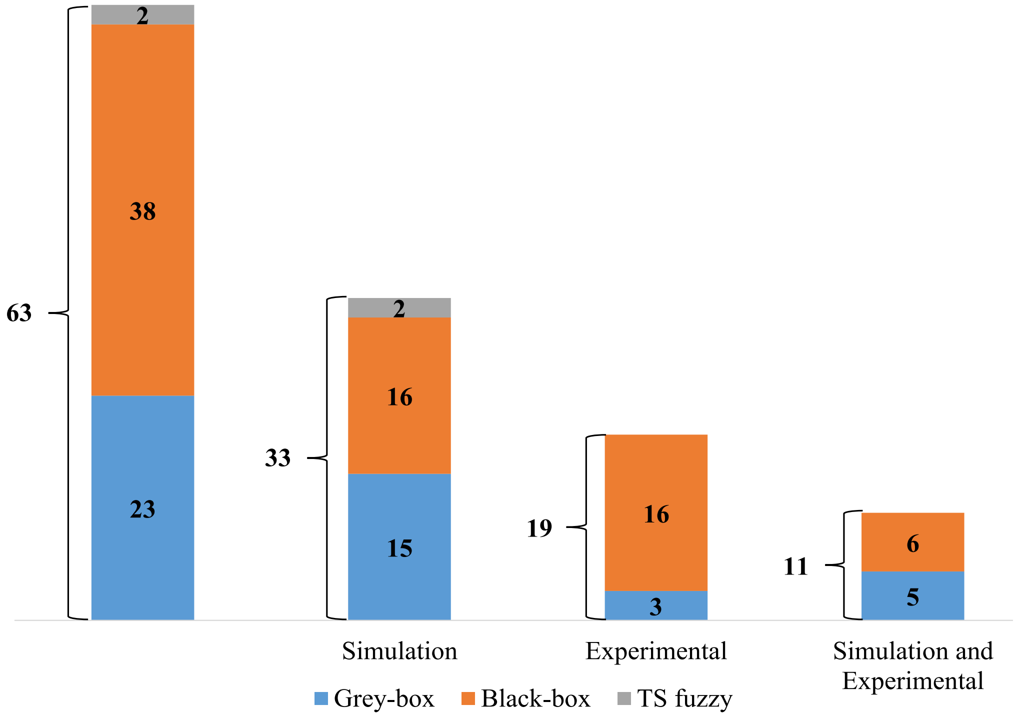

Source: From author.

2.4.1 *Identification techniques*

The identification of systems comprises a primordial step to obtain a dynamic model of the process to be controlled. Different methodologies, mathematical tools, and algorithms can be used to describe the system.

In general, the most common identification models are white-box, gray-box, and black-box. The white-box modeling is based on the fundamental principles of mechanics (Newton's laws). The gray-box modeling is built based on fundamental physical principles and experimental data. In this type of modeling, some internal features of the system may not be fully known. Whereas, the black-box is considered when there is no full understanding of the physical behavior of the process. In the black-box model, the dynamic system is represented mathematically in a more complex way, making it impossible to associate its description with the physical principles involved.

Fuzzy models can also be used to describe the dynamic behavior of a nonlinear system. There are two types of rule-based fuzzy models: the Mamdani and the Takagi-Sugeno (TS).

Figure 5 - Main topologies of control system applied to electrical stimulation: (a) open-loop; (b) closed-loop with output or state feedback; (c) closed-loop with feedforward-feedback controller; (d) adaptive.

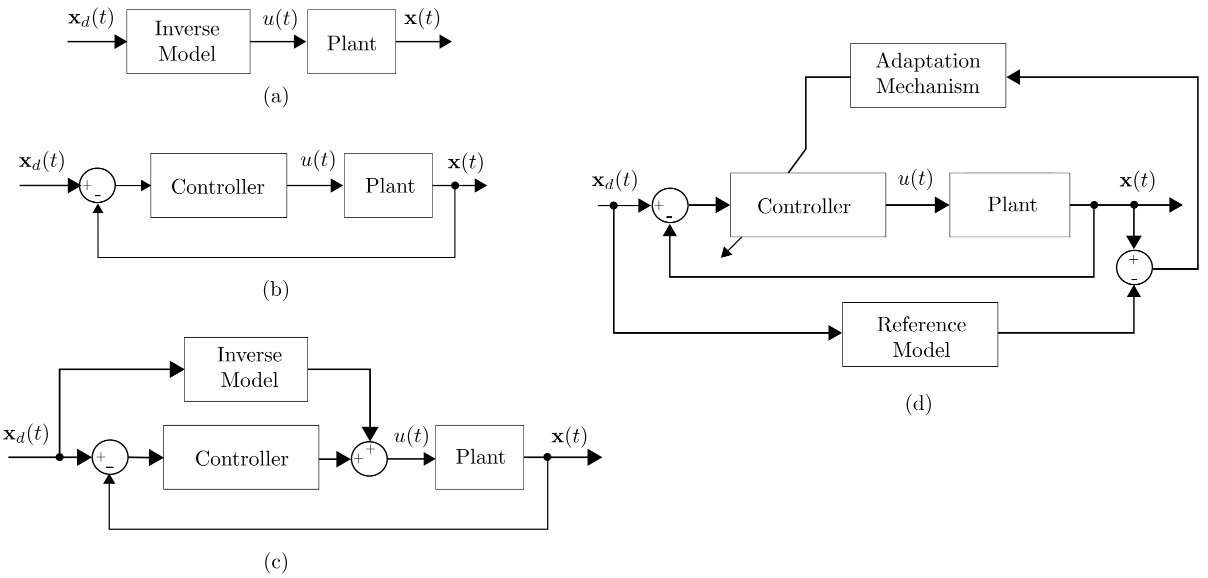

Source: From author.

Compared to the Mamdani, TS fuzzy models can, from few rules, approximate with greater accuracy a complex nonlinear system.

As can be observed in the Table, 37 papers used the black-box approach, 20 used the gray-box approach, and 2 used TS fuzzy models. Approximately 73% of the papers experimentally validated treated the dynamic system as a black-box.

2.4.2 *Closed-loop control techniques*

Furthermore, Table 1 allows evaluating the chronology of the control techniques evaluated to regulate the angular position of the knee joint. Note that several proposals have already been investigated. In general, we can categorize them as (a) open-loop using inverse model as compensator; (b) closed-loop with output or state feedback; (c) closed-loop with feedforward-feedback controller; (d) adaptive structure for controller based on a reference model.

2.4.3 *Specifications for experimental validation*

Generally, an electrical stimulator allows the adjustment of some specific parameters of the waveform, such as pulse width (μs or ms), voltage or current amplitude (V or mA, respectively), and burst frequency and pulses. The burst frequency is lower than the pulse frequency.

For frequencies $f_{burst} < 20$Hz, muscle tissue develops an inefficient response for movement generation, while for frequencies $f_{burst} > 70$Hz there is faster fatigue and discomfort due to nociceptive sensitivity in healthy individuals.

An electrical stimulator, in turn, is composed of electronic circuits capable of transforming the input signal from the electrical network into a pulsed type output signal with high voltage or current amplitude. An electrical stimulation device consists of the following circuits: (1) protection and power supply, responsible for providing and regulating the electrical signal coming from the external environment (battery or source voltage of the power grid); (2) pulse generator, consisting of oscillator or microcontroller circuits that generate a high frequency carrier signal of small amplitude; (3) modulator, whose function is to modulate the signal from the pulse generator circuit; and (4) output or power stage, which amplifies electrical signals and provides adequate energy to stimulate neuromuscular tissue (SOUZA et al., 2017).

With regard to modulation type, there are three basic categories: pulse amplitude modulation (PAM), pulse width (PWM) and frequency modulation (FM).

The energy applied to muscle tissue from the stimulator output stage may be constant current or voltage. The flow of electrons in muscle tissue determines the type of waveform: single phase or biphasic. Thus, a stimulator with single-phase output stage only allows one-way electron flow. While the biphasic allows the bidirectional flow of electric charges in the muscle tissue, thus avoiding a possible accumulation of charges, which can be detrimental to the patient.

Table 2 shows the differences among the experiments that carried out experimental validation concerning the modulation type (PWM or PAM), stimulator with current or voltage output stage, output stage topology for single-phase or biphasic signals, and electrode dimensions used.

The stimulation patterns are (1) the constant-frequency trains (CFT), that is, equally spaced constant-frequency (20-50 Hz) pulse trains; (2) the doublet-frequency trains (DFT) refer to close spaced pulses (doublets) throughout the train; (3) variable-frequency trains, for example, doublets at the beginning of CFT.

A body limb movement may involve isometric and/or isotonic muscle contraction. Isometric contraction refers to the case where the joint angle and the insertion length of the muscle remain constant. Isotonic and the length of the muscle vary, and can be: (1) concentric when muscular shortening occurs because the increase of muscular tension surpasses the resistance; or (2) eccentric when there is muscle stretching due to resistance overcoming muscle strength.

Table 3 presents a comparison of specifications in the experimental works regarding the stimulation frequency, pulse width range, voltage amplitude or current at the stimulator output stage.

Table 2 - Experimental features on modulation type, stimulator, output topology, and electrode dimension.

Author(s)	Modulation (PWM/PAM)	Stimulator (I/V)	Output topology	Electrodes (cm x cm)
(HATWELL et al., 1991)	PMW	V	NI	NI
(ABBAS et al., 1997)	PWM	I	NI	Implanted
(CHANG et al., 1997)	PAM	I	Biphasic	4×8
(SCHAUER; HUNT, 2000)	PWM	I	NI	NI
(RIESS; ABBAS, 2000)	PAM	I	Biphasic	NI
(FERRARIN et al., 2001)	PWM	I	Biphasic	5×9
(SCHAUER; HOLDERBAUM; HUNT, 2002)	PWM	I	NI	NI
(JEZERNIK; WASSINK; KELLER, 2004)	PWM	I	Biphasic	NI
(FERRANTE et al., 2004)	PWM	I	NI	NI
(MOHAMMED et al., 2005)	PAM	I	NI	NI
(AJOUDANI; ERFANIAN, 2006)	PWM	I	Biphasic	NI
(STEGATH et al., 2008)	PAM	I	Biphasic	NI
(SHARMA et al., 2009b)	PAM	I	Biphasic	NI
(AJOUDANI; ERFANIAN, 2009)	PWM	I	Biphasic	5×10
(LONGLONG et al., 2009)	PAM	I	Biphasic	NI
(SHARMA; GREGORY; DIXON, 2011)	PAM	I	Biphasic	NI
(IBRAHIM et al., 2011c)	PWM	I	Biphasic	5×13
(MIURA et al., 2011)	PAM	V	Mono/Biphasic	NI
(MOHAMMED et al., 2012)	PAM	I	NI	NI
(SHARMA et al., 2012)	PAM	V	Monophasic	NI
(WANG et al., 2013)	PAM	V	Monophasic	NI
(SANCHES et al., 2014)	PWM	I	Biphasic	4×4
(OBUZ et al., 2015)	PAM	I	NI	7.5×13
(DOWNEY et al., 2015b)	PWM	I	Biphasic	7.5×13 4×9 5×9
(CHENG et al., 2016)	PAM	V	Monophasic	7.5×13
(DOWNEY et al., 2017)	PWM	I	Biphasic	7.5×13 4×9 5×9
(ALIBEJI et al., 2017)	PAM	I	Biphasic	NI
(KIRSCH; ALIBEJI; SHARMA, 2017)	PAM	I	Biphasic	NI
(LI et al., 2017)	PWM	I	NI	NI
(SHARMA et al., 2017)	PAM	I	Biphasic	7×13
UNESP-Theses/Dissertations				
(KOZAN, 2012)	PWM	I	Biphasic	NI
(JUNQUEIRA, 2013)	PWM	I	Biphasic	NI
(SANCHES, 2013)	PWM	I	Biphasic	5×5
(KOZAN, 2016)	PWM	I	Biphasic	5×5
(TEODORO, 2018)	PWM	I	Biphasic	5×9

Legend - I: Electrical Current; NI: Not informed; V: Voltage.

Source: From author.

2.4.4 Controller performance indexes

Tests to track trajectories are performed to artificially mimic the movements of a limb by electrical stimulation. Different signs of tracing allow to know some behaviors of the mus-

Table 3 - FES parameter specifications in the experimental papers.

Author(s)	**Frequency [Hz]**	**PW** $[\mu s]$	**Voltage [V]**	**Current [mA]**
(HATWELL et al., 1991)	20	$[-70 \quad 200]$	NI	NI
(ABBAS et al., 1997)	20	$[5 \quad 150]$	-	20
(CHANG et al., 1997)	25	200	-	$[0 \quad 80]$
(SCHAUER; HUNT, 2000)	25	$[0 \quad 500]$	-	$[50 \quad 90]$
(RIESS; ABBAS, 2000)	20	360	-	NI
(FERRARIN et al., 2001)	20	$[0 \quad 520]$	-	$[80 \quad 100]$
(SCHAUER; HOLDERBAUM; HUNT, 2002)	20	NI	-	$[40 \quad 80]$
(JEZERNIK; WASSINK; KELLER, 2004)	20	$[0 \quad 500]$	-	$[0 \quad 125]$
(FERRANTE et al., 2004)	20	$[20 \quad 500]$	-	$[30 \quad 110]$
(MOHAMMED et al., 2005)	NI	NI	-	$[0 \quad 200]$
(AJOUDANI; ERFANIAN, 2006)	25	$[0 \quad 600]$	-	NI
(PEDROCCHI et al., 2006)	20	$[0 \quad 500]$	-	NI
(STEGATH et al., 2008)	100	100	$[20 \quad 35]$	-
(SHARMA et al., 2009b)	30	100	$[25 \quad 35]$	-
(AJOUDANI; ERFANIAN, 2009)	25	$[0 \quad 700]$	-	NI
(LONGLONG et al., 2009)	25	150	-	$[0 \quad 120]$
(SHARMA; GREGORY; DIXON, 2011)	30	$[100 \quad 400]$	$[5 \quad 50]$	-
(IBRAHIM et al., 2011c)	25	$[0 \quad 230]$	-	40
(MIURA et al., 2011)	20	300	$[0 \quad 80]$	
(MOHAMMED et al., 2012)	25	NI	NI	NI
(SHARMA et al., 2012)	30	400	$[15 \quad 38]$	-
(WANG et al., 2013)	28	400	$[1 \quad 50]$	-
(SANCHES et al., 2014)	50	$[0 \quad 230]$	-	$[60 \quad 120]$
(OBUZ et al., 2015)	35	NI	-	$[30 \quad 50]$
(DOWNEY et al., 2015b)	$[16, 64]$	$[80 \quad 170]$	-	NI
(CHENG et al., 2016)	$[25, 60]$	400	-	NI
(DOWNEY et al., 2017)	$[16, 64]$	$[0 \quad 150]$	-	$[70, 90]$
(ALIBEJI et al., 2017)	35	400	-	$[20 \quad 80]$
(KIRSCH; ALIBEJI; SHARMA, 2017)	35	400	-	$[20 \quad 80]$
(LI et al., 2017)	25	$[0 \quad 400]$	-	25
(SHARMA et al., 2017)	35	400	-	$[20 \quad 100]$
UNESP-Theses/Dissertations				
(KOZAN, 2012)	50	$[0 \quad 325]$	$-$	$[60, 65, 80]$
(JUNQUEIRA, 2013)	50	$[0 \quad 325]$	$-$	$[60, 65, 80]$
(SANCHES, 2013)	50	$[0 \quad 400]$	$-$	$[80, 100]$
(KOZAN, 2016)	50	$[100 \quad 280]$	$-$	120
(TEODORO, 2018)	50	$[0 \quad 400]$	$-$	$[70, 80, 120, 140]$

Legend - NI: Not informed; PW: Pulse Width.

Source: From author.

cle under stimulation. Table 4 summarizes the experimental validations for trajectory tracing, showing: the number of healthy and paraplegic individuals; the total stimulation interval; the tracking reference; and the RMS error. Note that the reference signal is smooth, and with low frequency, and only nine studies validated their control techniques with paraplegic individuals.

In addition to tracking, some studies evaluate the control system for step-type reference signals. However, maintaining the operation around an operating point for an extended period of time shows a difficult task, shown in Table 5.

Table 4 - Comparison among studies addressing the control by electrical stimulation of the knee joint for trajectory tracking.

Author(s)	N_h	N_p	T_t[s]	**Tracking signal**	**RMS error**
(HATWELL et al., 1991)	1	1	30	Sinusoidal $T = 10$ s	8°
(ABBAS et al., 1997)	-	**4**	-	-	-
(CHANG et al., 1997)	1	1	6	Sinusoidal $T = 2$ s	7.24°(H)
					7.18°(P)
				Sinusoidal $T = 1$ s	5.32°(H)
					5.14°(P)
(SCHAUER; HUNT, 2000)	1	–	25	Step of 10 s	NI
(RIESS; ABBAS, 2000)	–	2	**125**	Raised cosine	≤ 10°
				1.5 s (on), 1.0 s (off)	
(FERRARIN et al., 2001)	-	2	60	Triangular 20°-60°	4.55°
(SCHAUER; HOLDERBAUM; HUNT, 2002)	1	-	45	Step of 10 s	NI
	6	2	20	Step of 10 s	4.33°
(JEZERNIK; WASSINK; KELLER, 2004)			20	Ramps of 4 s	3.43°
			20	Raised cosine 2 s	4.76°
(FERRANTE et al., 2004)	1	1	25	Step of	≈ 5°
				4 s (on), 1 s (off)	
(MOHAMMED et al., 2005)	1	-	12	Step of	NI
				3 s (on), 2 s (off)	
(AJOUDANI; ERFANIAN, 2006)	3	3	120	Ramp of 14 s and	0.44°(H)
				hold to 6 s	0.90°(P)
(STEGATH et al., 2008)	1	-	8	Step of 8 s	7.62°
	1	-	20	Sinusoidal 20° to 45°	3.56°
(SHARMA et al., 2009b)	5	-	30	Two periodic	2.75°
				trajectory	
	5	-	30	Sinusoidal $T = 6$ s	2.88°
	5	-	30	Sinusoidal $T = 2$ s	4.11°
	5	-	30	Triple periodic	3.27°
				$6, 4, 2$ s	
	5	-	30	Triple periodic	5.46°
				$6, 4, 2$ s (higher range)	
(AJOUDANI; ERFANIAN, 2009)	5	**4**	120	Ramp of 14 s and	3.76°(H)
				hold to 6 s	5.41°(P)
	1		180	Raised cosine 12 s	3.77°(H)
(LONGLONG et al., 2009)	5	-	60	Variable from 10° to 80°	NI
(SHARMA; GREGORY; DIXON, 2011)	**10**	-	20	Sinusoidal $T = 2$ s	3.91°
(IBRAHIM et al., 2011c)	1	-	10	Sinusoidal $T = 1$ s	NI
(MIURA et al., 2011)	5	2*	NI	Variable from 45° to 70°	NI
(MOHAMMED et al., 2012)	1	2	10	Step of 8 s	NI
				Sinusoidal $T = 10$ s	NI
(SHARMA et al., 2012)	7	-	30	Sinusoidal $T = 1.5$ s	2.92°
	3	-	30	Dual periodic	2.29°
	2	-	30	Step of 15 s	NI

Continued on next page

Table 4 – *Continued from previous page*

Author(s)	N_h	N_p	T_t[s]	**Tracking signal**	**RMS error**
(WANG et al., 2013)	5	-	30	Sinusoidal	2.54°
	3	-	20	Step of 20 s	1.38°
(SANCHES et al., 2014)	-	1	4	Step of 4 s	NI
(OBUZ et al., 2015)	3	-	30	Sinusoidal $T = 2$ s	4.73°
(DOWNEY et al., 2015b)	4	-	45	Sinusoidal $T = 2$ s	4.96°
(CHENG et al., 2016)	5	-	20	Sinusoidal $T = 2.5$ s	7.22°
(DOWNEY et al., 2017)	6	-	35	Sinusoidal $T = 2$ s	9.9°
(ALIBEJI et al., 2017)	2	1	30	Dual periodic	3.74°
(KIRSCH; ALIBEJI; SHARMA, 2017)	3	-	25	Step	1.34°
(LI et al., 2017)	2	-	20	Step of 10 s	0.38°
(SHARMA et al., 2017)	3	-	30	Sinusoidal $T = 2$ s	3.78°
	3	-	30	Sinusoidal $T = 1$ s	4.86°
	3	-	30	Sinusoidal $T = 4$ s	3.63°
Average	**3.4**	**2**	**36**	-	-

Legend - N_h, N_p are the numbers of healthy and paraplegic individuals, respectively; T_t is the total stimulation period; T is the signal period; H: Healthy; P: Paraplegic; NI: Not informed.

Source: From author.

2.4.5 Level and time of spinal cord injury

The spinal cord lesion characterizes the partial or total interruption of the neurological signs of the spinal cord, resulting in paralysis and/or lack of sensitivity from the level of the lesion.

Table 5 - Comparison among studies involving control by electrical stimulation of the knee joint using step response.

Author(s)		**Healthy**			**Paraplegics**		
	N_T	N_h	T_{th}[s]	RMS error	N_p	T_{tp}[s]	RMS error
(PREVIDI; CARPANZANO, 2003)	1	-	-	-	1	5	NI
(JEZERNIK; WASSINK; KELLER, 2004)	**8**	**6**	10	4.33*	**2**	**10**	*
(STEGATH et al., 2008)	2	2	8	3.5	-	-	-
(WANG et al., 2010a)	3	3	20	1.38	-	-	-
(KIRSCH; ALIBEJI; SHARMA, 2017)	3	3	**25**	**1.34**	-	-	-
	1	1	**60**	**6.17**	-	-	-
UNESP-Theses/Dissertations							
(KOZAN, 2012)	3	3	7.1	NI	-	-	-
(JUNQUEIRA, 2013)	1	1	7.1	NI	-	-	-
(SANCHES, 2013)[5]	2	1	4.7	NI	1	5	NI
(KOZAN, 2016)	6	4	5.8	NI	2	6.3	NI
(TEODORO, 2018)	9	5	50	10	4	13.8	10

Legend - N_h, N_p are the numbers of healthy and paraplegic individuals, respectively; $N_T = N_h + N_p$ is the total number of individuals; T_{th}, T_{tp} are the stimulation interval associated with the RMS error considered for healthy and paraplegic individuals, respectively; *It presents results among all individuals; NI: Not informed.

Source: From author.

Table 6 - Characteristics of individuals with spinal cord injury.

Author(s)	Age (Years)	Level of injury	Time after injury (months)
(HATWELL et al., 1991)	40	T5	72
(ABBAS et al., 1997)	NI	NI	NI
(CHANG et al., 1997)	28	T8	2
(RIESS; ABBAS, 2000)	NI	T4,T10,T11	36
(FERRARIN et al., 2001)	33,40	T1,T7	24,48
(JEZERNIK; WASSINK; KELLER, 2004)	NI	NI	NI
(FERRANTE et al., 2004)	NI	NI	NI
(AJOUDANI; ERFANIAN, 2006)	NI	NI	NI
(AJOUDANI; ERFANIAN, 2009)	NI	T5-T6,T6,T7,T9-T10,T10-T11	4,12,2,48,24
(MOHAMMED et al., 2012)	29	T5,T12	5,12
(SANCHES et al., 2014)	40	T6	NI
(ALIBEJI et al., 2017)	41	T10	NI

Source: From author.

The lesion levels are divided into cervical (C1-C8), thoracic (T1-T12), lumbar (L1-L5) and sacral (S1-S5) levels. In addition to impairment of motor sensitivity and activity, spinal cord injured individuals also present alterations in the urinary, intestinal and autonomic systems.

Spinal cord injuries may be traumatic (motor accidents, falls or violence) and non-traumatic (tumors, spina bifida, and tuberculosis) According to the WHO, approximately 90% of the spinal cord injuries are traumatic, and about 1/3 of the individuals with spinal cord injuries present clinically significant signs of depression.

Table 6 indicates the level of injury, age and injury time. The most prominent level in the studies is T10, T5, and T6, with individuals with a mean age of 35 years and injury time on average equal to 27 months.

2.4.6 Benefits of FES

In addition to motor rehabilitation, electrical stimulation avoids muscle atrophy, ulceration, thrombosis, bone demineralization, spasticity, and promotes improved bowel, sexual and breathing function of the individual (RAGNARSSON, 2008).

2.4.7 Limitations of closed-loop FES systems

Some challenges still limit the large-scale application of FES control systems, such as muscle fatigue, spasticity, and number of individuals.

2.4.7.1 Fatigue

The decrease in muscle strength induced by FES has strongly affected the performance of control systems. For example, in less than one minute, muscle strength may fall by half in a neuroprosthesis. The causes of fatigue are diverse and include: reverse order of recruitment; high activation of motor units (stimulation frequency); synchronous activation of axons (DOWNEY et al., 2015a); among others.

Rapid muscle fatigue due to artificial activation has been minimized using spatiotemporal strategies such as decreasing stimulation frequency; modify the stimulation pattern (switching from CFT to DFT)(DING; WEXLER; BINDER-MACLEOD, 2003); switch the stimulation electrodes in asynchronous mode (DOWNEY et al., 2015a); among others.

However, even using these strategies presents other difficulties. By decreasing the stimulation frequency, control gains become larger. Moreover, although VFT and DFT stimulation trains can be employed to obtain greater isometric strength in fatigued muscles and potency in dynamic contraction, however, they produce a greater decline in strength than CFT.

2.4.7.2 Spasticity

Spasticity is common in individuals with spinal cord injury and is characterized by unpredictable increased muscle tone, occurrence of spasms, and hyperactive reflexes. For example, given an instant of time, the movement generated from electrical stimulation may be affected by an unexpected event of muscle spasticity. The paralyzed muscle tends to contract to the maximum, not in response to brain signals, but in response to a variety of sensory stimuli. In FES control systems, spasticity should be considered because the controller should be able to compensate for the increase in muscle tone (LYNCH; POPOVIC, 2008).

2.4.7.3 Number of volunteers

The clinical application of FES with control systems depends on more conclusive studies on the associated benefits in a higher number of paraplegic individuals. For example, to date, the highest number of paraplegic individuals with experimental validation was equal to six in (AJOUDANI; ERFANIAN, 2009).

2.4.8 Perspectives

Recent studies are still limited to obtaining more efficient performance control techniques, quantified by RMS error index for tracking or regulation applications. However, it is noted that the maximum application interval is still restricted to a few seconds.

Scientific findings describing the muscular behavior under the action of electric stimuli promoted the development and validation of different control techniques. However, some factors limit clinical and even experimental validation. From the point of view of rehabilitation professionals, the supervisory and control system should be easy to handle. From the point of view of the individual, in turn, the whole set of hardware, from sensors to the acquisition and command system, the system should prioritize the user's comfort and mobility.

2.5 Conclusion

This chapter has shown that the research field is vast and promising. However, studies focused on long-term motor rehabilitation for individuals with spinal cord injury are still scarce.

Performing closed-loop control of a physiological system is very complex. Such complexity is due both to the mathematical modeling of the biological system, which has non-linearities and parametric uncertainties and to the hardware implementation of more sophisticated controllers.

In addition to the challenges to be overcome, a question remains: how can an FES control system that achieves less tracking error, less muscle fatigue for an extended time of stimulation be developed?

3 ISOMETRIC CONTRACTION IMPROVEMENT FOR ELECTRICAL STIMULATION UNDER NON-IDEAL CONDITIONS USING SWITCHED CONTROLLER SUBJECT TO ACTUATOR SATURATION

"It is not your business to succeed, but to do right; when you have done so, the rest lies with God."
C. S. Lewis

Electrically stimulated lower limb systems contain higher order nonlinearities as well as uncertainties in their physical parameters. Nonlinear systems can be modeled using Takagi-Sugeno (TS) fuzzy models. Techniques such as parallel distributed compensation (PDC) are dependent on the membership functions that constitute the TS fuzzy model. In several cases, these functions are not explicitly available due to uncertainties or singularities in the system. In this chapter, we propose a switched controller that effectively handles system uncertainties. The closed-loop control system containing non-idealities (such as fatigue, spasms, tremor, muscle recruitment, and fault in the actuator) is compared using PDC and switched control.

3.1 Introduction

Every year, thousands of individuals worldwide suffer from spinal cord injuries arising from traffic accidents, acts of violence, or falls. For such individuals, neuromuscular electrical stimulation is widely used method for motor rehabilitation.

Current research efforts in this field are focused on enhancing the stimulation systems by improving the controllers used in the closed-loop system. Electrical stimulations address the stimulation of different body functions in the upper and lower limbs. In the case of lower limbs, for example, functional electrical stimulation (FES) is used for the rehabilitation of knee joint control (GAINO et al., 2017; YANG; QUEIROZ, 2018), standing up (RIENER; FUHR, 1998; KOBRAVI; ERFANIAN, 2012), sitting pivot transfer (JOVIC et al., 2015), gait (SHARMA; MUSHAHWAR; STEIN, 2014; HA; MURRAY; GOLDFARB, 2016), swimming (WIESENER et al., 2018), and cycling (BELLMAN et al., 2016; BO et al., 2017), among others. Activities that involve greater degrees of freedom and muscles require a more complex control system. For the current state-of-the-art, even simple motor activities still present great challenges and are subject to intense scientific research.

Several studies have been recently proposed to regulate knee joint utilizing controllers capable of handling non-linearities and uncertainties. Kirsch, Alibeji and Sharma (2017) presented a predictive control model for knee extension with the goal of minimizing muscular fatigue. However, the performance of the predictive controller for steady state regulation was not ideal and could not be maintained for a time interval over 30 s; as the controller could not simultaneously achieve error minimization and control. Gaino et al. (2017) proposed a PDC controller based on the TS fuzzy model that is capable of regulation at different operating points. One major limitation of this work is the fact that it assumes ideal conditions in its simulations and does not consider the uncertainties of the plant, and other practical aspects of the actuator such as saturation and possible failure modes such as power decrease. Yang and Queiroz (2018) presented a robust adaptive controller based on convex/concave parameterization, and Lipschitziana evaluated them under weak fatigue conditions. Downey et al. (2017) adopted a strategy for switching stimulation channels with the aim of maintaining controllability for a long time under fatigue conditions.

Future research will focus on FES systems associated with controllers for compensating muscular fatigue and other disturbances. This will enable individuals to perform functional movements, and the controlled system state variables will be close to the desired ones and operate for the longest possible time.

The major challenge is the achievement of regulation in the presence of nonlinear behavior and/or uncertainties in the musculoskeletal complex. Another significant issue is the non-linear effect of actuator saturation in the control design. Some authors do not consider the saturation effects, although it is a major problem and affects system performance. The current trend in medical devices is miniaturization, low energy consumption, and improved wearability. Therefore, it is important to consider the behavior of the system when the actuator fails or experiences a decrease in power due to power source limitations.

In this chapter, we propose a switched controller to address the problem of regulation in the electrical stimulation of the lower limbs as they have uncertain nonlinear dynamics. The switched control is compared to other control scheme described in the literature for regulation at different operating points. The design of the proposed switched controller is based on linear matrix inequalities (LMIs) for a non-linear uncertain plant described by TS fuzzy models with unknown membership functions. We expanded the analysis by considering saturation and fault in the actuator, and consider severe intensity levels of fatigue, spasms, tremor as additional sources of uncertainty. Results obtained indicate we can obtain a much lower RMS error in steady-state using the proposed switched controller.

This study contributes to the state-of-the-art by improving the steady-state regulation results by considering uncertainties such as fatigue, spasms, tremor, muscular recruitment, and faults in the actuator. The system under study has several uncertainties, and the advantage of the switched controller design is that it does not depend on the membership functions that constitute the TS fuzzy model, which in this case are unknown. In the addition, the switched control law minimizes the temporal derivative of the quadratic function of Lyapunov.

Throughout this paper, the notation adopted is standard. The symbol $\otimes$ denotes the Kronecker product. The symbol $\mathbf{sl}_{p,j} \in \mathbb{R}^{1\times p}$ denotes a row vector whose j-th element is 1 and the others are equal to zero, and $\overrightarrow{\overleftarrow{p}} = p2^{p-1}$, $p \geqslant 1$. For a symmetric matrix, the symbol $\star$ denotes the symmetric blocks in relation to the main diagonal. The set $\mathbb{I}_k = \{1,\, 2,\, \cdots,\, k\}$, $k \in \mathbb{N}$. Let $\mathrm{co}\left\{v_1,\, v_2,\, \cdots,v_p\right\}$ denote the convex hull of the vectors v_h, $h \in \mathbb{I}_p = \{1,\, 2,\, \cdots,\, p\}$. Besides that $\varsigma = \arg^* \min_{i\in\mathbb{I}_{n_r}} \{x_i\}$ denotes the smallest index $\varsigma \in \mathbb{I}_{n_r}$, such that, for the set $\{x_1,\, x_2,\, \cdots,x_{n_r}\}$, $x_\varsigma = \min_{i\in\mathbb{I}_{n_r}} \{x_i\}$.

The rest of this chapter is organized as follows. Section 3.2 presents the derivation of the torque-based nonlinear dynamic model for leg extension using electrical stimulation. Section 3.3 describes the switched control design subject to actuator saturation using LMIs. In Section 3.4, simulation results that demonstrate the controller performance improvement when compared to PDC in dealing with actuator failure, muscle activation uncertainty, and non-idealities like fatigue, spasms, and tremor are presented. Section 3.5 finally concludes this study.

3.2 Nonlinear dynamic model for leg extension using electrical stimulation

We consider the model widely disseminated in the literature. This model refers to a standard and consolidated technique for identifying parameters related to the dynamic model of knee joint movement from the electrical stimulation in the quadriceps. More details about this procedures can be obtained in Ferrarin and Pedotti (2000).

Consider the leg extension system using electrical stimulation with load cell added in the experimental apparatus, whose mathematical model is given by:

$$J\ddot{\theta} = H_g(\theta) + \Lambda_p(\theta,\dot{\theta}) + \Gamma_{ke}(M_a); \tag{1}$$

where $\theta, \dot{\theta}, \ddot{\theta}, M_a \in \mathbb{R}$ are angular position, velocity, acceleration and torque of the lower limb (shank-foot); $J \in \mathbb{R}$ is the moment of inertia, and $H_g(\theta)$ is the gravitational torque, given by:

$$H_g(\theta) = -mgl\sin(\theta), \tag{2}$$

where m, $l \in \mathbb{R}$ are the mass and distance between knee and the shank-foot complex mass center, respectively; g is the gravitational acceleration.

The passive musculoskeletal torque of the knee $\Lambda_p(\theta,\dot{\theta})$ is expressed as:

$$\Lambda_p(\theta,\dot{\theta}) = -\lambda e^{-E_v\left(\theta+\frac{\pi}{2}\right)}\left(\theta + \frac{\pi}{2} - \omega\right) - B\dot{\theta}, \tag{3}$$

where λ, $E_v \in \mathbb{R}$ are the coefficients of the exponential terms related to knee stiffness; $\omega \in \mathbb{R}$ is elastic rest angle of the knee; and $B \in \mathbb{R}$ is viscous friction coefficient.

Concerning the worst scenarios that can occur during electrically stimulated contractions, we incorporate non-idealities indicated by (LYNCH; GRAHAM; POPOVIC, 2011a; LYNCH; POPOVIC, 2012). The FES induced muscle contraction produces the muscular torque $\Gamma_{ke}(M_a)$ is expressed as:

$$\Gamma_{ke}(M_a) = (1+\kappa_{sp}+\kappa_{tr})\,\kappa_{fat}M_a = \kappa_{stf}M_a, \tag{4}$$

where $\kappa_{sp},\ \kappa_{tr},\ \kappa_{fat} \in \mathbb{R}$ are related to spasms, tremor, and fatigue. Three levels of spasms, tremor and fatigue were used: mild, moderate and severe. The criterion adopted for the classification of tremor waveforms and muscle spasm were chosen through the significance in functional movement. For example, the occurrence of spikes in the angular position of the knee refer to spasms classified as: *i*) mild, for amplitudes less than 10°; *ii*) moderate, for amplitudes between $10^\circ - 20^\circ$; *iii*) severe, for amplitudes greater than 20°. Whereas oscillations in knee position are due to tremors classified as: *i*) mild, those that modify knee dynamics in amplitude less than 7.5°; *ii*) moderate, for amplitude less than 15°; and *iii*) severe, for amplitude greater than 15°. The fatigue severity rating was established in such a way that: *i*) $\kappa_{fat} = 1$ indicates absence of fatigue; *ii*) $0 < \kappa_{fat} < 1$ corresponds to partially fatigued muscle; and *iii*) $\kappa_{fat} = 0$ suggests completely fatigued muscle.

The muscle activation M_a, that can be modeled by first order system as:

$$\frac{M_a}{\breve{u}_f} = \frac{\hat{G}}{\tau s+1} \quad \Longleftrightarrow \quad \dot{M}_a = \frac{1}{\tau}\left(-M_a + \hat{G}\breve{u}_f\right), \tag{5}$$

where $\breve{u}_f \in \mathbb{R}$ is the current amplitude of the electrical stimulation, $\tau \in \mathbb{R}$ is time constant of muscle activation, and $\hat{G} \in \mathbb{R}$ is the uncertain parameter.

Furthermore, in this chapter is considered an actuator fault. The actuator fault is a power loss from the stimulator power supply. In the model, this is represented by $\breve{u}_f(t) = \kappa_{flt}\breve{u}(t)$, which may correspond to the following operating conditions of the actuator: *i*) $\kappa_{flt} = 1$, implies that the actuator has no fault; *ii*) $0 < \kappa_{flt} < 1$ is a partial fault in the actuator; and *iii*) $\kappa_{flt} = 0$, represent a complete fault in the actuator.

Defining the state variables $\breve{x}_1 = \theta$, $\breve{x}_2 = \dot{\theta}$ and $\breve{x}_3 = M_a$. Then, (1) can be written as:

$$\begin{cases} \dot{\breve{x}}_1 = & \breve{x}_2 \\ \dot{\breve{x}}_2 = & \dfrac{1}{J}[-mgl\sin(\breve{x}_1) - \lambda e^{-E_v\left(\breve{x}_1+\frac{\pi}{2}\right)}\left(\breve{x}_1+\dfrac{\pi}{2}-\omega\right) - B\breve{x}_2 + \kappa_{stf}\breve{x}_3] \\ \dot{\breve{x}}_3 = & -\dfrac{1}{\tau}\breve{x}_3 + \dfrac{\kappa_{flt}\hat{G}}{\tau}\breve{u}, \end{cases} \tag{6}$$

The parameter values for healthy and paraplegic subjects are indicated in Table 7.

The goal is to maintain the leg angle in a desired position $\breve{x}_1 = \theta = \theta^d$. Considering that the equilibrium point of the system (6) is $\breve{\mathbf{x}}_e = [\breve{x}_1 \quad \breve{x}_2 \quad \breve{x}_3]^T = [\theta^d \quad 0 \quad M_a^d]^T$. So, $\dot{\breve{x}}_1 = 0$, $\dot{\breve{x}}_2 = 0$

Table 7 - Parameters from healthy and paraplegic subjects.

Subject	H1	H2	H3	H4	H5	P1	P2	P3
J [kg.m^2]	0.377	0.358	0.399	0.375	0.384	0.362	0.292	0.394
m [kg]	4.05	4.63	4.38	3.83	4.36	4.37	3.42	4.76
l [m]	0.253	0.239	0.248	0.237	0.243	0.238	0.231	0.233
B [N.m.s/rad]	0.377	0.311	0.400	0.305	0.332	0.270	0.302	0.289
λ [N.m/rad]	1.199	4.679	3.657	4.490	3.889	41.208	3.761	15.352
E_v [rad^{-1}]	-0.486	0.041	-0.031	0.257	-0.079	2.024	1.317	1.644
ω [rad]	2.548	2.427	2.710	2.701	2.412	2.918	2.520	3.896
G_n [N.m/A]	266.67	266.67	256.67	266.67	333.33	283.33	83.33	76.67
τ [s]	0.454	0.426	0.491	0.406	0.438	0.951	0.203	0.215

Source: Adapted from (FERRARIN; PEDOTTI, 2000).

and $\dot{\breve{x}}_3 = 0$, $\breve{u} = \breve{u}^d$, and from (6) it follows that:

$$0 = \frac{1}{J}\left[-mgl\sin(\theta^d) - \lambda e^{-E_v\left(\theta^d+\frac{\pi}{2}\right)}\left(\theta^d + \frac{\pi}{2} - \omega\right) + \kappa_{stf} M_a^d\right],$$

$$M_a^d = \frac{mgl\sin(\theta^d) + \lambda e^{-E_v\left(\theta^d+\frac{\pi}{2}\right)}\left(\theta^d + \frac{\pi}{2} - \omega\right)}{\kappa_{stf}}. \tag{7}$$

Moreover, from (6) one can also obtain that:

$$0 = -\frac{1}{\tau} M_a^d + \frac{\hat{G}}{\tau}\breve{u}_f^d,$$

$$\breve{u}^d = \frac{\breve{u}_f^d}{k_{flt}} = \frac{M_a^d}{\kappa_{stf}\kappa_{flt}\hat{G}} = \frac{mgl\sin(\theta^d) + \lambda e^{-E_v\left(\theta^d+\frac{\pi}{2}\right)}\left(\theta^d + \frac{\pi}{2} - \omega\right)}{\kappa_{stf}\kappa_{flt}\hat{G}}. \tag{8}$$

In addition, note that the equilibrium point is not the origin $[\breve{x}_1 \quad \breve{x}_2 \quad \breve{x}_3]^T = [0 \quad 0 \quad 0]^T$. For stability analysis it is necessary to modify the coordinates as:

$$\begin{aligned} &x_1 = \breve{x}_1 - \theta^d, \quad x_2 = \breve{x}_2, \quad x_3 = \breve{x}_3 - M_a^d, \quad u = \breve{u} - \breve{u}^d \quad i.e., \\ &\breve{x}_1 = x_1 + \theta^d, \quad \breve{x}_2 = x_2, \quad \breve{x}_3 = x_3 + M_a^d, \quad \breve{u} = u + \breve{u}^d. \end{aligned}$$

And $\dot{x}_1 = \dot{\breve{x}}_1$, $\dot{x}_2 = \dot{\breve{x}}_2$, and $\dot{x}_3 = \dot{\breve{x}}_3$, so

$$\dot{\mathbf{x}}(t) = \begin{bmatrix} 0 & 1 & 0 \\ f_{21}(\mathbf{z}) & -\frac{B}{J} & f_{23}(\mathbf{z}) \\ 0 & 0 & -\frac{1}{\tau} \end{bmatrix} \mathbf{x}(t) + \begin{bmatrix} 0 \\ 0 \\ g_{31}(\mathbf{z}) \end{bmatrix} \mathbf{u}(t), \tag{9}$$

$$f_{21}(\mathbf{z}) = \frac{1}{Jx_1}\left[-mgl\sin(x_1+\theta^d) - \lambda e^{-E_v\left(x_1+\theta^d+\frac{\pi}{2}\right)}\left(x_1 + \theta^d + \frac{\pi}{2} - \omega\right)\right.$$

$$+mgl\sin(\theta^d)+\lambda e^{-E_v\left(\theta^d+\frac{\pi}{2}\right)}\left(\theta^d+\frac{\pi}{2}-\omega\right)\Big], \tag{10}$$

$$f_{23}(\mathbf{z})=\frac{(1+\kappa_{sp}+\kappa_{tr})\,\kappa_{fat}}{J}=\frac{\kappa_{stf}}{J}, \tag{11}$$

$$g_{31}(\mathbf{z})=\frac{\kappa_{flt}\hat{G}}{\tau}, \tag{12}$$

where $\mathbf{x}=[x_1 \quad x_2 \quad x_3]^T$, $\mathbf{z}=[x_1 \quad \hat{G} \quad \theta^d \quad \kappa_{stf} \quad \kappa_{flt}]^T\in\mathbb{R}^5$.

Note that $\dot{x}_3=-\frac{1}{\tau}x_3+g_{31}(\mathbf{z})\breve{u}$, $u=\breve{u}-\breve{u}^d$, and $x_3=\breve{x}_3-M_a^d$, such that $\breve{u}^d$ and M_a^d are uncertain value for different operating point θ^d. The challenge of this system is to regulate at an operating point considering the uncertainties $\breve{u}^d$, and M_a^d. In Section 3.3, analysis of the control system design is presented considering the uncertainties of plant modeling.

3.2.1 TS fuzzy models

TS fuzzy models can approximate any continuous function uniformly $f:\mathbb{W}\subset\mathbb{R}^n\rightarrow\mathbb{R}^p$ in a compact domain $\mathbb{W}$.

The main idea about TS inference system is to use the description by means of fuzzy rules IF-THEN, to represent a nonlinear dynamic model by a linear subsystems association.

Therefore, given a time-invariant dynamic system, the local description in local models is established by:

$$\dot{\mathbf{x}}(t)=\mathbf{A}_\varphi\mathbf{x}(t)+\mathbf{B}_\varphi\mathbf{u}(t), \tag{13}$$

where $\varphi\in\mathbb{I}_{n_r}$ (n_r is the number of linear models), $\mathbf{x}(t)\in\mathbb{R}^{n_x}$ is the state vector, $\mathbf{u}(t)\in\mathbb{R}^{n_u}$ is the input vector, $\mathbf{A}_\varphi\in\mathbb{R}^{n_x\times n_x}$, and $\mathbf{B}_\varphi\in\mathbb{R}^{n_x\times n_u}$. This local models are used by the IF-THEN rules, where the φ-th fuzzy rule R^φ is given by:

$$\begin{aligned}R^\varphi:\ &\text{IF } z_1(t) \text{ is } M_1^\varphi \text{ AND } \cdots \text{ AND } z_{n_z}(t) \text{ is } M_{n_z}^\varphi,\\ &\text{THEN } \dot{\mathbf{x}}(t)=\mathbf{A}_\varphi\mathbf{x}(t)+\mathbf{B}_\varphi\mathbf{u}(t),\end{aligned}$$

such that $\varphi\in\mathbb{I}_{n_r}$; M_j^φ, $j\in\mathbb{I}_{n_z}$ is the j-th fuzzy set of φ-th fuzzy rule, and $z_1(t),\ \cdots,\ z_{n_z}(t)$, are the premise variables.

Define ω^φ the activation level of φ-th implication, $\mu_j^\varphi\left(z_j(t)\right)$ the membership function of the variable $z_j(t)$ to the fuzzy set M_j^φ, and $\mathbf{z}(t)=\left[z_1(t),\, z_2(t),\, \cdots,\, z_{n_z}(t)\right]$:

$$\omega^\varphi(\mathbf{z}(t))=\prod_{j=1}^{n_z}\mu_j^\varphi(z_j(t),$$

where $\mu_j^{\varphi}\left(z_j(t)\right) \geqslant 0$, for $\varphi \in \mathbb{I}_{n_r}$, then

$$\omega^{\varphi}\left(\mathbf{z}(t)\right) \geqslant 0 \text{ and } \sum_{\varphi=1}^{n_r} \omega^{\varphi}\left(\mathbf{z}(t)\right) > 0.$$

Then, the inferred fuzzy model is obtained by the weighted average of the local models described by:

$$\begin{aligned}
\dot{\mathbf{x}}(t) &= \frac{\sum_{\varphi=1}^{n_r} \omega^{\varphi}\left(\mathbf{z}(t)\right)\left(\mathbf{A}_{\varphi}\mathbf{x}(t) + \mathbf{B}_{\varphi}\mathbf{u}(t)\right)}{\sum_{\varphi=1}^{n_r} \omega^{\varphi}\left(\mathbf{z}(t)\right)}, \\
&= \sum_{\varphi=1}^{n_r} \alpha_{\varphi}\left(\mathbf{z}(t)\right)\left(\mathbf{A}_{\varphi}\mathbf{x}(t) + \mathbf{B}_{\varphi}\mathbf{u}(t)\right), \\
&= \left(\sum_{\varphi=1}^{n_r} \alpha_{\varphi}\left(\mathbf{z}(t)\right)\mathbf{A}_{\varphi}\right)\mathbf{x}(t) + \left(\sum_{\varphi=1}^{n_r} \alpha_{\varphi}\left(\mathbf{z}(t)\right)\mathbf{B}_{\varphi}\right)\mathbf{u}(t), \\
&= \mathbf{A}\left(\mathbf{z}(t)\right)\mathbf{x}(t) + \mathbf{B}\left(\mathbf{z}(t)\right)\mathbf{u}(t).
\end{aligned} \tag{14}$$

for $\varphi \in \mathbb{I}_{n_r}$. Thus, the inferred fuzzy model is given by a convex combination of the local models, where

$$\alpha_{\varphi}\left(\mathbf{z}(t)\right) = \frac{\omega^{\varphi}\left(\mathbf{z}(t)\right)}{\sum_{\varphi=1}^{n_r} \omega^{\varphi}\left(\mathbf{z}(t)\right)} \geqslant 0,\ \sum_{\varphi=1}^{n_r} \alpha_{\varphi}\left(\mathbf{z}(t)\right) = 1, \text{ and } \varphi = 1,\ 2,\ \cdots,\ n_r.$$

Therefore, considering the nonlinear system

$$\dot{\mathbf{x}}(t) = \mathbf{A}\left(\mathbf{z}(t)\right)\mathbf{x}(t) + \mathbf{B}\left(\mathbf{z}(t)\right)\mathbf{u}(t), \tag{15}$$

where $\mathbf{x}(t) = [x_1(t) \cdots x_{n_x}(t)]^T \in \mathbb{R}^{n_x}$ is the state vector; $\mathbf{u}(t) = [u_1(t) \cdots u_{n_u}(t)]^T$ is the control signal vector; $\mathbf{z}(t) = \left[\mathbf{x}(t)^T \zeta(t)^T\right]^T \in \mathscr{X} \in \mathbb{R}^{n_z}$, where ζ is the vector of uncertain parameters, $\mathscr{X}$ is a compact set, $n_z = n_x + n_{\zeta}$; $\tilde{f}_{ij}\left(\mathbf{z}(t)\right) : \mathbb{R}^{n_z} \to \mathbb{R}$, and $\tilde{g}_{lk}\left(\mathbf{z}(t)\right) : \mathbb{R}^{n_z} \to \mathbb{R}$ are linear or nonlinear continuous function located in elements (i, j) and (l, k) of matrices $\mathbf{A}(\mathbf{z}(t)) \in \mathbb{R}^{n_x \times n_x}$ and $\mathbf{B}(\mathbf{z}(t)) \in \mathbb{R}^{n_x \times n_u}$, respectively.

The Taniguchi's generalized approach, see Taniguchi et al. (2001), it considers the following variables

$$\begin{aligned}
a_{ij}^1 &\equiv \max_{\mathbf{z}(t) \in \mathscr{X}} \left\{\tilde{f}_{ij}\left(\mathbf{z}(t)\right)\right\}, \quad a_{ij}^2 \equiv \min_{\mathbf{z}(t) \in \mathscr{X}} \left\{\tilde{f}_{ij}\left(\mathbf{z}(t)\right)\right\}, \\
b_{lk}^1 &\equiv \max_{\mathbf{z}(t) \in \mathscr{X}} \left\{\tilde{g}_{lk}\left(\mathbf{z}(t)\right)\right\}, \quad b_{lk}^2 \equiv \min_{\mathbf{z}(t) \in \mathscr{X}} \left\{\tilde{g}_{lk}\left(\mathbf{z}(t)\right)\right\}.
\end{aligned} \tag{16}$$

Therefore, the system representation requires 2^s local models, where s is the number of the distinct terms $\tilde{f}_{ij}$ or $\tilde{g}_{lk}$ in the dynamic (15), which are not constant or depend on uncertain parameters.

The membership functions are used to relate (or combine) the local models describing the nonlinear dynamic.

Consider the generalized system class proposed in (15) and using the variables defined in (16), $\tilde{f}_{ij}(\mathbf{z}(t))$ and $\tilde{g}_{lk}(\mathbf{z}(t))$ can be represented as

$$\tilde{f}_{ij}(\mathbf{z}(t)) = \sum_{t^a_{(i,j)}=1}^{2} \sigma_{ij}^{t^a_{(i,j)}}(\mathbf{z}(t))\, a_{ij}^{t^a_{(i,j)}}, \tag{17}$$

$$\tilde{g}_{lk}(\mathbf{z}(t)) = \sum_{t^b_{(l,k)}=1}^{2} \xi_{lk}^{t^b_{(l,k)}}(\mathbf{z}(t))\, b_{lk}^{t^b_{(l,k)}}. \tag{18}$$

such that $\sigma_{ij}^{t^a_{(i,j)}}(\mathbf{z}(t))$, and $\xi_{lk}^{t^b_{(l,k)}}(\mathbf{z}(t))$ have the following characteristics:

$$\sum_{t^a_{(i,j)}=1}^{2} \sigma_{ij}^{t^a_{(i,j)}}(\mathbf{z}(t)) = 1, \sum_{t^b_{(l,k)}=1}^{2} \xi_{lk}^{t^b_{(l,k)}}(\mathbf{z}(t)) = 1,$$

$$\sigma_{ij}^{1}(\mathbf{z}(t)) = \frac{\tilde{f}_{ij}(\mathbf{z}(t)) - a_{ij}^{2}}{a_{ij}^{1} - a_{ij}^{2}}, \tag{19}$$

$$\sigma_{ij}^{2}(\mathbf{z}(t)) = \frac{a_{ij}^{1} - \tilde{f}_{ij}(\mathbf{z}(t))}{a_{ij}^{1} - a_{ij}^{2}}, \tag{20}$$

$$\xi_{lk}^{1}(\mathbf{z}(t)) = \frac{\tilde{g}_{lk}(\mathbf{z}(t)) - b_{lk}^{2}}{b_{lk}^{1} - b_{lk}^{2}}, \tag{21}$$

$$\xi_{lk}^{2}(\mathbf{z}(t)) = \frac{b_{lk}^{1} - \tilde{g}_{lk}(\mathbf{z}(t))}{b_{lk}^{1} - b_{lk}^{2}}, \tag{22}$$

and the elements $t^a_{(i,j)}$ and $t^b_{(l,k)}$ are related to the maximum and minimum values of the functions $\tilde{f}_{ij}(\mathbf{z}(t))$ and $\tilde{g}_{lk}(\mathbf{z}(t))$ in the considered compact set $\mathscr{X}$. The notation adopted in this study uses the superscript 1 related to the maximum, and superscript 2 to the minimum.

Let the sets of ordered pairs given by $\mathscr{P}_A = \{(i,j)\}$, $i,\ j \in \mathbb{I}_{n_x}$ associated to $\tilde{f}_{ij}(\mathbf{z}(t))$, and $\mathscr{P}_B = \{(l,k)\}$, $l \in \mathbb{I}_{n_x}$, and $k \in \mathbb{I}_{n_u}$ associated to $\tilde{g}_{lk}(\mathbf{z}(t))$. Define the matrices $\mathbb{A}_{ij} \in \mathbb{R}^{n_x \times n_x}$ such that their respective elements (i,j) are equal to 1 and the others ones are 0, and $\mathbb{B}_{lk} \in \mathbb{R}^{n_x \times n_u}$ such that their respective elements (l,k) are equal to 1 and the others ones are 0, see (ALVES, 2017) for more details. Then the system (15) can be rewritten as:

$$\dot{x}(t) = \left(\bar{\mathbb{A}} + \sum_{(i,j)\in\mathscr{P}_A} \tilde{f}_{ij}(\mathbf{z}(t))\,\mathbb{A}_{ij}\right)\mathbf{x}(t) + \left(\bar{\mathbb{B}} + \sum_{(l,k)\in\mathscr{P}_B} \tilde{g}_{lk}(\mathbf{z}(t))\,\mathbb{B}_{lk}\right)\mathbf{u}(t), \tag{23}$$

where $\bar{\mathbb{A}} \in \mathbb{R}^{n_x \times n_x}$ and $\bar{\mathbb{B}} \in \mathbb{R}^{n_x \times n_u}$, matrices whose elements (i,j) and (l,k) are the constant and known elements (independent of $\mathbf{z}(t)$) in $\mathbf{A}(\mathbf{z}(t))$ and $\mathbf{B}(\mathbf{z}(t))$ from (15), or 0 case $(i,j) \in \mathscr{P}_A$ or $(l,k) \in \mathscr{P}_B$, respectively.

From (17)-(22) and (23) one obtains

$$\dot{x}(t) = \left(\bar{\mathbb{A}} + \sum_{(i,j)\in\mathscr{P}_A} \sum_{t^a_{(i,j)}=1}^{2} \sigma_{ij}^{t^a_{(i,j)}}\left(\mathbf{z}(t)\right) a_{ij}^{t^a_{(i,j)}} \mathbb{A}_{ij} \right) \mathbf{x}(t) + \left(\bar{\mathbb{B}} + \sum_{(l,k)\in\mathscr{P}_B} \sum_{t^b_{(l,k)}=1}^{2} \xi_{lk}^{t^b_{(l,k)}}\left(\mathbf{z}(t)\right) b_{lk}^{t^b_{(l,k)}} \mathbb{B}_{lk} \right) \mathbf{u}(t). \quad (24)$$

Defining $\Gamma_{pq}(\mathbf{z}(t)) = \left[\sigma^1_{pq}(\mathbf{z}(t)) + \sigma^2_{pq}(\mathbf{z}(t))\right]$, $\Xi_{rs}(\mathbf{z}(t)) = \left[\xi^1_{rs}(\mathbf{z}(t)) + \xi^2_{rs}(\mathbf{z}(t))\right]$,

$$\hat{\sigma}_{ij} = \prod_{\substack{(p,q)\in\mathscr{P}_A \\ (p,q)\neq(i,j)}} \prod_{(r,s)\in\mathscr{P}_B} \Gamma_{pq}(\mathbf{z}(t))\Xi_{rs}(\mathbf{z}(t)) = 1, \quad (25)$$

$$\hat{\xi}_{ij} = \prod_{(p,q)\in\mathscr{P}_A} \prod_{\substack{(r,s)\in\mathscr{P}_B \\ (r,s)\neq(l,k)}} \Gamma_{pq}(\mathbf{z}(t))\Xi_{rs}(\mathbf{z}(t)) = 1, \quad (26)$$

$$\psi = \prod_{(p,q)\in\mathscr{P}_A} \prod_{(r,s)\in\mathscr{P}_B} \Gamma_{pq}(\mathbf{z}(t))\Xi_{rs}(\mathbf{z}(t)) = 1. \quad (27)$$

Given (24) and (25)-(27), one can obtain

$$\dot{\mathbf{x}}(t) = \left(\psi\bar{\mathbb{A}} + \sum_{(i,j)\in\mathscr{P}_A} \hat{\sigma}_{ij} \sum_{t^a_{(i,j)}=1}^{2} \sigma_{ij}^{t^a_{(i,j)}}(\mathbf{z}(t)) a_{ij}^{t^a_{(i,j)}} \mathbb{A}_{ij} \right) \mathbf{x}(t) + \left(\psi\bar{\mathbb{B}} + \sum_{(l,k)\in\mathscr{P}_B} \hat{\xi}_{lk} \sum_{t^b_{(l,k)}=1}^{2} \xi_{lk}^{t^b_{(l,k)}}(\mathbf{z}(t)) b_{lk}^{t^b_{(l,k)}} \mathbb{B}_{lk} \right) \mathbf{u}(t). \quad (28)$$

Note that in (28) it appears all the combinations of $\prod_{(i,j)\in\mathscr{P}_A} \prod_{(l,k)\in\mathscr{P}_B} \sigma_{ij}^{t^a_{(i,j)}}\left(\mathbf{z}(t)\right) \xi_{lk}^{t^a_{(l,k)}}\left(\mathbf{z}(t)\right)$. In order to make change of variables, consider the bijections of counting $c_A : \mathscr{P}_A \to \mathbb{I}_{n_A}$ and $c_B : \mathscr{P}_B \to \mathbb{I}_{n_B}$, where n_A and n_B are the numbers of elements $\tilde{f}_{ij}\left(\mathbf{z}(t)\right)$ and $\tilde{g}_{lk}\left(\mathbf{z}(t)\right)$ in (15), respectively, which are continuous functions of $\mathbf{z}(t)$.

In addition, the local model index φ is a function of the values t^a_{ij} and t^b_{lk}, defined by

$$\varphi = 1 + \sum_{(i,j)\in\mathscr{P}_A} 2^{(c_A(i,j)-1)} \left(t^a_{(i,j)} - 1\right) + 2^{n_A} \sum_{(l,k)\in\mathscr{P}_B} 2^{(c_B(l,k)-1)} \left(t^b_{(l,k)} - 1\right), \quad (29)$$

and more details can be found at (ALVES, 2017).

Therefore, to describe (28) as (14), consider the index φ and the values of t^a_{ij} and t^b_{lk}, thus

$$\alpha_\varphi(\mathbf{z}(t)) = \prod_{(i,j)\in\mathscr{P}_A} \prod_{(l,k)\in\mathscr{P}_B} \sigma_{ij}^{t^a_{(i,j)}}\left(\mathbf{z}(t)\right) \xi_{lk}^{t^b_{(l,k)}}\left(\mathbf{z}(t)\right), \quad (30)$$

$$\mathbf{A}_{\varphi} = \bar{\mathbb{A}} + \sum_{(i,j)\in\mathscr{P}_A} a_{ij}^{t^a_{(i,j)}} \mathbb{A}_{ij}, \tag{31}$$

$$\mathbf{B}_{\varphi} = \bar{\mathbb{B}} + \sum_{(l,k)\in\mathscr{P}_B} b_{lk}^{t^b_{(l,k)}} \mathbb{B}_{lk}, \tag{32}$$

from (17)-(22), $\sigma_{ij}^{t^a_{(i,j)}}(\mathbf{z}(t)) \geqslant 0$ and $\xi_{lk}^{t^b_{(l,k)}}(\mathbf{z}(t)) \geqslant 0$, therefore $\alpha_{\varphi}(\mathbf{z}(t)) \geqslant 0$ and from (25)-(27)

$$\sum_{\varphi=1}^{2^{(n_A+n_B)}} \alpha_{\varphi}(\mathbf{z}(t)) = \psi = 1.$$

3.2.2 TS fuzzy representation of the knee joint

To find the local models, the maximum and minimum values of the function $f_{21}(z)$, $f_{23}(z)$, and $g_{31}(z)$ must be obtained.

Then, suppose that the operation region is defined in the interval $\frac{\pi}{18} \leqslant \check{x}_1(t) \leqslant \frac{\pi}{2}$, desired position belongs to set $\theta^d \in [\pi/6 \quad \pi/3]$, and the uncertain parameters $\hat{G} \in [0.9G_n \quad G_n]$, $\kappa_{stf} \in [0.1 \quad 1]$, and $\kappa_{flt} \in [0.8 \quad 1]$.

Assuming the following set:

$$\mathbb{D} = \Big\{ z \in \mathbb{R}^4 : -\frac{5\pi}{18} \leqslant x_1 \leqslant \frac{\pi}{3}, \quad -5 \leqslant x_3 \leqslant 5, \quad 0.9G_n \leqslant \hat{G} \leqslant G_n, \quad 0.1 \leqslant \kappa_{stf} \leqslant 1,$$
$$0.8 \leqslant \kappa_{flt} \leqslant 1, \quad \frac{\pi}{6} \leqslant \theta^d \leqslant \frac{\pi}{3} \Big\}. \tag{33}$$

Thus, considering the paraplegic subject P1, the minimum and maximum values of nonlinear functions are:

$$a_{21}^1 \equiv \max\{f_{21}(\mathbf{z}(t))\} = -0.2117, a_{21}^2 \equiv \min\{f_{21}(\mathbf{z}(t))\} = -44.3100,$$

$$a_{23}^1 \equiv \max\{f_{23}(\mathbf{z}(t))\} = 2.7624, a_{23}^2 \equiv \min\{f_{23}(\mathbf{z}(t))\} = 0.2762,$$

$$b_{31}^1 \equiv \max\{g_{31}(\mathbf{z}(t))\} = 297.9320 \times 10^4, b_{31}^2 \equiv \min\{g_{31}(\mathbf{z}(t))\} = 214.5110 \times 10^4.$$

From (19)-(22) one obtains, respectively:

$$\sigma_{21}^1(\mathbf{z}(t)) = \frac{f_{21}(\mathbf{z}(t)) - a_{21}^2}{a_{21}^1 - a_{21}^2}, \sigma_{21}^2(\mathbf{z}(t)) = \frac{a_{21}^1 - f_{21}(\mathbf{z}(t))}{a_{21}^1 - a_{21}^2},$$

$$\sigma_{23}^1(\mathbf{z}(t)) = \frac{f_{23}(\mathbf{z}(t)) - a_{23}^2}{a_{23}^1 - a_{23}^2}, \sigma_{23}^2(\mathbf{z}(t)) = \frac{a_{23}^1 - f_{23}(\mathbf{z}(t))}{a_{23}^1 - a_{23}^2},$$

$$\xi_{31}^1(\mathbf{z}(t)) = \frac{g_{31}(\mathbf{z}(t)) - b_{31}^2}{b_{31}^1 - b_{31}^2}, \xi_{31}^2(\mathbf{z}(t)) = \frac{b_{31}^1 - g_{31}(\mathbf{z}(t))}{b_{31}^1 - b_{31}^2}.$$

The nonlinear function $f_{21}(\mathbf{z}(t))$ can be represented by a TS fuzzy model, considering two local models: a^1_{21} and a^2_{21}, that is, according to (17) exist $\sigma^1_{21}(\mathbf{z}(t))$ and $\sigma^2_{21}(\mathbf{z}(t))$ such that,

$$f_{21}(\mathbf{z}(t)) = \sigma^1_{21}(\mathbf{z}(t))a^1_{21} + \sigma^2_{21}(\mathbf{z}(t))a^2_{21}, \sum_{t^a_{(i,j)}=1}^{2} \sigma^{t^a_{(i,j)}}_{21}(\mathbf{z}(t)) = 1, \text{ and } 0 \leqslant \sigma^{t^a_{(i,j)}}_{21}(\mathbf{z}(t)) \leqslant 1.$$

Similarly, the function $f_{23}(\mathbf{z}(t))$ can be represented by:

$$f_{23}(\mathbf{z}(t)) = \sigma^1_{23}(\mathbf{z}(t))a^1_{23} + \sigma^2_{23}(\mathbf{z}(t))a^2_{23}, \sum_{t^a_{(i,j)}=1}^{2} \sigma^{t^a_{(i,j)}}_{23}(\mathbf{z}(t)) = 1, \text{ and } 0 \leqslant \sigma^{t^a_{(i,j)}}_{23}(\mathbf{z}(t)) \leqslant 1.$$

Likewise, from (18) the function $g_{31}(\mathbf{z}(t))$ can be represented by:

$$g_{31}(\mathbf{z}(t)) = \xi^1_{31}(\mathbf{z}(t))b^1_{31} + \xi^2_{31}(\mathbf{z}(t))_{31}b^2_{31}, \sum_{t^b_{(i,j)}=1}^{2} \xi^{t^b_{(i,j)}}_{31}(\mathbf{z}(t)) = 1, \text{ and } 0 \leqslant \xi^{t^b_{(i,j)}}_{31}(\mathbf{z}(t)) \leqslant 1.$$

Considering the dynamic expressed in (9), note the following sets of ordered pairs $\mathscr{P}_A = \{(2,3),(2,1)\}$ and $\mathscr{P}_B = \{(3,1)\}$. Therefore, $n_A = 2$, $n_B = 1$, and counting bijections are defined as $c_A(2,3) = 1$, $c_A(2,1) = 2$, and $c_B(3,1) = 1$. From (29) obtains the index φ for changing combinations of variable given by $t^a_{(i,j)}$, $t^b_{(l,k)}$ and expressed by

$$\varphi = 2^{n_B} \sum_{(i,j)\in\mathscr{P}_A} 2^{(c_A(i,j)-1)}\left(t^a_{(i,j)} - 1\right) + \sum_{(l,k)\in\mathscr{P}_B} 2^{(c_B(l,k)-1)}\left(t^b_{(l,k)} - 1\right) + 1,$$

$$\varphi = 4\left(t^a_{(2,1)} - 1\right) + 2\left(t^a_{(2,3)} - 1\right) + \left(t^b_{(3,1)} - 1\right) + 1. \tag{34}$$

From (30) and (34) obtains the membership functions

$$\begin{cases} \alpha_1(\mathbf{z}(t)) = \sigma^1_{21}(\mathbf{z}(t))\sigma^1_{23}(\mathbf{z}(t))\xi^1_{31}(\mathbf{z}(t)), \\ \alpha_2(\mathbf{z}(t)) = \sigma^1_{21}(\mathbf{z}(t))\sigma^1_{23}(\mathbf{z}(t))\xi^2_{31}(\mathbf{z}(t)), \\ \alpha_3(\mathbf{z}(t)) = \sigma^1_{21}(\mathbf{z}(t))\sigma^2_{23}(\mathbf{z}(t))\xi^1_{31}(\mathbf{z}(t)), \\ \alpha_4(\mathbf{z}(t)) = \sigma^1_{21}(\mathbf{z}(t))\sigma^2_{23}(\mathbf{z}(t))\xi^2_{31}(\mathbf{z}(t)), \\ \alpha_5(\mathbf{z}(t)) = \sigma^2_{21}(\mathbf{z}(t))\sigma^1_{23}(\mathbf{z}(t))\xi^1_{31}(\mathbf{z}(t)), \\ \alpha_6(\mathbf{z}(t)) = \sigma^2_{21}(\mathbf{z}(t))\sigma^1_{23}(\mathbf{z}(t))\xi^2_{31}(\mathbf{z}(t)), \\ \alpha_7(\mathbf{z}(t)) = \sigma^2_{21}(\mathbf{z}(t))\sigma^2_{23}(\mathbf{z}(t))\xi^1_{31}(\mathbf{z}(t)), \\ \alpha_8(\mathbf{z}(t)) = \sigma^2_{21}(\mathbf{z}(t))\sigma^2_{23}(\mathbf{z}(t))\xi^2_{31}(\mathbf{z}(t)), \end{cases} \tag{35}$$

satisfying to $\sum_{\varphi=1}^{8} \alpha_\varphi(\mathbf{z}(t)) = 1$.

Table 8 - Parameters of the TS fuzzy local models for healthy and paraplegic individuals.

Subject	a_{21}^1	a_{21}^2	a_{23}^1	a_{23}^2	b_{31}^1	b_{31}^2
H1	-19.3868	-30.5984	2.6525	0.2653	587.3715	422.9075
H2	-11.1563	-41.8621	2.7933	0.27933	625.9781	450.7042
H3	-10.2394	-35.1688	2.5063	0.25063	522.7427	376.3747
H4	-4.7823	-32.8802	2.6667	0.2667	656.8144	472.9064
H5	-13.7400	-37.1348	2.6042	0.2604	761.0350	547.9452
P1	-0.2117	-44.3100	2.7624	0.2762	297.9320	214.5110
P2	-0.0745	-29.0451	3.4247	0.3425	410.5090	295.5665
P3	-0.6219	-40.0962	2.5381	0.2538	356.5891	256.7442

Source: From author.

The dynamic (9) can be described by a convex combination (35) of TS fuzzy local models as expressed in (14). The local models are obtained from (31)-(32), considering $\varphi \in \mathbb{I}_8$. In such a way that from (31) one obtains

$$
\begin{aligned}
\mathbf{A}_1 = \mathbf{A}_2 &= \bar{\mathbb{A}} + a_{21}^1 \mathbb{A}_{21} + a_{23}^1 \mathbb{A}_{23}, \\
\mathbf{A}_3 = \mathbf{A}_4 &= \bar{\mathbb{A}} + a_{21}^1 \mathbb{A}_{21} + a_{23}^2 \mathbb{A}_{23}, \\
\mathbf{A}_5 = \mathbf{A}_6 &= \bar{\mathbb{A}} + a_{21}^2 \mathbb{A}_{21} + a_{23}^1 \mathbb{A}_{23}, \\
\mathbf{A}_7 = \mathbf{A}_8 &= \bar{\mathbb{A}} + a_{21}^2 \mathbb{A}_{21} + a_{23}^2 \mathbb{A}_{23}, \\
\mathbf{B}_1 = \mathbf{B}_3 = \mathbf{B}_5 = \mathbf{B}_7 &= \bar{\mathbb{B}} + b_{31}^1 \mathbb{B}_{31}, \\
\mathbf{B}_2 = \mathbf{B}_4 = \mathbf{B}_6 = \mathbf{B}_8 &= \bar{\mathbb{B}} + b_{31}^2 \mathbb{B}_{31},
\end{aligned}
$$

where the matrices $\bar{\mathbb{A}}$ and $\bar{\mathbb{B}}$ respectively are composed by constant and known elements of the state matrix and control-input matrix and assigning null value to the remaining elements, and the matrices $\mathbb{A}_{31}$, $\mathbb{A}_{23}$, and $\mathbb{B}_{31}$ are expressed as

$$
\bar{\mathbb{A}} = \begin{bmatrix} 0 & 1 & 0 \\ 0 & -0.7459 & 0 \\ 0 & 0 & -1.0515 \end{bmatrix}, \bar{\mathbb{B}} = \begin{bmatrix} 0 \\ 0 \\ 0 \end{bmatrix}, \mathbb{A}_{31} = \begin{bmatrix} 0 & 0 & 0 \\ 1 & 0 & 0 \\ 0 & 0 & 0 \end{bmatrix}, \mathbb{A}_{23} = \begin{bmatrix} 0 & 0 & 0 \\ 0 & 0 & 1 \\ 0 & 0 & 0 \end{bmatrix}, \mathbb{B}_{31} = \begin{bmatrix} 0 \\ 0 \\ 1 \end{bmatrix}.
$$

Observe that the system (9) has three uncertain nonlinear functions $f_{21}(\mathbf{z}(t))$, $f_{23}(\mathbf{z}(t))$, and $g_{31}(\mathbf{z}(t))$. Consequently, one obtains $n_r = 2^3 = 8$ local models for exact representation of the system through TS fuzzy models, being

$$
\mathbf{A}_1=\mathbf{A}_2=\begin{bmatrix}0 & 1 & 0\\ -0.21172 & -0.74586 & 2.7624\\ 0 & 0 & -1.0515\end{bmatrix}, \mathbf{A}_3=\mathbf{A}_4=\begin{bmatrix}0 & 1 & 0\\ -0.21172 & -0.74586 & 0.27624\\ 0 & 0 & -1.0515\end{bmatrix},
$$
$$
\mathbf{A}_5=\mathbf{A}_6=\begin{bmatrix}0 & 1 & 0\\ -44.3100 & -0.74586 & 2.7624\\ 0 & 0 & -1.0515\end{bmatrix}, \mathbf{A}_7=\mathbf{A}_8=\begin{bmatrix}0 & 1 & 0\\ -44.31 & -0.74586 & 0.27624\\ 0 & 0 & -1.0515\end{bmatrix},
$$
$$
\mathbf{B}_1=\mathbf{B}_3=\mathbf{B}_5=\mathbf{B}_7=\begin{bmatrix}0\\ 0\\ 297.932\end{bmatrix}, \mathbf{B}_2=\mathbf{B}_4=\mathbf{B}_6=\mathbf{B}_8=\begin{bmatrix}0\\ 0\\ 214.511\end{bmatrix}. \tag{36}
$$

In the next section will show the switched control design subject to saturation and determine the gains through LMIs conditions.

3.3 Switched control design subject to actuator saturation

Consider a nonlinear system subject to actuator saturation described by the following TS fuzzy model

$$
\dot{\mathbf{x}}=\mathbf{A}(\alpha)\mathbf{x}(t)+\mathbf{B}(\alpha)\mathrm{sat}(\mathbf{u}(t))+\mathbf{B}(\alpha)d(t), \tag{37}
$$

where $\mathbf{A}(\alpha)$ defined in (14), $\mathbf{B}(\alpha)=\mathbf{B}_0 g(\alpha)$, $g(\alpha)\geqslant 0$, for all α,

$$
\mathrm{sat}(\mathbf{u}(t))=\left[\mathrm{sat}\left(u_{(1)}(t)\right)\cdots\mathrm{sat}\left(u_{(n_u)}(t)\right)\right]^T,
$$
$$
\mathrm{sat}\left(u_{(l)}(t)\right)=\mathrm{sgn}\left(u_{(l)}(t)\right)\min\left\{\rho_{(l)},|u_{(l)}(t)|\right\}, \tag{38}
$$

$\forall l\in\mathbb{I}_{n_u}$, $\vartheta_1\leqslant d(t)\leqslant\vartheta_2$, $\rho_{(l)}$ are the actuator saturation values.

We propose the application of the switched control law subject to saturation. The proposed procedure uses an switching index ς, as described in (40), which it selects a state-feedback controller gain belonging to the set $\left\{\mathbf{K}_i\in\mathbb{R}^{n_u\times n_x},\ i\in\mathbb{I}_{n_r}\right\}$, and an index ψ that compensates uncertainty in the signal control, as defined in (41). The index ς is determined by auxiliary symmetric matrices $\mathbf{Q}_j$. The control law is defined as follows

$$
\mathbf{u}(t)=\mathrm{sat}_0\left(\mathbf{u}_\varsigma(t)\right)-\vartheta_\psi(t), \tag{39}
$$
$$
\mathbf{u}_\varsigma(t)=-\mathbf{K}_\varsigma\mathbf{x}(t),\ \varsigma=\arg^*\min_{i\in\mathbb{I}_{n_r}}\left\{\mathbf{x}^T(t)\mathbf{Q}_j\mathbf{x}(t)\right\},\ \varsigma,\,j\in\mathbb{I}_{n_r}, \tag{40}
$$
$$
\psi=\arg^*\min_{m\in\mathbb{I}_2}\left\{-\mathbf{x}^T\mathbf{P}\mathbf{B}_0\vartheta_m\right\}, \tag{41}
$$

where $\text{sat}_0\left(\mathbf{u}_\varsigma(t)\right) = \left[\text{sat}_0\left(u_{\varsigma(1)}(t)\right)\cdots\text{sat}_0\left(u_{\varsigma(n_u)}(t)\right)\right]^T$, and

$$\text{sat}_0\left(u_{\varsigma(l)}(t)\right) = \text{sgn}\left(u_{\varsigma(l)}(t)\right)\min\left\{\rho_{0(l)}, |u_{\varsigma(l)}(t)|\right\}, \tag{42}$$

being $\rho_{0(l)} = \rho_{(l)} - \max\limits_{m\in\mathbb{I}_2}\{|\vartheta_m|\}$, $\forall l \in \mathbb{I}_{n_u}$, $m \in \mathbb{I}_2$, and ϑ_m, ρ, ρ_0, $\mathbf{B}_0$ will be defined later. The state-feedback matrices $\mathbf{K}_\varsigma$ and decision matrices $\mathbf{Q}_j$ will be obtained in the design procedure, ensuring the local stability of the system (37)-(42) and with decay rate.

The TS fuzzy representation of a nonlinear system is adequate in a bounded domain of validity (KLUG et al., 2015). A low performance or system instability may occur when the state trajectories do not belong to the validity domain of the model. The domain of validity can be represented by a polyhedral set

$$\mathscr{O} \triangleq \left\{\mathbf{x}(t) \in \mathbb{R}^{n_x} : \left|\mathbf{N}_{(h)}\mathbf{x}(t)\right| \leqslant \phi_{(h)},\ h \in \mathbb{I}_p\right\}, \tag{43}$$

where $\mathbf{N} = \begin{bmatrix}\mathbf{N}_{(1)}^T & \mathbf{N}_{(2)}^T\cdots\mathbf{N}_{(p)}^T\end{bmatrix}^T \in \mathbb{R}^{p\times n_x}$ and $\phi = \begin{bmatrix}\phi_{(1)} & \phi_{(2)}\cdots\phi_{(p)}\end{bmatrix}^T \in \mathbb{R}^p$ are known.

In addition, considering the quadratic Lyapunov function $V(\mathbf{x}) = \mathbf{x}^T\mathbf{P}\mathbf{x}$, denote the ellipsoid $\mathscr{E}(\mathbf{P},\delta)$, and the constant $\delta > 0$ as:

$$\mathscr{E}(\mathbf{P},\delta) = \{\mathbf{x}(t) \in \mathbb{R}^{n_x} : \mathbf{x}(t)^T\mathbf{P}\mathbf{x}(t) \leqslant \delta\}. \tag{44}$$

An invariant region for the operation of the system is considered. Then the system state, initiated with an initial condition in a suitable region within an operating region, will remain in this region for all $t \geqslant 0$. In other words, determining an invariant region, say $\mathscr{E} \subset \mathscr{O}$, $\forall\mathbf{x}(0) \in \mathscr{E}$, the state vector $\mathbf{x}(t)$ of (37) remains in the operating region $\mathscr{O}$, $\forall t \geqslant 0$. Consequently, (14) exactly represents the system (37) for $t \geqslant 0$, and for all $\mathbf{x}(0) \in \mathscr{E}$, following the procedure described in the Subsection 3.2.1.

Lemma 1. *(KLUG et al., 2015; ALVES et al., 2016) Consider a nonlinear system described by* (15) *and an operation region $\mathbf{x}(t) \in \mathscr{O}$, for $t \geqslant 0$, given in* (43)*. Assume that there exist a symmetric positive definite matrix $\mathbf{X} \in \mathbb{R}^{n_x\times n_x}$, such that*

$$\begin{bmatrix}\phi_{(h)}^2 & \mathbf{N}_{(h)}\mathbf{X} \\ \star & \mathbf{X}\end{bmatrix} \geqslant \mathbf{0}, \tag{45}$$

hold for all i and $h \in \mathbb{I}_p$. Therefore, if $\mathbf{x}(0) \in \mathscr{E}(\mathbf{P},1)$, given in (44)*, where $\mathbf{P} = \mathbf{X}^{-1}$, then $\mathbf{x}(t) \in \mathscr{O}$, $t \geqslant 0$.*

Proof. More details are in Klug et al. (2015), Alves et al. (2016). □

Let the polyhedral set $\mathscr{L}(\mathbf{H}_k)$

$$\mathscr{L}(\mathbf{H}_k) := \left\{\mathbf{x}(t) \in \mathbb{R}^{n_x} : \left|\mathbf{H}_{k(l)}\mathbf{x}(t)\right| \leqslant \rho_{(l)},\ k \in \mathbb{I}_{n_r},\ \text{and } l \in \mathbb{I}_{n_u}\right\}, \tag{46}$$

where $\mathbf{H}_k = \left[\mathbf{H}_{k(1)}^T \cdots \mathbf{H}_{k(n_u)}^T\right] \in \mathbf{R}^{n_u \times n_x}$ and $\phi = \left[\rho_{(1)} \cdots \rho_{(n_u)}\right]^T \in \mathbb{R}^{n_u}$, $\rho_{(l)} > 0$ are known vectors.

Consider the set $\mathscr{D}_{n_u}$ composed of 2^{n_u} diagonal matrices $\mathbf{D}_s \in \mathbb{R}^{n_u \times n_u}$, $s \in \mathbb{I}_{2^{n_u}}$, whose diagonal elements are either 1 or 0. For any $\mathbf{D}_s \in \mathscr{D}_{n_u}$, consider that $\mathbf{D}_s^- = \mathbf{I}_{n_u} - \mathbf{D}_s$.

Now, define a function $q_{n_u} : \mathbb{I}_{2^{n_u}} \to \mathbb{I}_{2^{n_u-1}}$ as follows:

$$\begin{cases} q_{n_u}(i_s) = q_{n_u}(i_s - 1) + 1, & \mathbf{D}_{i_s} + \mathbf{D}_{j_s} \neq \mathbf{I}_{n_u},\ \forall j_s \in \mathbb{I}_{i_s},\ i_s \in \mathbb{I}_{2^{n_u}}, \\ q_{n_u}(i_s) = q_{n_u}(i_s), & \mathbf{D}_{i_s} + \mathbf{D}_{j_s} = \mathbf{I}_{n_u},\ \exists j_s \in \mathbb{I}_{i_s},\ i_s \in \mathbb{I}_{2^{n_u}}. \end{cases} \tag{47}$$

This function will be useful for convex hull representation of saturation nonlinearity. In this chapter, we adopted the saturation representation provided by Zhou (2013).

Lemma 2. *(ZHOU, 2013) Let $n_u \geqslant 1$ be a given integer and $\check{\mathbf{v}} \in \mathbb{R}^{\overset{\rightleftharpoons}{n}_u}$ be such that $\|\check{\mathbf{v}}\|_\infty \leqslant 1$. Let the elements in $\mathscr{D}_{n_u}$ be labeled as $\mathbf{D}_s$, $s \in \mathbb{I}_{2^{n_u}}$ and the vector $\mathbf{sl}_{2^{n_u-1},\, q_{n_u}(i_s)}$, $i_s \in \mathbb{I}_{2^{n_u}}$, where the function $q_{n_u}(i_s)$ be defined in* (47). *Then, for any $\mathbf{u} \in \mathbb{R}^{n_u}$, there holds*

$$sat(\mathbf{u}) \in co\left\{\mathbf{D}_s\mathbf{u} + \check{\mathbf{D}}_s^-\check{\mathbf{v}}\right\},\ s \in \mathbb{I}_{2^{n_u}}, \tag{48a}$$

where $\check{\mathbf{D}}_s \in \mathbb{R}^{n_u \times \overset{\rightleftharpoons}{n}_u}$, defined as

$$\check{\mathbf{D}}_s = \mathbf{sl}_{2^{n_u-1},\, q_{n_u}(i_s)} \otimes \mathbf{D}_s^-,\ \forall s, i_s \in \mathbb{I}_{2^{n_u}}. \tag{48b}$$

Proof. Further details can be found at Zhou (2013). □

Remark 1. *Note that Lemma 2 is less conservative than (HU; LIN; CHEN, 2002), because it contains $\overset{\rightleftharpoons}{n}_u = n_u 2^{n_u-1}$ slack variables for representation of the convex hull. For example, if $n_u = 2$, then $\overset{\rightleftharpoons}{n}_u = 4$, $\mathbf{D}_s$, $s \in \mathbb{I}_{2^{n_u}}$ are the matrices as follows:*

$$\mathscr{D}_2 = \{\mathbf{D}_1,\ \mathbf{D}_2,\ \mathbf{D}_3,\ \mathbf{D}_4\},$$
$$\mathscr{D}_2 = \left\{\begin{bmatrix}1 & 0\\0 & 1\end{bmatrix}, \begin{bmatrix}1 & 0\\0 & 0\end{bmatrix}, \begin{bmatrix}0 & 0\\0 & 1\end{bmatrix}, \begin{bmatrix}0 & 0\\0 & 0\end{bmatrix}\right\}.$$

From (47)*, adopting $q_2(0) = 0$, the associated function to elements of the set $\mathscr{D}_2$ is expressed as $q_2(1) = 1$, $q_2(2) = 2$, $q_2(3) = q_2(2) = 2$, and $q_2(4) = q_2(1) = 1$. Consequently, the row vectors are $\mathbf{sl}_{2,\, q_2(1)} = [1 \quad 0]$, $\mathbf{sl}_{2,\, q_2(2)} = [0 \quad 1]$, $\mathbf{sl}_{2,\, q_2(3)} = [0 \quad 1]$, and $\mathbf{sl}_{2,\, q_2(4)} = [1 \quad 0]$.*

From (48b) *one obtains:*

$$\breve{\mathbf{D}}_s^- = \mathbf{sl}_{2,\,q_2(i_s)} \otimes \mathbf{D}_s^-,\ \forall s, i_s \in \mathbb{I}_4,$$

$$\breve{\mathscr{D}}_2^- = \left\{\breve{\mathbf{D}}_1^-, \breve{\mathbf{D}}_2^-, \breve{\mathbf{D}}_3^-, \breve{\mathbf{D}}_4^-\right\},$$
$$\breve{\mathscr{D}}_2^- = \left\{ \begin{bmatrix} 0 & 0 & 0 & 0 \\ 0 & 0 & 0 & 0 \end{bmatrix}, \begin{bmatrix} 0 & 0 & 0 & 0 \\ 0 & 0 & 0 & 1 \end{bmatrix}, \begin{bmatrix} 0 & 0 & 1 & 0 \\ 0 & 0 & 0 & 0 \end{bmatrix}, \begin{bmatrix} 1 & 0 & 0 & 0 \\ 0 & 1 & 0 & 0 \end{bmatrix} \right\}.$$

Thus, (48a) *can be written as:*

$$sat(\mathbf{u}) \in co \left\{ \begin{bmatrix} u_1 \\ u_2 \end{bmatrix}, \begin{bmatrix} u_1 \\ \breve{v}_4 \end{bmatrix}, \begin{bmatrix} \breve{v}_3 \\ u_2 \end{bmatrix}, \begin{bmatrix} \breve{v}_1 \\ \breve{v}_2 \end{bmatrix} \right\}.$$

Note that the variables $\breve{v}_3$ and $\breve{v}_4$ do not appear in the switched control design proposed by Alves et al. (2016), Oliveira et al. (2017).

Remark 2. *If $\mathbf{x}(t) \in \mathscr{L}_k$ defined in* (46)*, $k \in \mathbb{I}_{n_r}$, then $\mathbf{x}(t) \in \mathscr{L}_\varsigma$ and $sat(\mathbf{u})$ can be rewritten as*

$$sat(\mathbf{u}) = \sum_{s=1}^{2^{n_u}} \lambda_s \left[\mathbf{D}_s(\mathbf{u}) + \breve{\mathbf{D}}_s^-(\breve{\mathbf{v}})\right], \tag{49}$$

where $\varsigma \in \mathbb{I}_{n_r}$, $\mathbf{D}_s \in \mathscr{D}$, $\breve{\mathbf{D}}_s \in \breve{\mathscr{D}}$, $\breve{\mathbf{D}}_s^- = \mathbf{I} - \breve{\mathbf{D}}_s$, $s \in \mathbb{I}_{2^{n_u}}$, and $\lambda_s \geqslant 0$, $\sum_{s=1}^{2^{n_u}} \lambda_s = 1$.

Considering (42)*, $\rho_{0(l)} = \rho_{(l)} - \max_{m \in \mathbb{I}_2}\left\{\left|\vartheta_{m(l)}\right|\right\}$, from* (39) *each element $u_{(l)}(t)$ of the control vector $\mathbf{u}(t) = \left[u_{(1)}(t)\ u_{(2)}(t)\ \cdots\ u_{(n_u)(t)}\right]^T$ one obtains*

$$\left|u_{(l)}(t)\right| = \left|sat_0\left(u_{\varsigma(l)}(t)\right) - \vartheta_{\psi(l)}\right| \leqslant \left|sat_0\left(u_{\varsigma(l)}(t)\right)\right| + \left|\vartheta_{\psi(l)}\right| \leqslant \rho_{0(l)} + \max_{m \in \mathbb{I}_2}\left\{\vartheta_{m(l)}\right\}.$$

$$\rho_{0(l)} + \max_{m \in \mathbb{I}_2}\left\{\vartheta_{m(l)}\right\} = \rho_{(l)} + \max_{m \in \mathbb{I}_2}\left\{\left|\vartheta_{m(l)}\right|\right\} - \max_{m \in \mathbb{I}_2}\left\{\left|\vartheta_{m(l)}\right|\right\} = \rho_{(l)},$$

therefore $sat\left(u_{(l)}(t)\right) = sat_0\left(u_{\varsigma(l)}(t)\right) - \vartheta_{\psi(l)}$, and $sat(\mathbf{u}(t)) = sat_0\left(\mathbf{u}_\varsigma(t)\right) - \vartheta_\psi$.

Similarly to (49)*, if $\mathbf{x}(t) \in \mathscr{L}_k$, $k \in \mathbb{I}_{n_r}$, then $\mathbf{x}(t) \in \mathscr{L}_\varsigma$ and $sat_0\left(-\mathbf{K}_\varsigma \mathbf{x}\right)$ one obtains*

$$sat_0\left(-\mathbf{K}_\varsigma \mathbf{x}\right) = \sum_{s=1}^{2^{n_u}} \lambda_s \left[\mathbf{D}_s\left(-\mathbf{K}_\varsigma \mathbf{x}\right) + \breve{\mathbf{D}}_s^-\left(\mathbf{H}_\varsigma \mathbf{x}\right)\right]. \tag{50}$$

The following lemma provides a sufficient condition for the constraint $\mathscr{E}(\mathbf{P}, \delta) \subset \mathscr{L}(\mathbf{H}_k)$.

Lemma 3. *(HU; LIN; CHEN, 2002; ALVES et al., 2016) Let the sets $\mathscr{E}(\mathbf{P}, \delta)$ and $\mathscr{L}(\mathbf{H}_k)$, the constraint $\mathscr{E}(\mathbf{P}, \delta) \subset \mathscr{L}(\mathbf{H}_k)$ is enforced if the LMIs*

$$\begin{bmatrix} \rho_{0(l)}^2 \delta^{-1} & \mathbf{G}_{k(l)} \\ \star & \mathbf{X} \end{bmatrix} \geqslant 0, \tag{51}$$

holds for all $k \in \mathbb{I}_{n_r}$*, and* $l \in \mathbb{I}_{n_u}$ *hold, where* $\mathbf{X} = \mathbf{P}^{-1}$ *and* $\mathbf{G}_{k(l)} = \mathbf{H}_{k(l)}\mathbf{X}$*.*

Proof. See Hu, Lin and Chen (2002), Alves et al. (2016). □

With all ellipsoids satisfying the invariance condition, a less conservative choice of the largest ellipsoid inside the domain of attraction can be guaranteed taking its shape into consideration. Let $\mathscr{W}_r \subset \mathbb{R}^{n_x}$

$$\mathscr{W}_r = \mathrm{co}\left\{\mathbf{w}_0^1,\ \mathbf{w}_0^2, \cdots, \mathbf{w}_0^q\right\}, \tag{52}$$

where $\mathbf{w}_0^{i_w} \in \mathbb{R}^{n_x}$, $\forall i_w \in \mathbb{I}_q$ are *a priori* given points. A guarantee that a convex hull is contained in the invariant region $\mathscr{E}(\mathbf{P}, 1)$ is described in the Lemma 4.

Lemma 4. *The constraint* $\bar{\omega}\, \mathscr{W}_r \subset \mathscr{E}(\mathbf{P},1)$*, where* $\mathscr{W}_r = co\left\{\mathbf{w}_0^1, \mathbf{w}_0^2, \cdots, \mathbf{w}_0^q\right\}$*,* $\mathbf{w}_0^{i_w} \in \mathbb{R}^n$ *for all* $i_w \in I_q$*, is the convex hull of known vectors* $\mathbf{w}_0^1$*,* $\mathbf{w}_0^2$*,* $\cdots$*,* $\mathbf{w}_0^q$*, and the constant* $\bar{\omega} > 0$*, is enforced if*

$$\begin{bmatrix} \bar{\omega}^{-2} & \star \\ \mathbf{w}_0^{i_w} & \mathbf{X} \end{bmatrix} \geqslant \mathbf{0}, \tag{53}$$

holds for all $i_w \in \mathbb{I}_q$*. Thus,* $\bar{\omega}$ *can be used as a variable to obtain a less conservative estimate of the domain of attraction and to search the 'largest' ellipsoid* $\mathscr{E}(\mathbf{P},1)$*.*

Proof. See Hu, Lin and Chen (2002), Cao and Lin (2003). □

On the other hand, constraints may adopted to avoid that controller assume large norm, e.g., using the Lemma 5.

Lemma 5. *(HU; LIN; CHEN, 2002; ALVES et al., 2016) It is possible to reduce the norm of the gain matrices* $\mathbf{K}_i$ *increasing the region* $\mathscr{L}(\mathbf{K}_i)$ *selecting appropriately* ξ *such that* $\mathscr{E}(\mathbf{P}, \xi^{-1}) \subset \mathscr{L}(\mathbf{K}_i)$ *imposed if the LMIs*

$$\begin{bmatrix} \xi \rho_{0(l)}^{-2} & \mathbf{M}_{i(l)} \\ \star & \mathbf{X} \end{bmatrix} \geqslant 0, \tag{54}$$

holds for all $i \in \mathbb{I}_{n_r}$*, and* $l \in \mathbb{I}_{n_u}$*.*

Proof. See Hu, Lin and Chen (2002), Alves et al. (2016), Boyd et al. (1994). □

Theorem 1. *(ALVES et al., 2016) Let the sets* $\mathscr{E}(\mathbf{P},1)$*,* $\mathscr{L}(\mathbf{H}_k)$*, and* $\mathscr{W}_r$*. Consider a nonlinear system subject to actuator saturation and an operation region* $\mathbf{x}(t) \in \mathscr{O}$*,* $t \geqslant 0$*,* $\rho \in \mathbb{R}^{n_u}$*,* $\phi \in \mathbb{R}^p$ *and* $\mathbf{N} \in \mathbb{R}^{p \times n_x}$ *are known. Assume that there exist a symmetric positive definite matrix* $\mathbf{X} \in \mathbb{R}^{n_x \times n_x}$ *symmetric matrices* $\bar{\mathbf{Q}}_i$ *and* $\bar{\mathbf{Z}}_i \in \mathbb{R}^{n_x \times n_x}$*, matrices* $\mathbf{G}_j = \left[\mathbf{G}_{j(1)}^T\, \mathbf{G}_{j(2)}^T\, \cdots \mathbf{G}_{j(n_u)}^T\right]$*,* $\mathbf{M}_i \in \mathbb{R}^{n_u \times n_x}$ *and a scalar* $\beta > 0$ *such that*

$$\mathbf{A}_i\mathbf{X} + \mathbf{X}\mathbf{A}_i^T + \bar{\mathbf{Z}}_i + \bar{\mathbf{Q}}_i + 2\beta\mathbf{X} < 0, \tag{55a}$$

$$-\mathbf{B}_i\mathbf{D}_s\mathbf{M}_j+\mathbf{B}_i\breve{\mathbf{D}}_s^-\mathbf{G}_j-\mathbf{M}_j^T\mathbf{D}_s^T\mathbf{B}_i^T+\mathbf{G}_j^T\breve{\mathbf{D}}_s^{-T}\mathbf{B}_i^T-\bar{\mathbf{Z}}_i-\bar{\mathbf{Q}}_j\leqslant 0, \tag{55b}$$

$$\begin{bmatrix}\rho_{0(l)}^2 & \mathbf{G}_{j(l)}\\ \star & \mathbf{X}\end{bmatrix}\geqslant 0, \tag{55c}$$

$$\begin{bmatrix}\phi_{(h)}^2 & \mathbf{N}_{(h)}\mathbf{X}\\ \star & \mathbf{X}\end{bmatrix}\geqslant 0, \tag{55d}$$

$$\begin{bmatrix}\xi\rho_{0(l)}^{-2} & \mathbf{M}_{i(l)}\\ \star & \mathbf{X}\end{bmatrix}\geqslant 0, \tag{55e}$$

$$\begin{bmatrix}\bar{w}^{-2} & \star\\ \mathbf{w}_0^{i_w} & \mathbf{X}\end{bmatrix}\geqslant 0, \tag{55f}$$

hold for all i and $j\in\mathbb{I}_{n_r}$, $l\in\mathbb{I}_{n_u}$, $h\in\mathbb{I}_p$, $i_w\in\mathbb{I}_q$, $s\in\mathbb{I}_{2^{n_u}}$, $\mathbf{D}_s\in\mathscr{D}$ *and* $\breve{\mathbf{D}}_s^-\in\breve{\mathscr{D}}$. *Then, the control law* (39)-(42), *where* $\mathbf{K}_i=\mathbf{M}_i\mathbf{X}^{-1}$ *and* $\mathbf{Q}_i=\mathbf{X}^{-1}\bar{\mathbf{Q}}_i\mathbf{X}^{-1}$ *for all* $i\in\mathbb{I}_{n_r}$, *makes the system* (37) *locally asymptotically stable with a decay rate equal to or greater than* β, $\forall\mathbf{x}(0)\in\mathscr{E}(\mathbf{P},1)$, *where* $\mathbf{P}=\mathbf{X}^{-1}$. *Furthermore,* $\mathbf{x}(t)\in\mathscr{O}$, $t\geqslant 0$.

Proof. Based on Alves et al. (2016), consider as Lyapunov function candidate $V(\mathbf{x}(t))=\mathbf{x}(t)^T\mathbf{P}\mathbf{x}(t)$, $\mathbf{P}=\mathbf{P}^T\in\mathbb{R}^{n_x\times n_x}$, $\mathbf{P}>0$. Therefore, from the system (37) and the control law (40)

$$\begin{aligned}\dot V(\mathbf{x}) &= \dot{\mathbf{x}}^T\mathbf{P}\mathbf{x}+\mathbf{x}^T\mathbf{P}\dot{\mathbf{x}},\\ &= [\mathbf{A}(\alpha)\mathbf{x}+\mathbf{B}(\alpha)\mathrm{sat}(\mathbf{u})+\mathbf{B}(\alpha)d]^T\mathbf{P}\mathbf{x}+\mathbf{x}^T\mathbf{P}[\mathbf{A}(\alpha)\mathbf{x}+\mathbf{B}(\alpha)\mathrm{sat}(\mathbf{u})+\mathbf{B}(\alpha)d],\\ &= \mathbf{x}^T\left[\mathbf{A}(\alpha)^T\mathbf{P}+\mathbf{P}\mathbf{A}(\alpha)\right]\mathbf{x}+\mathrm{sat}(\mathbf{u})^T\mathbf{B}(\alpha)^T\mathbf{P}\mathbf{x}+\mathbf{x}^T\mathbf{P}\mathbf{B}(\alpha)\mathrm{sat}(\mathbf{u})+2\mathbf{x}^T\mathbf{P}\mathbf{B}(\alpha)d.\end{aligned} \tag{56}$$

Replacing (39)-(40) in (56)

$$\begin{aligned}\dot V(\mathbf{x}) = \mathbf{x}^T\left[\mathbf{A}(\alpha)^T\mathbf{P}+\mathbf{P}\mathbf{A}(\alpha)\right]\mathbf{x}&+\left[\mathrm{sat}_0\left(\mathbf{u}_\varsigma(t)\right)-\vartheta_\psi(t)\right]^T\mathbf{B}(\alpha)^T\mathbf{P}\mathbf{x}\\ &+\mathbf{x}^T\mathbf{P}\mathbf{B}(\alpha)\left[\mathrm{sat}_0\left(\mathbf{u}_\varsigma(t)\right)-\vartheta_\psi(t)\right]+2\mathbf{x}^T\mathbf{P}\mathbf{B}(\alpha)d,\end{aligned}$$

$$\begin{aligned}\dot V(\mathbf{x}) = \mathbf{x}^T\left[\mathbf{A}(\alpha)^T\mathbf{P}+\mathbf{P}\mathbf{A}(\alpha)\right]\mathbf{x}&+\mathrm{sat}_0\left(-\mathbf{K}_\varsigma\mathbf{x}\right)^T\mathbf{B}(\alpha)^T\mathbf{P}\mathbf{x}\\ &+\mathbf{x}^T\mathbf{P}\mathbf{B}(\alpha)\mathrm{sat}_0\left(-\mathbf{K}_\varsigma\mathbf{x}\right)+2\mathbf{x}^T\mathbf{P}\mathbf{B}(\alpha)\left[d-\vartheta_\psi(t)\right].\end{aligned} \tag{57}$$

Considering (50), (57) can be rewritten as

$$\begin{aligned}\dot V(\mathbf{x}) &= \mathbf{x}^T\left[\mathbf{A}(\alpha)^T\mathbf{P}+\mathbf{P}\mathbf{A}(\alpha)\right]\mathbf{x}\\ &+\left\{\sum_{s=1}^{2^{n_u}}\lambda_s\left[\mathbf{D}_s\left(-\mathbf{K}_\varsigma\mathbf{x}\right)+\breve{\mathbf{D}}_s^-\left(\mathbf{H}_\varsigma\mathbf{x}\right)\right]\right\}^T\mathbf{B}(\alpha)^T\mathbf{P}\mathbf{x}\\ &+\mathbf{x}^T\mathbf{P}\mathbf{B}(\alpha)\left\{\sum_{s=1}^{2^{n_u}}\lambda_s\left[\mathbf{D}_s\left(-\mathbf{K}_\varsigma\mathbf{x}\right)+\breve{\mathbf{D}}_s^-\left(\mathbf{H}_\varsigma\mathbf{x}\right)\right]\right\}+2\mathbf{x}^T\mathbf{P}\mathbf{B}(\alpha)\left[d-\vartheta_\psi\right].\end{aligned} \tag{58}$$

Note that $d(t)$ can be rewritten as $d(t)=\gamma_1(t)\vartheta_1+\gamma_2(t)\vartheta_2$

$$\sum_{m=1}^{2}\gamma_m(t)=1,\ \gamma_1(t),\gamma_2(t)\geqslant 0,\ \gamma_2(t)=\frac{d(t)-\vartheta_1}{\vartheta_2-\vartheta_1};\ \gamma_1(t)=1-\gamma_2(t). \tag{59}$$

Therefore, replacing $\mathbf{B}(\alpha)=\mathbf{B}_0 g(\mathbf{x})$, $g(\mathbf{x})\geqslant 0$, $\forall\mathbf{x}\neq 0$, from (41) and considering $\vartheta_\psi=\min_{m\in\mathbb{I}_2}\{\vartheta_m\}\leqslant\sum_{m=1}^{2}\gamma_m(t)\vartheta_m$, it follows that

$$\begin{aligned}\mathbf{x}^T\mathbf{P}\mathbf{B}(\alpha)\left[d-\vartheta_\psi\right]&=\mathbf{x}^T\mathbf{P}\mathbf{B}_0\left[\sum_{m=1}^{2}\gamma_m(t)\vartheta_m+\min_{m\in\mathbb{I}_2}\left\{-\mathbf{x}^T\mathbf{P}\mathbf{B}_0\vartheta_m\right\}\right]\\&\leqslant\mathbf{x}^T\mathbf{P}\mathbf{B}_0\sum_{m=1}^{2}\gamma_m(t)\vartheta_m-\mathbf{x}^T\mathbf{P}\mathbf{B}_0\sum_{m=1}^{2}\gamma_m(t)\vartheta_m=0.\end{aligned} \tag{60}$$

Then, one obtains

$$\begin{aligned}\dot V(\mathbf{x})=\mathbf{x}^T\left[\mathbf{A}(\alpha)^T\mathbf{P}+\mathbf{P}\mathbf{A}(\alpha)\right]\mathbf{x}+\left\{\sum_{s=1}^{2^{n_u}}\lambda_s\left[\mathbf{D}_s\left(-\mathbf{K}_\varsigma\mathbf{x}\right)+\breve{\mathbf{D}}_s^-\left(\mathbf{H}_\varsigma\mathbf{x}\right)\right]\right\}^T\mathbf{B}(\alpha)^T\mathbf{P}\mathbf{x}\\+\mathbf{x}^T\mathbf{P}\mathbf{B}(\alpha)\left\{\sum_{s=1}^{2^{n_u}}\lambda_s\left[\mathbf{D}_s\left(-\mathbf{K}_\varsigma\mathbf{x}\right)+\breve{\mathbf{D}}_s^-\left(\mathbf{H}_\varsigma\mathbf{x}\right)\right]\right\}.\end{aligned} \tag{61}$$

Now, assume that there exist symmetric matrices $\mathbf{Z}_i$ and $\mathbf{Q}_j$ such that

$$\left[-\mathbf{D}_s\mathbf{K}_j+\breve{\mathbf{D}}_s^-\mathbf{H}_j\right]^T\mathbf{B}_i^T\mathbf{P}+\mathbf{P}\mathbf{B}_i\left[-\mathbf{D}_s\mathbf{K}_j+\breve{\mathbf{D}}_s^-\mathbf{H}_j\right]\leqslant\mathbf{Z}_i+\mathbf{Q}_j, \tag{62}$$

$\forall i,\ j\in\mathbb{I}_{n_r}$, $\forall\mathbf{D}_s\in\mathscr{D}$, and $\forall\breve{\mathbf{D}}_s^-\in\breve{\mathscr{D}}^-$. Then, for $j=\varsigma$, multiplying by α_i, where $\alpha_i\geqslant 0$, and taking the sum from $i=1$ to n_r, $\sum_{i=1}^{n_r}\alpha_i=1$ and then multiplying the result by λ_s, $\lambda_s\geqslant 0$ and taking the sum from $s=1$ to 2^{n_u}, $\sum_{s=1}^{2^{n_u}}\lambda_s=1$, considering $\mathbf{B}(\alpha)=\sum_{i=1}^{n_r}\alpha_i\mathbf{B}_i$, $\alpha\geqslant 0$, $\sum_{i=1}^{n_r}\alpha_i=1$, $i\in\mathbb{I}_{n_r}$ one has

$$\sum_{s=1}^{2^{n_u}}\lambda_s\left\{\left[-\mathbf{D}_s\mathbf{K}_\varsigma+\breve{\mathbf{D}}_s^-\mathbf{H}_\varsigma\right]^T\mathbf{B}(\alpha)^T\mathbf{P}+\mathbf{P}\mathbf{B}(\alpha)\left[-\mathbf{D}_s\mathbf{K}_\varsigma+\breve{\mathbf{D}}_s^-\mathbf{H}_\varsigma\right]\right\}\leqslant\mathbf{Z}(\alpha)+\mathbf{Q}_\varsigma, \tag{63}$$

where $\mathbf{Z}(\alpha)=\sum_{i=1}^{n_r}\alpha_i\mathbf{Z}_i$. Observe that, from the control law (40), $\mathbf{x}^T\mathbf{Q}_\varsigma\mathbf{x}=\min_{i\in\mathbb{I}_{n_r}}\left\{\mathbf{x}^T\mathbf{Q}_i\mathbf{x}\right\}\leqslant\sum_{i=1}^{n_r}\alpha_i\mathbf{x}^T\mathbf{Q}_i\mathbf{x}=\mathbf{x}^T\mathbf{Q}(\alpha)\mathbf{x}$. Thus, from (61) and (63),

$$\dot V(\mathbf{x})\leqslant\mathbf{x}^T\left\{\mathbf{A}(\alpha)^T\mathbf{P}+\mathbf{P}\mathbf{A}(\alpha)+\mathbf{Z}(\alpha)+\mathbf{Q}(\alpha)\right\}\mathbf{x}. \tag{64}$$

Because to achieve a decay rate greater than or equal to β it is sufficient that $\dot V(\mathbf{x})\leq$

$-2\beta V(\mathbf{x})$. Hence, from (64) is sufficient that, $\forall i \in \mathbb{I}_{n_r}$,

$$\mathbf{A}_i^T\mathbf{P} + \mathbf{P}\mathbf{A}_i + \mathbf{Z}_i + \mathbf{Q}_i + 2\beta\mathbf{P} \leq 0. \tag{65}$$

Premultiplying and postmultiplying (62) and (65) by $\mathbf{X} = \mathbf{P}^{-1}$ and performing the change of variables $\mathbf{G}_j = \mathbf{H}_j\mathbf{X}$, $\mathbf{M}_j = \mathbf{K}_j\mathbf{X}$, $\bar{\mathbf{Z}}_i = \mathbf{X}\mathbf{Z}_i\mathbf{X}$ and $\bar{\mathbf{Q}}_i = \mathbf{X}\mathbf{Q}_i\mathbf{X}$, one obtains (55a) and (55b). Note that as $V(\mathbf{x}) = \mathbf{x}^T\mathbf{P}\mathbf{x}$ and $\dot{V}(\mathbf{x}) < 0$, $\mathbf{x} \neq 0$, from (44), if $\mathbf{x}(0) \in \mathscr{E}(\mathbf{P},\delta)$ then $\mathbf{x}(t) \in \mathscr{E}(\mathbf{P},\delta)$, $\forall t \geqslant 0$. Considering Lemma 3 with $\delta = 1$, LMI (55c) ensure $\mathscr{E}(\mathbf{P},1) \in \mathscr{L}(\mathbf{H}_k)$, a sufficient condition such that (50) holds. And considering Lemma 1, LMI (55d) ensure $\mathscr{E}(\mathbf{P},1) \subset \mathscr{O}$, a sufficient condition for a state trajectory started with an initial condition $\mathbf{x}(0) \in \mathscr{E}(\mathbf{P},1)$ to be in $\mathscr{O}$ for all $t \geqslant 0$. In addition, considering the Lemma 4, LMI (55f) guarantees that convex hull is contained in the invariant region $\mathscr{E}(\mathbf{P},1)$, and LMI (55e) minimizes the norm of the matrices $\mathbf{K}_i$, selecting appropriately ξ such that $\mathscr{E}(\mathbf{P},\xi^{-1}) \subset \mathscr{L}(\mathbf{K}_i)$. The proof is complete. □

Remark 3. *The Gaino et al. (2017) approach treated the plant model without uncertainties, consequently the values of $\breve{u}^d$ and nominal torque M_a are not uncertain. Now assuming non-idealities, the state vector becomes an estimate, since M_a^d is uncertain. However, we add to the control signal a term $\vartheta_\psi(t)$ that will dominate the error from the uncertainty of the desired torque. Thus,*

$$\breve{u} = -\mathbf{K}_\varsigma\mathbf{x}_e(t) + \vartheta_\psi(t), \tag{66}$$

where $\mathbf{K}_\varsigma = \begin{bmatrix}\mathbf{K}_{\varsigma1} & \mathbf{K}_{\varsigma2} & \mathbf{K}_{\varsigma3}\end{bmatrix}$, $\mathbf{x}_e(t) = [x_1(t) \quad x_2(t) \quad x_{3e}(t)]^T$, $x_{3e}(t) = \check{x}_3 - M^d_{a\,nom}$, $M_{a\,nom}$ is the nominal torque.

Considering the following relationship $x_{3e}(t) = \check{x}_3 - M_a^d + \Delta M_a$, $\Delta M_a = M_a^d - M^d_{a\,nom}$, (66) can be rewritten as

$$\breve{u} = -\begin{bmatrix}\mathbf{K}_{\varsigma1} & \mathbf{K}_{\varsigma2} & \mathbf{K}_{\varsigma3}\end{bmatrix}\begin{bmatrix} x_1 \\ x_2 \\ x_3 + \Delta M_a \end{bmatrix} + \vartheta_\psi(t),$$

Therefore,

$$u = \breve{u} - \breve{u}_e^d = -\begin{bmatrix}\mathbf{K}_{\varsigma1} & \mathbf{K}_{\varsigma2} & \mathbf{K}_{\varsigma3}\end{bmatrix}\begin{bmatrix} x_1 \\ x_2 \\ x_3 \end{bmatrix} - \mathbf{K}_{\varsigma3}\Delta M_a - \breve{u}_e^d + \vartheta_\psi(t),$$

$$u = -\mathbf{K}_\varsigma\mathbf{x} - \breve{u}^d + u_{error} + \vartheta_\psi(t),$$

where $u_{error} = \left(\breve{u}^d - \breve{u}_e^d - \mathbf{K}_{\varsigma3}\Delta M_a\right)$ will be dominated by the term $\vartheta_\psi(t)$.

3.3.1 Example: paraplegic individual P1

The LMIs (55) were solved using the MatLab® software, and the modeling language YALMIP (EFBERG; LÖFBERG, 2004) with the solver LMILab (GAHINET et al., 1994).

Consider the TS fuzzy modeling of the paraplegic individual P1, whose local models are described in (36). The operating region $\mathscr{O}$, described in (43), where $p = 3$, $\mathbf{N} = \mathbf{I}_3$, and $\phi = [\frac{\pi}{3} \quad 4 \quad 10]^T$. Note that $\mathbf{B}(\alpha) = \mathbf{B}_0 g(\mathbf{z})$, where $\mathbf{B}_0 = [0 \quad 0 \quad 1]^T$, and $g(\mathbf{z}) \geqslant 0$, $g_0(\mathbf{z}) = \max_{\mathbf{z}\in\mathbb{D}} \{g(\mathbf{z})\} = 297.9320$.

Solving the LMIs (55) present in Theorem 1, the aforementioned parameters, $\beta = 1.0$, $\rho_0 = 0.3$, $q = 2$, $\mathbf{w}_0^1 = \left[\frac{\pi}{6} \quad 0 \quad 5\right]$, $\mathbf{w}_0^2 = \left[\frac{-\pi}{9} \quad 0 \quad -5\right]$, minimizing $\bar{w}$, one obtains

$$\bar{\mathbf{Q}}_1 = 10^3 \times \begin{bmatrix} -14774.7641 & -4312.2519 & -791.3337 \\ -4312.2519 & -1041.3075 & -172.6256 \\ -791.3337 & -172.6256 & -26.7213 \end{bmatrix},$$

$$\bar{\mathbf{Q}}_2 = 10^3 \times \begin{bmatrix} -14774.7668 & -4312.2538 & -791.3343 \\ -4312.2538 & -1041.3087 & -172.626 \\ -791.3343 & -172.626 & -26.7214 \end{bmatrix},$$

$$\bar{\mathbf{Q}}_3 = 10^3 \times \begin{bmatrix} -14774.7637 & -4312.2518 & -791.3335 \\ -4312.2518 & -1041.3075 & -172.6255 \\ -791.3335 & -172.6255 & -26.7213 \end{bmatrix},$$

$$\bar{\mathbf{Q}}_4 = 10^3 \times \begin{bmatrix} -14774.7665 & -4312.2537 & -791.334 \\ -4312.2537 & -1041.3088 & -172.6259 \\ -791.334 & -172.6259 & -26.7214 \end{bmatrix},$$

$$\bar{\mathbf{Q}}_5 = 10^3 \times \begin{bmatrix} -14774.7205 & -4312.241 & -791.331 \\ -4312.241 & -1041.3074 & -172.6256 \\ -791.331 & -172.6256 & -26.7213 \end{bmatrix},$$

$$\bar{\mathbf{Q}}_6 = 10^3 \times \begin{bmatrix} -14774.7208 & -4312.2418 & -791.3313 \\ -4312.2418 & -1041.3085 & -172.6259 \\ -791.3313 & -172.6259 & -26.7214 \end{bmatrix},$$

$$\bar{\mathbf{Q}}_7 = 10^3 \times \begin{bmatrix} -14774.7202 & -4312.2409 & -791.3307 \\ -4312.2409 & -1041.3075 & -172.6255 \\ -791.3307 & -172.6255 & -26.7212 \end{bmatrix},$$

$$\bar{\mathbf{Q}}_8 = 10^3 \times \begin{bmatrix} -14774.7208 & -4312.242 & -791.331 \\ -4312.242 & -1041.3086 & -172.6258 \\ -791.331 & -172.6258 & -26.7213 \end{bmatrix},$$

$$
\begin{aligned}
&\mathbf{K}_1 = \begin{bmatrix}0.2600 & 0.1311 & 0.0463\end{bmatrix}, \quad \mathbf{K}_2 = \begin{bmatrix}0.2822 & 0.1384 & 0.0473\end{bmatrix},\\
&\mathbf{K}_3 = \begin{bmatrix}0.2482 & 0.1339 & 0.0467\end{bmatrix}, \quad \mathbf{K}_4 = \begin{bmatrix}0.2736 & 0.1411 & 0.0475\end{bmatrix},\\
&\mathbf{K}_5 = \begin{bmatrix}-0.0367 & 0.1240 & 0.0439\end{bmatrix}, \quad \mathbf{K}_6 = \begin{bmatrix}-0.0734 & 0.1272 & 0.0423\end{bmatrix},\\
&\mathbf{K}_7 = \begin{bmatrix}-0.0438 & 0.1322 & 0.0424\end{bmatrix}, \quad \mathbf{K}_8 = \begin{bmatrix}-0.0679 & 0.1319 & 0.0379\end{bmatrix},\\
&\mathbf{P} = \begin{bmatrix}4.9616 & 0.8501 & 0.1052\\ 0.8501 & 0.3784 & 0.0804\\ 0.1052 & 0.0804 & 0.0272\end{bmatrix}.
\end{aligned}
$$

In order to compare with the literature, a control strategy proposed by Gaino et al. (2017) was evaluated. The authors adopted the PDC controller. It is noteworthy that Gaino et al. (2017) did not consider uncertainties (fatigue, tremor, spasms and fault in the actuator) in the model. Therefore, the state-feedback gains are obtained for ideal conditions. From Gaino et al. (2017), the LMIs conditions were solved considering $\mu = 300$ mA, $\beta = 1.0$, one obtains

$$
\mathbf{P} = \begin{bmatrix}44.2076 & 5.6622 & 1.2298\\ 5.6622 & 1.5778 & 0.3441\\ 1.2300 & 0.3441 & 0.1509\end{bmatrix},
$$

$$
\begin{aligned}
\mathbf{F}_1 = \mathbf{M}_1\mathbf{X} &= \begin{bmatrix}0.2592 & 0.1363 & 0.0302\end{bmatrix},\\
\mathbf{F}_2 = \mathbf{M}_1\mathbf{X} &= \begin{bmatrix}0.2563 & 0.1359 & 0.0301\end{bmatrix}.
\end{aligned} \tag{67}
$$

3.4 Results and discussion

3.4.1 Ideal conditions

Usually, the results of controllers from simulation consider ideal conditions for electrical stimulation of the lower limbs, i.e., without fatigue, tremor, spasms and other uncertainties.

In ideal conditions, the PDC and switched controllers were applied to regulation at three operating points in the time interval $0 \leqslant t \leqslant 30$ s. The results were determined for healthy and paraplegic subjects.

The root mean square error value in the periods transient ($TRMSE$), steady-state ($SSRMSE$), and over the total time (0-60s) ($TTRMSE$) were analyzed. The $TRMSE$ values were obtained during the initial 5 s of the transient response. Meanwhile, the $SSRMSE$ corresponds the last 5 s of regulation in the reference position.

Figure 6 indicates the mean of the RMS error in the time intervals ($TRMSE$, $SSRMSE$, $TTRMSE$) for each individual, and the mean value obtained for the healthy and paraplegic group.

In general, it can be concluded that $TRMSE$ is lower using PDC controller. However, both controllers had a satisfactory performance for regulation around the operating point, i.e., $SSRMSE$ tending to zero.

Remark 4. *It is important to note that although Gaino et al. (2017) establishes a design procedure applied to trajetory tracking based on TS fuzzy models, the analysis was restricted to regulation at three operation points.*

3.4.2 Non-ideal conditions

Simulations were run for non-ideal conditions of fault in the actuator, parametric uncertainty in the recruitment function as well as combinations of severity in fatigue, spasms, and tremor. The test conditions of each individual were the same for both controllers (PDC and switched).

The controllers performance based on the steady-state error value for a step at the desired position reference was not investigated in Lynch and Popovic (2012). In this paper, we evaluated and compared the steady-state error of the PDC and switched controllers in the non-ideal conditions.

3.4.2.1 Fault in the actuator and parametric uncertainty in the muscle recruitment

The fault in the actuator was considered as a decrease in energy (80% of the nominal) applied to the muscles. It was also assumed an uncertainty in the muscular recruitment function, expressed by the parameter $\hat{G}$. Figure 7 indicates a discrepancy between the knee angular position and the desired value using the PDC controller. Otherwise, the switched controller was able to reach the desired operation point, even in presence of parametric uncertainties.

Lynch and Popovic (2012) obtained closed-loop control results from PID, gain shedulling, and sliding mode. An emphasis given by the authors is that all controllers were sensitive to parameter variation. Therefore, the incompatibility error between model and control design explains the degraded performance.

3.4.2.2 Muscle fatigue, tremor and spasms

Muscle non-idealities (fatigue, spasms, and tremor) alters muscle torque. These non-idealities were evaluated at the instant $t = 30$s, Figure 8.

The literature does not establish a metric to categorize the unwanted behavior level in the muscle response provided by electrical stimulus.

Figure 6 - RMS error in transient (TRMSE), steady-state (SSRMSE), and total time (TTRMSE), and average of the healthy and paraplegic groups.

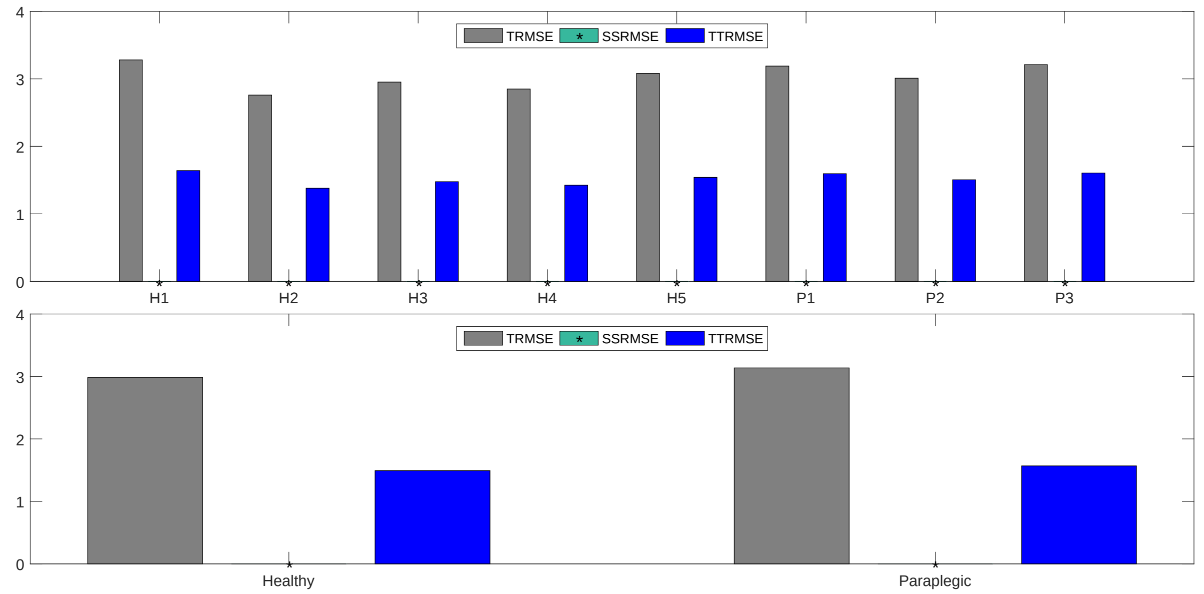

(a) PDC controller

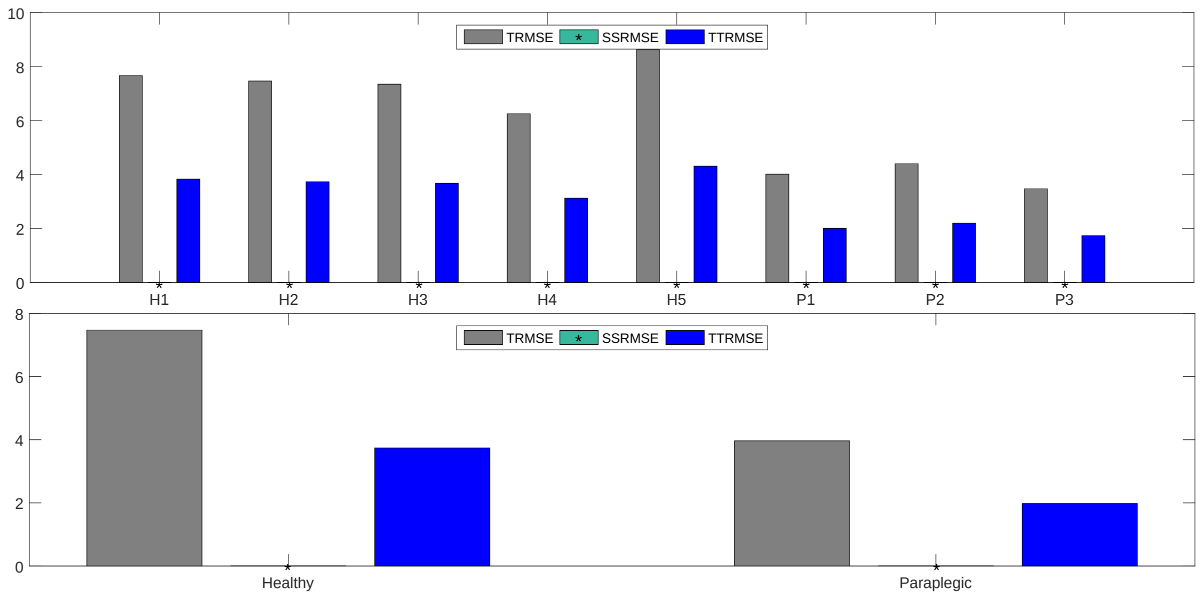

(b) Switched controller

Source: From author.

Table 9 lists the RMS steady-state error for the PDC and switched controllers. The situations of non-idealities due to fatigue are listed first. Fatigue was assessed at three levels: mild, moderate and severe. Next, the same level of intensity for each non-ideality (fatigue, spasms and tremor) is indicated. Note that for all individuals and in all non-ideal conditions the switched controller obtained the best result, achieving the lowest RMS error for the angular position.

Figures 9a and 9b illustrate the performance of the controllers for the mild and severe

Figure 7 - Comparative analysis between PDC and switched controller considering fault in the actuator (80% nominal), and uncertainty in the muscle recruitment function ($\hat{G} = 0.8G$) of the individual P1.

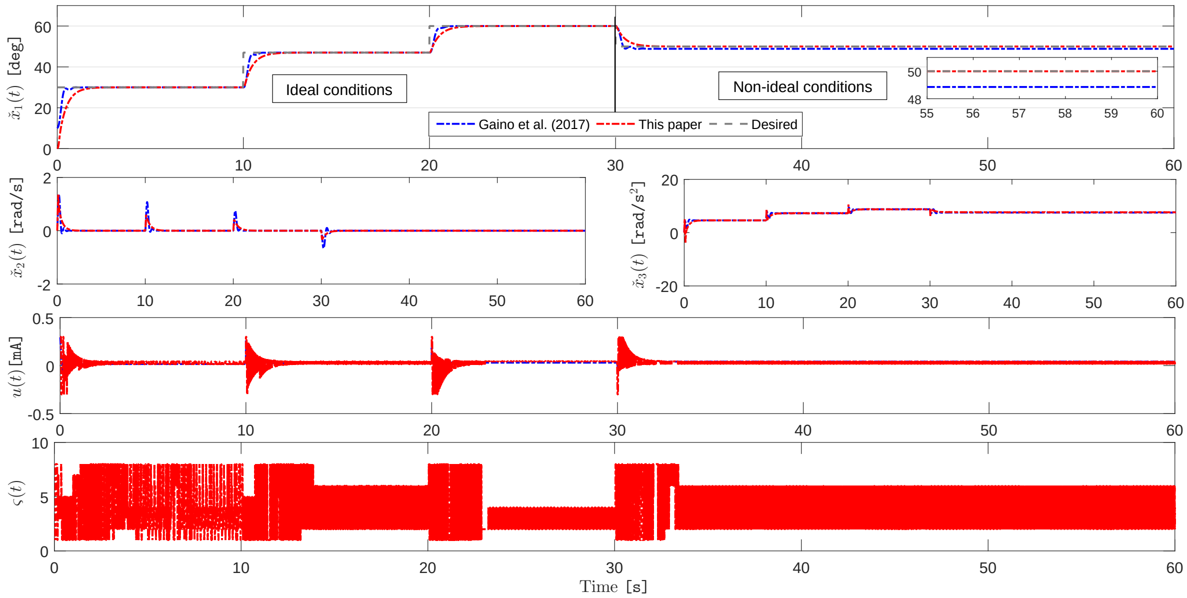

Source: From author.

condition of muscular non-idealities. The performance of the PDC controller in ideal conditions induces to conclude that it is suitable for validation in humans. However, the performance under non-ideal conditions shows an unsatisfactory result.

Note that even the switched controller reducing steady-state error, the fatigue precludes null error. Muscle torque is reduced substantially. Consequently, maintaining the angular position and muscular activation applied to a single motor point is a difficult task, because the fatigue effect modifies the musculoskeletal system to null torque. Even by electrically stimulating a motor point, one way to achieve better results is to delay the action of fatigue, such as initiating the volunteers in a pre-training aimed at muscle strengthening, and to increase the rest time between stimulation attempts.

For all individuals the highest RMS error was obtained for the severe fatigue situation. It is interesting to note that this condition presents a greater error than considering all non-idealities in maximum severity degree. This behavior is due to spasticity (LYNCH; GRAHAM; POPOVIC, 2011a). In this case, spasticity effectively increases the knee joint stiffness, contributing to a smaller error in the controllers' performance.

Figure 8 - Muscle behavior in different non-idealities levels inserted during the tests: (8a) fatigue, (8b) spasms, and (8c) tremor.

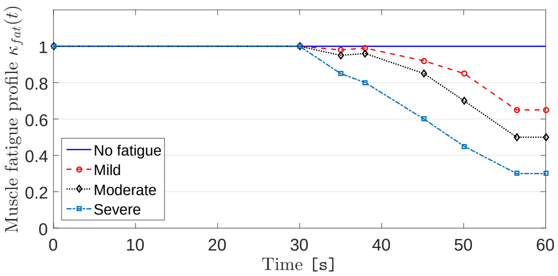

(a) Muscle fatigue.

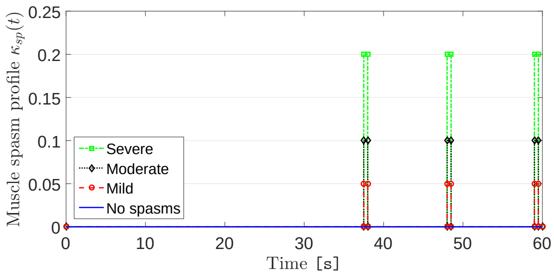

(b) Muscle spasms.

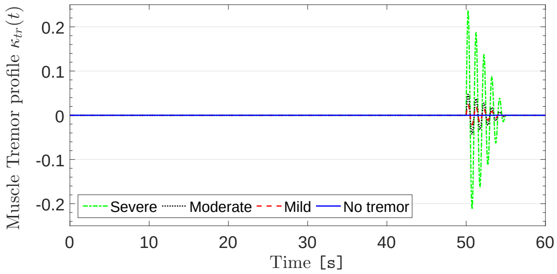

(c) Muscle tremor.

Source: From author.

3.4.3 Critical analysis

3.4.3.1 Switched controller perfomance: advantages and limitations

The switched controller handled uncertainties inherent in the individual such as: muscle fatigue, spasms, tremor; and also features of the system such as: saturation and actuator failure. The results show a regulation response similar to Gaino et al. (2017) under ideal conditions at the proposed operating points. However, under non-ideal conditions the performance of the switched controller is better than Gaino et al. (2017).

For nonlinear system described by TS fuzzy model, the PDC controller depends on known membership functions. When dealing with uncertain systems, the result obtained with PDC becomes unsatisfactory, because the membership functions become unsuitable for model uncertainties. Thus, the switched controller is presented as an advantageous proposal, since it does not depend explicitly on the membership functions for the convex combination of controller gains. Other applications of the switched controller for uncertain nonlinear plants can be found in the studies of Souza et al. (2014), Alves et al. (2016), Oliveira et al. (2017).

One observed limitation is that by increasing the number and range of uncertain parameters, the LMIs of the switched control design tend to become infeasible.

Finally, chattering in the control signal promoted by the switched controller can be smoothed.

Table 9 - RMS error for healthy and paraplegic individuals.

Individual	Fatigue	Spasms	Tremor	RMS error [deg] (GAINO et al., 2017)	RMS error [deg] This study
H1	Mild	-	-	7.63	**4.14**
	Moderate	-	-	10.94	**7.34**
	Severe	-	-	17.43	**14.33**
H2	Mild	-	-	4.70	**2.54**
	Moderate	-	-	7.53	**4.58**
	Severe	-	-	13.42	**9.81**
H3	Mild	-	-	5.04	**2.15**
	Moderate	-	-	7.75	**4.05**
	Severe	-	-	13.22	**8.79**
H4	Mild	-	-	4.26	**1.53**
	Moderate	-	-	6.83	**2.94**
	Severe	-	-	12.31	**6.86**
H5	Mild	-	-	6.78	**2.81**
	Moderate	-	-	9.89	**5.30**
	Severe	-	-	16.01	**11.08**
P1	Mild	-	-	6.43	**1.50**
	Moderate	-	-	10.08	**2.79**
	Severe	-	-	17.39	**6.28**
	Mild	Mild	Mild	6.376	**1.48**
	Moderate	Moderate	Moderate	9.98	**2.75**
	Severe	Severe	Severe	17.29	**6.21**
P2	Mild	-	-	7.51	**1.51**
	Moderate	-	-	10.83	**2.92**
	Severe	-	-	18.04	**7.21**
	Mild	Mild	Mild	10.26	**1.50**
	Moderate	Moderate	Moderate	10.74	**2.86**
	Severe	Severe	Severe	17.94	**7.16**
P3	Mild	-	-	9.14	**1.16**
	Moderate	-	-	12.44	**2.30**
	Severe	-	-	19.11	**9.22**
	Mild	Mild	Mild	9.08	**1.15**
	Moderate	Moderate	Moderate	12.34	**2.28**
	Severe	Severe	Severe	19.00	**9.67**

Source: From author.

In Alves et al. (2016) was introduced the idea of smooth minimum function. Although the smooth switched control law may mitigate the effect of chattering on the control signal, the steady-state error may be greater than the switched, due to the guarantee of uniform ultimate boundedness of the controlled system.

3.4.3.2 *Complementing the design procedure proposed by Gaino et al. (2017)*

Further details on the procedure for determining the nonlinear function presented in Gaino et al. (2017) are presented. The proposed approach consists in obtaining a new representation of the equations of the plant using change of variables and adopting a virtual state, in order to

Figure 9 - Lower limb dynamic behavior for muscle non-idealities (fatigue, spasms, and tremor) in conditions: (9a) mild, (9b) severe, and considering fault in the actuator (80% of the nominal).

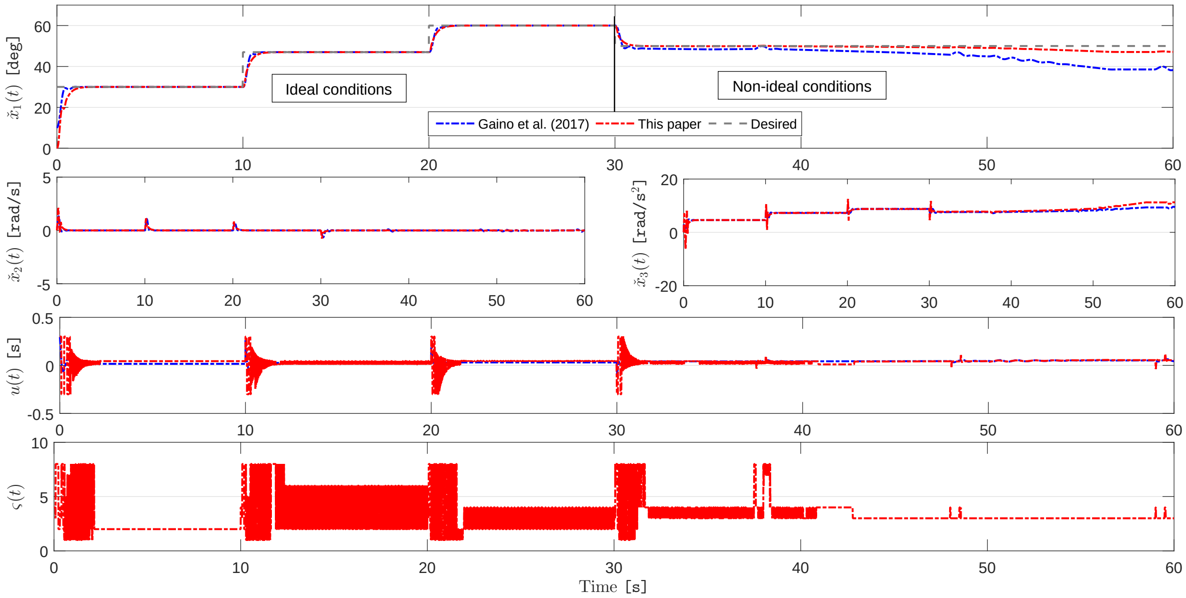

(a) All muscle non-idealities in mild conditions.

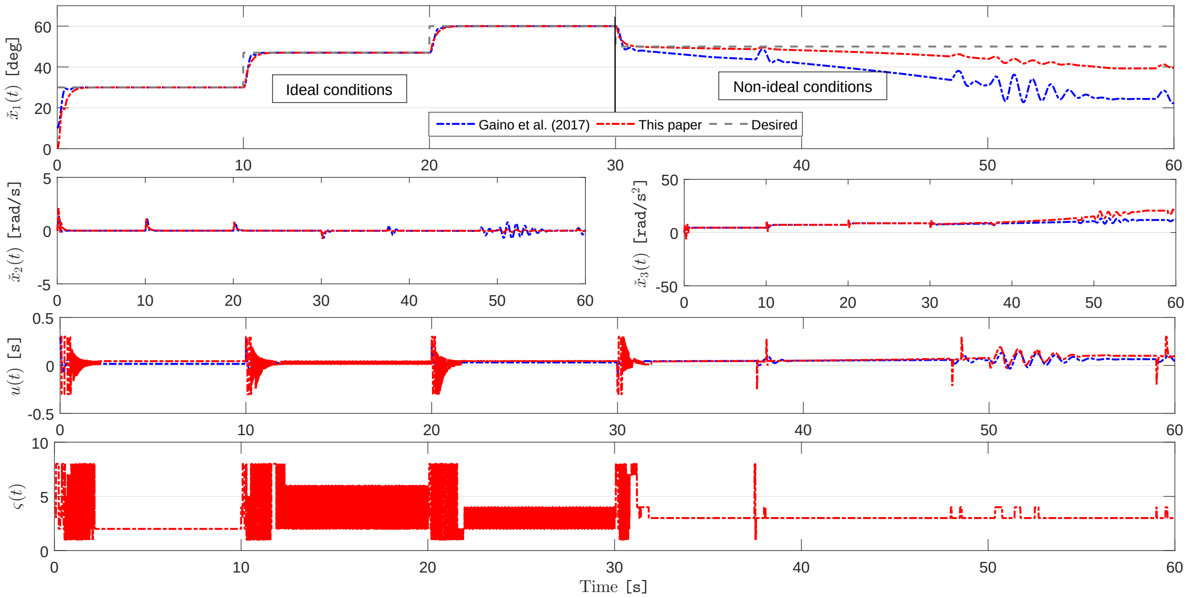

(b) All muscle non-idealities in severe conditions and fault in the actuator.

Source: From author.

group the nonlinear function $f_{21}(x_1)$ such that

$$x_{1n} = f_{21}(x_1)x_1 = f(x_1), \tag{68}$$

and assuming that $f(x_1)$ is an invertible function, one obtains the following relation

$$f(x_1) = x_{1n} \Longleftrightarrow f^{-1}(x_{1n}) = x_1. \tag{69}$$

A new representation of the system was obtained using the (68) and (69) expressed as

$$\underbrace{\begin{bmatrix} \dot{x}_{1n} \\ \dot{x}_{2n} \\ \dot{x}_{3n} \end{bmatrix}}_{\dot{\mathbf{x}}_n} = \underbrace{\begin{bmatrix} 0 & f_{12n}(x_{1n}) & 0 \\ 1 & -\dfrac{B}{J} & \dfrac{1}{J} \\ 0 & 0 & -\dfrac{1}{\tau} \end{bmatrix}}_{\mathbf{A}(\mathbf{x}_n)} \underbrace{\begin{bmatrix} x_{1n} \\ x_{2n} \\ x_{3n} \end{bmatrix}}_{\mathbf{x}_n} + \underbrace{\begin{bmatrix} 0 \\ 0 \\ \dfrac{G}{\tau} \end{bmatrix}}_{\mathbf{B}} \mathbf{u}, \tag{70}$$

where the new nonlinear function is

$$f_{12n}(x_{1n}) = \left[\frac{\partial f^{-1}(x_{1n})}{\partial x_{1n}} \right]^{-1}. \tag{71}$$

However, Gaino et al. (2017) does not explicitly indicate the expression of $f_{12n}(x_{1n})$. In this case, the problem lies in the definition of the new variable:

$$x_{1n} = f(x_1) = f_{21}(x_1)x_1 = \frac{1}{J}\left[-mgl\sin(x_1) - \lambda e^{-E\left(x_1+\frac{\pi}{2}\right)} \left(x_1 + \frac{\pi}{2} - \omega \right) \right], \tag{72}$$

which refers to a transcendental equation. Thus, there is the following question: how to calculate the local models having $f_{12n}(x_{1n})$ depending on the inverse of the function $f(x_{1n})$?

Next, we propose a complement to elucidate the procedure by explicitly indicating an expression for the nonlinear function $f_{12n}(x_{1n})$.

Theorem 2. *Let $x_{1n} = f(x_1)$ be invertible with inverse $x_1 = f^{-1}(x_{1n})$. If $f(x_1)$ is derivable at $x_1^d = f^{-1}(x_{1n}^d)$, $f'(x_1^d) \neq 0$, and if $f^{-1}(x_{1n})$ is continuous in x_{1n}^d then it will be derivable in x_{1n}^d with*

$$\left(f^{-1}\right)'(x_{1n}) = \frac{1}{f'\left(f^{-1}(x_{1n})\right)} = \frac{1}{f'(x_1)}. \tag{73}$$

Proof. Consider

$$\frac{f^{-1}(x_{1n}) - f^{-1}(x_{1n}^d)}{x_{1n} - x_{1n}^d} = \frac{f^{-1}(x_{1n}) - f^{-1}(x_{1n}^d)}{f\left(f^{-1}(x_{1n})\right) - f\left(f^{-1}(x_{1n}^d)\right)} = \left[\frac{f\left(f^{-1}(x_{1n})\right) - f\left(f^{-1}(x_{1n}^d)\right)}{f^{-1}(x_{1n}) - f^{-1}(x_{1n}^d)} \right]^{-1}, \tag{74}$$

$x_{1n} \neq x_{1n}^d$.

Let $x_1 = f^{-1}(x_{1n})$, as $f^{-1}(x_{1n})$ is continuous in x_{1n}^d, one obtains

$$\lim_{x_{1n} \to x_{1n}^d} f^{-1}(x_{1n}) = f^{-1}(x_{1n}^d), \tag{75}$$

Figure 10 - Nonlinear function $f_{12n}(x_{1n})$ in the system (70) proposed by Gaino et al. (2017).

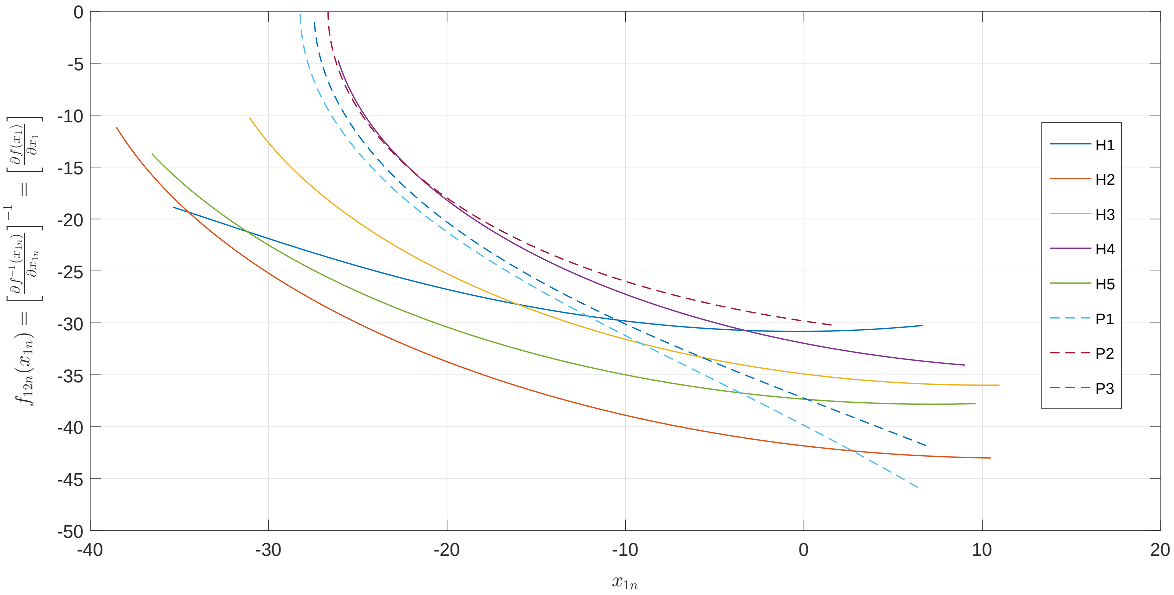

Source: From author.

i.e., when $x_{1n} \to x_{1n}^d$, $f^{-1}(x_{1n}) \to f^{-1}(x_{1n}^d)$, $x_1 \to x_1^d$, then

$$\lim_{x_{1n} \to x_{1n}^d} \frac{f^{-1}(x_{1n}) - f^{-1}\left(x_{1n}^d\right)}{x_{1n} - x_{1n}^d} = \lim_{x_1 \to x_1^d} \left[\frac{f^{-1}(x_1) - f^{-1}\left(x_1^d\right)}{x_1 - x_1^d}\right]^{-1} = \left[\frac{\partial f(x_1)}{\partial x_1}\right]^{-1}\Bigg|_{x_1 = x_1^d} \tag{76}$$

being $f(x_1)$ derivable in $x_1^d = f^{-1}(x_{1n}^d)$, $f'(x_1^d) \neq 0$. Thus, the proof is complete. □

Remark 5. *Given the representation of the system in* (70), *and consider the function* $f(x_1)$ *defined by*

$$f(x_1) = f_{21}(x_1)x_1 = \frac{1}{J}\left[-mgl\sin(x_1) - \lambda e^{-E\left(x_1 + \frac{\pi}{2}\right)}\left(x_1 + \frac{\pi}{2} - \omega\right)\right], \tag{77}$$

$$\frac{\partial f(x_1)}{\partial x_1} = \frac{1}{J}\left[-mgl\cos(x_1) + \lambda E\left(x_1 + \frac{\pi}{2} - \omega\right)e^{-E\left(x_1 + \frac{\pi}{2}\right)} - \lambda e^{-E\left(x_1 + \frac{\pi}{2}\right)}\right]. \tag{78}$$

Thus, (71) *can be rewritten from* (73) *and* (78),

$$f_{12n}(x_{1n}) = \left[\frac{\partial f^{-1}(x_{1n})}{\partial x_{1n}}\right]^{-1} = \left[\frac{\partial f(x_1)}{\partial x_1}\right],$$

$$f_{12n}(x_{1n}) = \left[-\frac{mgl}{J}\cos(x_1) + \frac{\lambda E}{J}\left(x_1 + \frac{\pi}{2} - \omega\right)e^{-E\left(x_1 + \frac{\pi}{2}\right)} - \frac{\lambda}{J}e^{-E\left(x_1 + \frac{\pi}{2}\right)}\right], \tag{79}$$

being $x_{1n} = f(x_1)$ *and* $f_{12n}(x_{1n}) = \left[\frac{\partial f^{-1}(x_{1n})}{\partial x_{1n}}\right]^{-1}$, *one obtains the representation shown in Figure 10.*

3.4.4 Future works

The control signal used in the system identification is a single-phase square energy signal. This study adopted the amplitude modulation of the current signal. Future works may investigate other schemes such as: pulse width modulation (PWM), or frequency. In PWM-type approaches, there are no LMIs conditions that guarantee asymmetric saturation and/or null constraint. Benzaouia et al. (2014) reported unsatisfactory results at each change of reference (control application in a Buck converter), evidencing overcoming physical limits imposed for the duty cycle.

3.5 Conclusions

The uncertainty from the recruitment function, fault in the actuator, and other non-ideality parameters add an error to the model, specifically to nominal torque $M^{d}_{a\,nom}$ and in the value of $\breve{u}^{d}$. This analysis explains why different muscle torque estimation-based control techniques yields regulation error.

The novelty of this work was to use switched control law subject to saturation applied to compensate plant uncertainties. This technique was compared to the literature using the PDC controller. The results showed better performance for the switched control.

Thus, the contribution of this work was improved performance of isometric contraction evoked by electrical stimuli dealing the non-ideal conditions (fatigue, spasms, tremor, muscular activation and fault in the actuator) as uncertainties in the control design.

Future works may investigate a new mathematical model for the plant, relating muscle activation and kinematic variables appropriately without relying on muscle torque estimation.

4 A NEW ACCELERATION-BASED MODEL APPLIED TO ELECTRICALLY STIMULATED LOWER LIMBS

"Just do not give up on the first attempts, persistence is a friend of conquest. If you want to get where most do not go, do what most do not".

Bill Gates

Electrical stimulation is an important technique, which minimizes muscle spasticity and restores paralyzed limb movements. A mathematical model of plant dynamics is fundamental to control design. Different control techniques have been proposed based on nonlinear model and with parametric uncertainties. However, most studies use models based on angular position, velocity, and torque as state variables. In practical applications, measuring torque is very difficult for isotonic contractions. In this Chapter, we present a new nonlinear model whose state variables are the angular position, velocity and acceleration. Thus, the torque is replaced by angular acceleration, which can be measured by accelerometers. In addition, the nonlinear plant modeled by the proposed approach is described by TS fuzzy models and the design of a fuzzy regulator is presented. At the significance level of 0.05, a statistical analysis of closed-loop control was performed for healthy and paraplegic individuals at different operating points.

4.1 Introduction

Functional electrical stimulation has been shown to be important for rehabilitation, muscle strengthening and movement execution in individuals with spinal cord injury.

The mathematical model of the plant to be controlled is fundamental for the controllers design. In particular, the relationship among voltage or current amplitude, pulse width, frequency and corresponding joint movement must be well understood. However, this process involves biomechanical interactions and complex, nonlinear and uncertain physiological phenomena (DORGAN; O'MALLEY, 1997; PREVIDI, 2002; SCHAUER et al., 2005).

Basically, the dynamic models of musculoskeletal systems for FES control are divided into two types. The first type refers to approaches whose purpose is to model internal processes of the muscle, such as the models proposed by Hill, Huxley or combination of both. From these derive mathematical models for isometric force prediction (DING; WEXLER; BINDER–MACLEOD, 2002; FREY LAW; SHIELDS, 2007), fatigue (MARION; WEXLER; HULL, 2010) and movement (PERUMAL; WEXLER; BINDER-MACLEOD, 2006) of the lower limb from muscle contraction coming from electrical stimuli. However, modeling may be more complex due to the analysis of biochemical factors and complicated measurement of internal parameters. Thus, this model complicates its experimental validation with closed-loop controllers. The second type of approach is the most common one for implementing real-time controllers because they use black-box or gray-box modeling strategies.

In black-box modeling, mathematical representations are determined without knowledge of the physical laws that describe the behavior of the system. For example, Previdi (2002) used a nonlinear autoregressive exogenous black-box (NARX). The drawback of empirical models based on the input-output relationship is that their parameters do not have a physical meaning. In turn gray-box modeling, the structure of the identification model and its parameters are associated with the dynamics of the system (FRANKEN et al., 1993; RIENER; QUINTERN; SCHMIDT, 1996; FERRARIN; PEDOTTI, 2000; KIRSCH; ALIBEJI; SHARMA, 2017). Riener, Quintern and Schmidt (1996) proposed a biomechanical model for the knee joint and introduced functions in the activation dynamics and muscle contraction to characterize the system regarding the stimulation parameters. The Ferrarin and Pedotti's model presented experimental tests to obtain a second-order nonlinear model (FERRARIN; PEDOTTI, 2000). The experimental procedure consists of two phases and takes into account the gravitational and inertial characteristics of the anatomical segments together with the damping and stiffness properties of the knee. Schauer et al. (2005) proposed an online approach to identify the parameters using normalized radial basis function network and an extended Kalman filter to estimate model parameters. Although the proposed technique is valid, obviously the implementation of this technique is a challenge for embedded systems. Lynch, Graham and Popovic (2011a) included a block of nonidealities to the Ferrarin and Pedotti's model. Experimental tests performed by Kirsch, Alibeji and Sharma (2017) improved the methods proposed by Stein et al. (1996), Riener, Quintern and Schmidt (1996) for parameter estimation.

The future expectation is that the closed-loop electrical stimulation allows injured individuals to perform precise movements in different applications such as cycling (BO et al., 2017), swimming, standing, sitting pivot transfer, walking, and among others. However, the most studies consider angular position, velocity, and muscle torque as state variables due to the fact that obtaining and monitoring the dynamic torque in real time is a difficult process for experimental validation (KIRSCH; ALIBEJI; SHARMA, 2017; TEIXEIRA et al., 2006; FERRARIN; PEDOTTI, 2000).

Overcoming this challenge, we propose a new model whose state variables are angular position, velocity and acceleration. And the electrical signals of these variables can be measurable by sensors like electrogoniometer, gyroscope, and accelerometer. Other techniques for measuring the state variables can also be employed. We exemplify the use of the model for the TS fuzzy controller design. Therefore, we intend that from this study, other control techniques can be tested and compared.

In addition, the model proposed in this chapter tends to the employment of wearable sensors. In lower limb applications, inertial sensors have been extensively studied for gait analysis, orientation and motion tracking (LUINGE; VELTINK, 2005; DEJNABADI et al., 2006; COOPER et al., 2009; SEEL; RAISCH; SCHAUER, 2014), evaluation of knee ligament injury (FAVRE et al., 2008), and monitoring of muscle fatigue, e.g. mechanomiography (KRUEGER; POPOVIĆ-MANESKI; NOHAMA, 2018).

The rest of the chapter is organized as follows. Section 4.2 presents the acceleration-based dynamic model. Section 4.3 describes the TS fuzzy representation for the nonlinear model proposed. Section shows the fuzzy control design of electrically stimulated lower limb based on LMIs, and discusses the results obtained. Section 4.5 presents a conclusion about the results and a perspective for future studies.

For convenience, in some places, the following notation is used: the symbols $\mathbb{R}$, $\mathbb{R}_+$, and $\mathbb{Z}_+^*$ represent the set of real, positive real, and non-zero positive integers numbers, respectively; the set $\mathbb{I}_{n_r} = \{1,\ 2, \cdots,\ n_r\}$, $n_r \in \mathbb{Z}_+^*$; $\mathbf{I}_n$ denotes the identity matrix of size $n \times n$; all state variables will be considered as time-dependent, for example $x_n(t) = x_n$, when $x_n(t)$ is explicit it will be to emphasize dependence in the time domain; $co\{a_1,\ a_2,\ \cdots,\ a_r\}$ is the convex hull of the vectors a_i, $i \in \mathbb{I}_r$; $\dot{x}_i(t)$ denotes $\dfrac{\partial x_i(t)}{\partial t}$, and $w_d(z) = \dfrac{\partial w(z)}{\partial z}$.

4.2 Acceleration-based proposed model

Consider the lower limb dynamic model, described by nonlinear functions $\tilde{\mathtt{w}}(z)$, $\tilde{\mathtt{r}}(z)$, $\tilde{\mathtt{b}}(z)$, $\tilde{\mathtt{m}}(z)$, $\tilde{\mathtt{n}}(z) : \mathbb{R} \to \mathbb{R}$, $\tilde{\mathtt{b}}(z) \neq 0$, and $\tilde{\mathtt{n}}(z) \neq 0$, for all $z(t) \in \mathbb{R}$:

$$\begin{cases} \dot{\check{x}}_1 = \check{x}_2 \\ \dot{\check{x}}_2 = \tilde{\mathtt{w}}(z) + \tilde{\mathtt{r}}(z)\check{x}_2 + \tilde{\mathtt{b}}(z)\check{x}_3\ , \\ \dot{\check{x}}_3 = \tilde{\mathtt{m}}(z)\check{x}_3 + \tilde{\mathtt{n}}(z)\check{u} \end{cases} \tag{80}$$

where the state vector $\check{\mathbf{x}}(t) = \begin{bmatrix} \check{x}_1 & \check{x}_2 & \check{x}_3 \end{bmatrix}^T$, $\check{x}_1$ is the angular position, $\check{x}_2$ is the angular velocity, $\check{x}_3$ is the muscle activation provided by an estimated muscle torque, and $\check{u}$ is the pulse width of the electric stimulus applied to the muscle.

Thus, from (80), considering that $\tilde{\mathtt{b}}(z) \neq 0$, and $\ddot{\check{x}}_1 = \dot{\check{x}}_2$:

$$\check{x}_3 = \frac{1}{\tilde{\mathtt{b}}(z)} \left[\ddot{\check{x}}_1 - \tilde{\mathtt{w}}(z) - \tilde{\mathtt{r}}(z)\check{x}_2\right]. \tag{81}$$

Applying time derivative in (81),

$$\dot{\check{x}}_3 = \frac{1}{\tilde{\mathtt{b}}(z)^2} \left\{ \left[\dddot{\check{x}}_1 - \tilde{\mathtt{w}}_d(z)\dot{z} - \tilde{\mathtt{r}}(z)\dot{\check{x}}_2 - \tilde{\mathtt{r}}_d(z)\dot{z}\check{x}_2\right] \tilde{\mathtt{b}}(z) - \left[\ddot{\check{x}}_1 - \tilde{\mathtt{w}}(z) - \tilde{\mathtt{r}}(z)\check{x}_2\right] \tilde{\mathtt{b}}_d(z)\dot{z} \right\}, \tag{82}$$

where $\tilde{\mathtt{w}}_d(z) = \dfrac{\partial \tilde{\mathtt{w}}}{\partial z}$, $\tilde{\mathtt{r}}_d(z) = \dfrac{\partial \tilde{\mathtt{r}}}{\partial z}$, and $\tilde{\mathtt{b}}_d(z) = \dfrac{\partial \tilde{\mathtt{b}}}{\partial z}$.

Again from (80), for $\tilde{\mathtt{n}}(z) \neq 0$,

$$\breve{u} = \frac{1}{\tilde{\mathtt{n}}(z)}\dot{\breve{x}}_3 - \frac{\tilde{\mathtt{m}}(z)}{\tilde{\mathtt{n}}(z)}\breve{x}_3. \tag{83}$$

Replacing (81) and (82) into (83) one obtains

$$\breve{u} = \frac{1}{\tilde{\mathtt{n}}(z)\tilde{\mathtt{b}}(z)^2}\left\{\left[\dddot{\breve{x}}_1 - \tilde{\mathtt{w}}_d(z)\dot{z} - \tilde{\mathtt{r}}(z)\dot{\breve{x}}_2 - \tilde{\mathtt{r}}_d(z)\dot{z}\breve{x}_2\right]\tilde{\mathtt{b}}(z) - \left[\ddot{\breve{x}}_1 - \tilde{\mathtt{w}}(z) - \tilde{\mathtt{r}}(z)\breve{x}_2\right]\tilde{\mathtt{b}}_d(z)\dot{z}\right\}$$
$$- \frac{\tilde{\mathtt{m}}(z)}{\tilde{\mathtt{n}}(z)\tilde{\mathtt{b}}(z)}\left[\ddot{\breve{x}}_1 - \tilde{\mathtt{w}}(z) - \tilde{\mathtt{r}}(z)\breve{x}_2\right]. \tag{84}$$

Defining new variables $\breve{x}_{1n} = \breve{x}_1$, $\breve{x}_{2n} = \breve{x}_2 = \dot{\breve{x}}_1$ and $\breve{x}_{3n} = \dot{\breve{x}}_2 = \ddot{\breve{x}}_1$, thus (84) can be rewritten as:

$$\breve{u} = \frac{1}{\tilde{\mathtt{n}}(z)\tilde{\mathtt{b}}(z)}\dot{\breve{x}}_{3n} + \frac{1}{\tilde{\mathtt{n}}(z)\tilde{\mathtt{b}}(z)}\left[\frac{\tilde{\mathtt{b}}_d(z)\dot{z}\tilde{\mathtt{w}}(z)}{\tilde{\mathtt{b}}(z)} + \tilde{\mathtt{m}}(z)\tilde{\mathtt{w}}(z)\right]$$
$$+ \frac{1}{\tilde{\mathtt{n}}(z)\tilde{\mathtt{b}}(z)}\left[-\frac{\tilde{\mathtt{w}}_d(z)\dot{z}}{\breve{x}_{2n}} + \frac{\tilde{\mathtt{b}}_d(z)\dot{z}\tilde{\mathtt{r}}(z)}{\tilde{\mathtt{b}}(z)} - \tilde{\mathtt{r}}_d(z)\dot{z} + \tilde{\mathtt{m}}(z)\tilde{\mathtt{r}}(z)\right]\breve{x}_{2n}$$
$$+ \frac{1}{\tilde{\mathtt{n}}(z)\tilde{\mathtt{b}}(z)}\left[-\tilde{\mathtt{r}}(z) - \frac{\tilde{\mathtt{b}}_d(z)\dot{z}}{\tilde{\mathtt{b}}(z)} - \tilde{\mathtt{m}}(z)\right]\breve{x}_{3n},$$

or rewriting,

$$\dot{\breve{x}}_{3n} = \left[\frac{-\tilde{\mathtt{b}}_d(z)\dot{z}\tilde{\mathtt{w}}(z)}{\tilde{\mathtt{b}}(z)} - \tilde{\mathtt{m}}(z)\tilde{\mathtt{w}}(z)\right]$$
$$+ \left[\frac{\tilde{\mathtt{w}}_d(z)\dot{z}}{\breve{x}_{2n}} - \frac{\tilde{\mathtt{b}}_d(z)\dot{z}\tilde{\mathtt{r}}(z)}{\tilde{\mathtt{b}}(z)} + \tilde{\mathtt{r}}_d(z)\dot{z} - \tilde{\mathtt{m}}(z)\tilde{\mathtt{r}}(z)\right]\breve{x}_{2n}$$
$$+ \left[\tilde{\mathtt{r}}(z) + \frac{\tilde{\mathtt{b}}_d(z)\dot{z}}{\tilde{\mathtt{b}}(z)} + \tilde{\mathtt{m}}(z)\right]\breve{x}_{3n} + \tilde{\mathtt{n}}(z)\tilde{\mathtt{b}}(z)\breve{u}.$$

Therefore, the novel acceleration-based nonlinear model is expressed:

$$\begin{cases} \dot{\breve{x}}_{1n} = \breve{x}_{2n} \\ \dot{\breve{x}}_{2n} = \breve{x}_{3n} \\ \dot{\breve{x}}_{3n} = \left[\dfrac{-\tilde{\mathtt{b}}_d(z)\dot{z}\tilde{\mathtt{w}}(z)}{\tilde{\mathtt{b}}(z)} - \tilde{\mathtt{m}}(z)\tilde{\mathtt{w}}(z)\right] + \left[\dfrac{\tilde{\mathtt{w}}_d(z)\dot{z}}{\breve{x}_{2n}} - \dfrac{\tilde{\mathtt{b}}_d(z)\dot{z}\tilde{\mathtt{r}}(z)}{\tilde{\mathtt{b}}(z)} + \tilde{\mathtt{r}}_d(z)\dot{z} - \tilde{\mathtt{m}}(z)\tilde{\mathtt{r}}(z)\right]\breve{x}_{2n} \\ \qquad + \left[\tilde{\mathtt{r}}(z) + \dfrac{\tilde{\mathtt{b}}_d(z)\dot{z}}{\tilde{\mathtt{b}}(z)} + \tilde{\mathtt{m}}(z)\right]\breve{x}_{3n} + \tilde{\mathtt{n}}(z)\tilde{\mathtt{b}}(z)\breve{u} \end{cases} \tag{85}$$

where the state vector $\breve{\mathbf{x}}_n(t) = \begin{bmatrix}\breve{x}_{1n} & \breve{x}_{2n} & \breve{x}_{3n}\end{bmatrix}^T$, $\breve{x}_{1n}$ is the angular position, $\breve{x}_{2n}$ is the angular velocity, and $\breve{x}_{3n}$ is angular acceleration.

4.2.1 Example: knee joint

The dynamic model for knee joint control is given by the equilibrium between inertial torque and the gravitational torque $\tilde{H}_g(\theta_v)$, passive musculoskeletal torque $\tilde{\Lambda}_p(\phi_k, \dot{\phi}_k)$ (composed by stiffness $\tilde{\Lambda}_s(\phi_k)$ and damping $\Lambda_d(\dot{\phi}_k)$ components), and muscular torque generated by the electrical stimulation $\Gamma_{ke}(\phi_k, \dot{\phi}_k, a_{ke})$:

$$J\ddot{\theta}_v = \tilde{H}_g(\theta_v) + \tilde{\Lambda}_p(\phi_k, \dot{\phi}_k) + \Gamma_{ke}(\phi_k, \dot{\phi}_k, a_{ke}),$$

where θ_v, $\dot{\theta}_v \in \mathbb{R}$ is the angular position and velocity of the leg (shank-foot complex), respectively; ϕ_k, $\dot{\phi}_k \in \mathbb{R}$ are the knee joint angle and velocity, respectively; and a_{ke} is muscle activation.

The technique proposed in this chapter is exemplified based on the Ferrarin and Pedotti's model (FERRARIN; PEDOTTI, 2000). The dynamic equilibrium is expressed by a second-order nonlinear differential equation:

$$J\ddot{\theta}_v = -mgl\sin(\theta_v) - \lambda e^{-E\phi_k}(\phi_k - \omega) - B\dot{\phi}_k + M_a, \tag{86}$$

where $J \in \mathbb{R}_+$ is the inertial moment of the shank-foot complex; $\phi_k = \theta_v + \dfrac{\pi}{2} \in \mathbb{R}$ is the knee angle, between the shank and the thigh on sagittal plane; $\dot{\phi}_k = \dot{\theta}_v \in \mathbb{R}$ is the knee angular velocity; $m \in \mathbb{R}_+$ is the mass of shank-foot complex; $g \in \mathbb{R}_+$ is the gravitational acceleration; $l \in \mathbb{R}$ is the distance between the knee and the shank-foot complex mass center; $B \in \mathbb{R}_+$ is the viscous friction coefficient; $\lambda, E \in \mathbb{R}_+$ are the coefficients of the exponential terms and $\omega \in \mathbb{R}_+$ is the elastic rest angle of the knee; and $M_a \in \mathbb{R}$ is muscular torque generated by electrical stimulation.

The muscle activation M_a, that can be modeled by first order system as:

$$\frac{M_a}{p} = \frac{G}{\tau s + 1} \quad \Longleftrightarrow \quad \dot{M}_a = \frac{1}{\tau}(-M_a + Gp) \tag{87}$$

where G, $\tau \in \mathbb{R}$ are positive constants related to muscular torque; $p \in \mathbb{R}_+$ electrical stimulation pulse width.

Ferrarin and Pedotti suggest an experimental method for obtaining the model's parameters. These parameters refer to healthy (H1-H5) and paraplegic individuals (P1-P3), as described in the Table 10.

Considering $\check{x}_1 = \theta_v$, $\check{x}_2 = \dot{\theta}_v$, $\check{x}_3 = M_a$, and $\check{u} = p$ the dynamic (86)-(87) can be expressed

Table 10 - Model's parameter proposed by Ferrarin and Pedotti for healthy (H1-H5) and paraplegic (P1-P3) individuals.

Parameter [unit]	**H1**	**H2**	**H3**	**H4**	**H5**	**P1**	**P2**	**P3**
J [kg.m^2]	0.377	0.358	0.399	0.375	0.384	0.362	0.292	0.394
m [kg]	4.05	4.63	4.38	3.83	4.36	4.37	3.42	4.76
l [m]	0.253	0.239	0.248	0.237	0.243	0.238	0.231	0.233
B [N.m.s/rad]	0.377	0.311	0.400	0.305	0.332	0.270	0.302	0.289
λ [N.m/rad]	1.199	4.679	3.657	4.490	3.889	41.208	3.761	15.352
E [rad^{-1}]	-0.486	0.041	-0.031	0.257	-0.079	2.024	1.317	1.644
ω [rad]	2.548	2.427	2.710	2.701	2.412	0.264	0.264	0.264
G [N.m/s]	40000	40000	38500	40000	50000	42500	12500	11500
τ [s]	0.454	0.426	0.491	0.406	0.438	0.951	0.203	0.215

Source: From (FERRARIN; PEDOTTI, 2000).

in a state-space formulation as (80), such that:

$$\begin{cases} \dot{\check{x}}_1 = \check{x}_2 \\ \dot{\check{x}}_2 = \dfrac{1}{J}\left[-mgl\sin(\check{x}_1) - \lambda e^{-E\left(\check{x}_1+\frac{\pi}{2}\right)}\left(\check{x}_1+\dfrac{\pi}{2}-\omega\right)\right] - \dfrac{B}{J}\check{x}_2 + \dfrac{1}{J}\check{x}_3 \\ \dot{\check{x}}_3 = -\dfrac{1}{\tau}\check{x}_3 + \dfrac{G}{\tau}\check{u}. \end{cases} \tag{88}$$

Teixeira et al. (2006) proposed the following state space representation of the system:

$$\dot{\check{\mathbf{x}}}(t) = \begin{bmatrix} 0 & 1 & 0 \\ \tilde{f}_{21}(\check{x}_1) & -\dfrac{B}{J} & \dfrac{1}{J} \\ 0 & 0 & -\dfrac{1}{\tau} \end{bmatrix} \check{\mathbf{x}}(t) + \begin{bmatrix} 0 \\ 0 \\ \dfrac{G}{\tau} \end{bmatrix} \check{\mathbf{u}}(t),$$

where $\check{\mathbf{x}}(t) = \begin{bmatrix} \check{x}_1 & \check{x}_2 & \check{x}_3 \end{bmatrix}^T$, $\check{\mathbf{u}}(t)$ is the control input, and $\tilde{f}_{21}(\check{x}_1)$ is given by:

$$\tilde{f}_{21}(\check{x}_1) = \frac{1}{J\check{x}_1}\left[-mgl\sin(\check{x}_1) - \lambda e^{-E\left(\check{x}_1+\frac{\pi}{2}\right)}\left(\check{x}_1+\frac{\pi}{2}-\omega\right)\right].$$

Note that the state variables are position, velocity, and torque. However, it is challenging to estimate the torque for each closed-loop operation point.

To overcome this problem, a novel state space model is obtained, and the torque variable is replaced by angular acceleration. Consequently, an adequate representation from measurable variables is obtained for state feedback control.

From (80) and (88), it follows that the function $\tilde{\mathtt{w}}(z)$ is associated with the gravitational and stiffness torque components. In addition, z is related only to angular position $\check{x}_1$, and then the following relation is valid:

$$\tilde{\mathtt{w}}(z)=\tilde{\mathtt{w}}(\check{x}_1)=\frac{1}{J}\left[-mgl\sin\left(\check{x}_1\right)-\lambda e^{-E\left(\check{x}_1+\frac{\pi}{2}\right)}\left(\check{x}_1+\frac{\pi}{2}-\omega\right)\right], \tag{89}$$

while the functions $\tilde{\mathtt{r}}(z)$ and $\tilde{\mathtt{b}}(z)$ are constant parameters,

$$\tilde{\mathtt{r}}(z)=\mathtt{r}=-\frac{B}{J}, \tag{90}$$

$$\tilde{\mathtt{b}}(z)=\mathtt{b}=\frac{1}{J}. \tag{91}$$

Furthermore, the functions $\tilde{\mathtt{m}}(z)$ and $\tilde{\mathtt{n}}(z)$ are associated with muscle activation parameters,

$$\tilde{\mathtt{m}}(z)=\mathtt{m}(\tau)=-\frac{1}{\tau}, \tag{92}$$

$$\tilde{\mathtt{n}}(z)=\mathtt{r}(G,\tau)=\frac{G}{\tau}. \tag{93}$$

Therefore, considering that from (88), $\dot{\check{x}}_1=\check{x}_2$, then the following relations hold:

$$\dot{\tilde{\mathtt{w}}}(z)\dot{z}=\frac{\partial\tilde{\mathtt{w}}(\check{x}_1)}{\partial\check{x}_1}\dot{\check{x}}_1=\frac{1}{J}\left[-mgl\cos\left(\check{x}_1\right)-\lambda e^{-E\left(\check{x}_1+\frac{\pi}{2}\right)}+\lambda Ee^{-E\left(\check{x}_1+\frac{\pi}{2}\right)}\left(\check{x}_1+\frac{\pi}{2}-\omega\right)\right]\check{x}_2, \tag{94}$$

$$\dot{\tilde{\mathtt{b}}}(z)=0, \tag{95}$$

$$\dot{\tilde{\mathtt{r}}}(z)=0. \tag{96}$$

Replacing (89)-(96) in (85) one obtains (98). The final aim is to design a controller that keeps the angular position at desired position $\theta_v=\check{x}_{1n}=\theta_0$, after a transient response. From the third equation in (98), in the equilibrium point, $\check{x}_{2n}=\check{x}_{3n}=0$, and $\check{u}=\check{u}_0$, such that

$$\check{u}_0=\frac{\left[mgl\sin\left(\theta_0\right)+\lambda e^{-E\left(\theta_0+\frac{\pi}{2}\right)}\left(\theta_0+\frac{\pi}{2}-\omega\right)\right]}{G}. \tag{97}$$

$$\begin{cases}\dot{\check{x}}_{1n}=\check{x}_{2n}\\ \dot{\check{x}}_{2n}=\check{x}_{3n}\\ \dot{\check{x}}_{3n}=\dfrac{1}{\tau J}\left[-mgl\sin\left(\check{x}_{1n}\right)-\lambda e^{-E\left(\check{x}_{1n}+\frac{\pi}{2}\right)}\left(\check{x}_{1n}+\dfrac{\pi}{2}-\omega\right)\right]\\ \qquad+\dfrac{1}{J}\left[-mgl\cos\left(\check{x}_{1n}\right)-\lambda e^{-E\left(\check{x}_{1n}+\frac{\pi}{2}\right)}+\lambda Ee^{-E\left(\check{x}_{1n}+\frac{\pi}{2}\right)}\left(\check{x}_{1n}+\dfrac{\pi}{2}-\omega\right)-\dfrac{B}{\tau}\right]\check{x}_{2n}\\ \qquad\qquad+\left[-\dfrac{B}{J}-\dfrac{1}{\tau}\right]\check{x}_{3n}+\dfrac{G}{\tau J}\check{u}.\end{cases} \tag{98}$$

The equilibrium point is not at the origin $[\check{x}_{1n}\quad\check{x}_{2n}\quad\check{x}_{3n}]^T=[0\quad 0\quad 0]^T$. Thus, the following change of coordinates is necessary for stability analysis: $x_1 = \check{x}_{1n} - \theta_0$, $x_2 = \check{x}_{2n}$, $x_3 = \check{x}_{3n}$, and $u = \check{u} - \check{u}_0$.

Hence, considering (97) the system (98) can be rewritten as:

$$\dot{\mathbf{x}}(t) = \begin{bmatrix} 0 & 1 & 0 \\ 0 & 0 & 1 \\ \tilde{\mathfrak{L}}(x_1,\theta_0) & \tilde{\mathfrak{I}}(x_1,\theta_0) & \mathfrak{E} \end{bmatrix} \mathbf{x}(t) + \begin{bmatrix} 0 \\ 0 \\ \mathfrak{B} \end{bmatrix} \mathbf{u}(t). \tag{99}$$

where state vector is $\mathbf{x}(t) = \begin{bmatrix} x_1 & x_2 & x_3 \end{bmatrix}^T$, x_1 is the error between the angular position $\check{x}_{1n}$ and reference θ_0, x_2 is the angular velocity, and x_3 is the angular acceleration. The functions $\tilde{\mathfrak{L}}(x_1,\theta_0)$, $\tilde{\mathfrak{I}}(x_1,\theta_0)$, and the parameters $\mathfrak{E}$ and $\mathfrak{B}$ are given by:

$$\tilde{\mathfrak{L}}(x_1,\theta_0) = \frac{1}{\tau J x_1}\left[-mgl\sin(x_1+\theta_0) - \lambda e^{-E\left(x_1+\theta_0+\frac{\pi}{2}\right)}\left(x_1+\theta_0+\frac{\pi}{2}-\omega\right)\right],$$

$$\begin{aligned}\tilde{\mathfrak{I}}(x_1,\theta_0) = \frac{1}{J}\Big[&-mgl\cos(x_1+\theta_0) - \lambda e^{-E\left(x_1+\theta_0+\frac{\pi}{2}\right)} \\ &+\lambda E e^{-E\left(x_1+\theta_0+\frac{\pi}{2}\right)}\left(x_1+\theta_0+\frac{\pi}{2}-\omega\right) - \frac{B}{\tau}\Big],\end{aligned}$$

$$\mathfrak{E} = \left(-\frac{B}{J} - \frac{1}{\tau}\right),$$

$$\mathfrak{B} = \frac{G}{\tau J}.$$

In the next section we present the TS fuzzy technique to describe nonlinear system using the local models convex combination.

4.3 TS fuzzy representation

Fuzzy systems are considered universal approximation of functions, because it has the capacity to infer qualitative and even uncertain information (WANG; MENDEL, 1992). Through fuzzy modeling we obtain exact representation of nonlinear functions, given by a number of local and time-invariant linear models. The fuzzy representation is established by the designer, in order to obtain a satisfactory description of the system at different points in the space of states. Thus, more sophisticated models can be obtained, considering the plant dynamics in distant regions of the desired operation point. The sector-nonlinearity approach is shown in the next section (TANIGUCHI et al., 2001).

In the following Subsection, it will be exemplified the procedure (presented in the Section 3.2.1) for obtaining a TS fuzzy model that describes an uncertain nonlinear system.

4.3.1 TS fuzzy models for acceleration-based knee joint model

Given the system defined in (99), and defining that $\tilde{f}_{31}(\mathbf{z}(t)) = \tilde{\mathfrak{L}}(x_1, \theta_0)$, and $\tilde{f}_{32}(\mathbf{z}(t)) = \tilde{\mathfrak{I}}(x_1, \theta_0)$. To obtain the generalized form it is necessary to determine the maximum and minimum values of the functions considering the compact set. The following set $\mathfrak{D}_0$ was assumed, where $\mathbf{z}(t) = [x_1(t) \quad x_2(t) \quad x_3(t) \quad \theta_0(t)]^T$,

$$\mathfrak{D}_0 = \big\{\mathbf{z} \in \mathbb{R}^4 : -1.2 \leqslant x_1(t) \leqslant 1.2, -4 \leqslant x_2(t) \leqslant 4,\\ -10 \leqslant x_3(t) \leqslant 10,\ 0 \leqslant \theta_0(t) \leqslant 1.2\big\}.$$

For example, considering the healthy subject H1, the minimum and maximum values of nonlinear functions are

$$a_{31}^1 \equiv \max\left\{\tilde{f}_{31}\left(\mathbf{z}(t)\right)\right\} = -11.6851,$$

$$a_{31}^2 \equiv \min\left\{\tilde{f}_{31}\left(\mathbf{z}(t)\right)\right\} = -96.4022,$$

$$a_{32}^1 \equiv \max\left\{\tilde{f}_{32}\left(\mathbf{z}(t)\right)\right\} = -18.0064,$$

$$a_{32}^2 \equiv \min\left\{\tilde{f}_{32}\left(\mathbf{z}(t)\right)\right\} = -33.0229.$$

From (19)-(22) one obtains, respectively:

$$\sigma_{31}^1\left(\mathbf{z}(t)\right) = \frac{\tilde{f}_{31}\left(\mathbf{z}(t)\right) - a_{31}^2}{a_{31}^1 - a_{31}^2},$$

$$\sigma_{31}^2\left(\mathbf{z}(t)\right) = \frac{a_{31}^1 - \tilde{f}_{31}\left(\mathbf{z}(t)\right)}{a_{31}^1 - a_{31}^2},$$

$$\sigma_{32}^1\left(\mathbf{z}(t)\right) = \frac{\tilde{f}_{32}\left(\mathbf{z}(t)\right) - a_{32}^2}{a_{32}^1 - a_{32}^2},$$

$$\sigma_{32}^2\left(\mathbf{z}(t)\right) = \frac{a_{32}^1 - \tilde{f}_{32}\left(\mathbf{z}(t)\right)}{a_{32}^1 - a_{32}^2}.$$

The nonlinear function $\tilde{f}_{31}(\mathbf{z}(t))$ can be represented by a TS fuzzy model, considering two local models: a_{31}^1 e a_{31}^2, that is, according to (17) there exist $\sigma_{31}^1(\mathbf{z}(t))$ and $\sigma_{31}^2(\mathbf{z}(t))$ such that,

$$\tilde{f}_{31}(\mathbf{z}(t)) = \sigma_{31}^1(\mathbf{z}(t))a_{31}^1 + \sigma_{31}^2(\mathbf{z}(t))a_{31}^2,$$

with $\sum_{t_{(i,j)}^a=1}^{2} \sigma_{31}^{t_{(i,j)}^a}\left(\mathbf{z}(t)\right) = 1$, and $0 \leqslant \sigma_{31}^{t_{(i,j)}^a}\left(\mathbf{z}(t)\right) \leqslant 1$.

Likewise, from (17) the function $\tilde{f}_{32}(\mathbf{z}(t))$ can be represented by:

$$\tilde{f}_{32}(\mathbf{z}(t)) = \sigma_{32}^1(\mathbf{z}(t))a_{32}^1 + \sigma_{32}^2(\mathbf{z}(t))a_{32}^2,$$

with $\sum_{t^a_{(i,j)}=1}^{2} \sigma_{32}^{t^a_{(i,j)}}(\mathbf{z}(t)) = 1$, and $0 \leqslant \sigma_{32}^{t^a_{(i,j)}}(\mathbf{z}(t)) \leqslant 1$.

Considering the dynamic expressed in (99), from its uncertain/nonlinear terms, it follows $\mathscr{P}_A = \{(3,1),(3,2)\}$ and $\mathscr{P}_B = \{\}$. Therefore, $n_A = 2$, $n_B = 0$, and counting bijections are defined as $c_A(3,1) = 1$, $c_A(3,2) = 2$. There is no bijection for c_B. From (29) obtains the index φ for changing combinations of variable given by $t^a_{(i,j)}$ and expressed by

$$\varphi = 1 + \sum_{(i,j)\in\mathscr{P}_A} 2^{(c_A(i,j)-1)}\left(t^a_{(i,j)} - 1\right),$$

$$\varphi = 1 + \left(t^a_{(3,1)} - 1\right) + 2\left(t^a_{(3,2)} - 1\right). \tag{100}$$

From (30) and (100) obtains the membership functions

$$\begin{cases} \alpha_1(\mathbf{z}(t)) = \sigma_{32}^1(\mathbf{z}(t))\sigma_{31}^1(\mathbf{z}(t)), \\ \alpha_2(\mathbf{z}(t)) = \sigma_{32}^1(\mathbf{z}(t))\sigma_{31}^2(\mathbf{z}(t)), \\ \alpha_3(\mathbf{z}(t)) = \sigma_{32}^2(\mathbf{z}(t))\sigma_{31}^1(\mathbf{z}(t)), \\ \alpha_4(\mathbf{z}(t)) = \sigma_{32}^2(\mathbf{z}(t))\sigma_{31}^2(\mathbf{z}(t)), \end{cases} \tag{101}$$

satisfying to $\sum_{\varphi=1}^{4} \alpha_\varphi(\mathbf{z}(t)) = 1$.

The dynamic (99) can be described by a convex combination (101) of local models of the T-S fuzzy system as expressed in (14). The local models are obtained from (31)-(32), considering $\varphi \in \mathbb{I}_4$. In such a way that from (31) one obtains

$$\begin{aligned} \mathbf{A}_1 &= \bar{\mathbb{A}} + a_{31}^1\mathbb{A}_{31} + a_{32}^1\mathbb{A}_{32}, \\ \mathbf{A}_2 &= \bar{\mathbb{A}} + a_{31}^2\mathbb{A}_{31} + a_{32}^1\mathbb{A}_{32}, \\ \mathbf{A}_3 &= \bar{\mathbb{A}} + a_{31}^1\mathbb{A}_{31} + a_{32}^2\mathbb{A}_{32}, \\ \mathbf{A}_4 &= \bar{\mathbb{A}} + a_{31}^2\mathbb{A}_{31} + a_{32}^2\mathbb{A}_{32}, \end{aligned}$$

where the matrices $\mathbb{A}_{31}$ and $\mathbb{A}_{32}$ are

$$\mathbb{A}_{31} = \begin{bmatrix} 0 & 0 & 0 \\ 0 & 0 & 0 \\ 1 & 0 & 0 \end{bmatrix}, \mathbb{A}_{32} = \begin{bmatrix} 0 & 0 & 0 \\ 0 & 0 & 0 \\ 0 & 1 & 0 \end{bmatrix}.$$

And from (32) one obtains

$$\mathbf{B}_1 = \mathbf{B}_2 = \mathbf{B}_3 = \mathbf{B}_4 = \bar{\mathbb{B}}.$$

Table 11 - Parameter of the TS fuzzy local models for healthy and paraplegic individuals.

Subjects	a_{31}^1	a_{31}^2	a_{32}^1	a_{32}^2
H1	-11.6851	-96.4022	-18.0064	-33.0229
H2	-22.9496	-104.9125	10.8242	-45.0638
H3	-10.2088	-73.3120	7.6172	-38.0379
H4	-19.7044	-85.3859	13.3598	-36.5745
H5	-29.7279	-77.2926	3.0928	-39.8012
P1	7.1275	-141.4784	20.8478	-358.5996
P2	-37.9580	-165.5286	15.3002	-45.5599
P3	-35.4149	-177.0747	17.6995	-162.8031

Source: From author.

The matrices $\bar{\mathbb{A}}$ and $\bar{\mathbb{B}}$, respectively, are composed by the constant and known elements of the state matrix and control-input matrix, and using zeros for the remaining elements. From (99) , $\mathfrak{C} = \left(-\dfrac{B}{J} - \dfrac{1}{\tau}\right) = -5.3847$, and $\mathfrak{B} = \left(\dfrac{G}{\tau J}\right) = 1.3576 \times 10^5$ one obtains

$$\bar{\mathbb{A}} = \begin{bmatrix} 0 & 1 & 0 \\ 0 & 0 & 1 \\ 0 & 0 & -5.3847 \end{bmatrix}, \bar{\mathbb{B}} = \begin{bmatrix} 0 \\ 0 \\ 1.3576 \times 10^5 \end{bmatrix}.$$

Observe that the system (99) has two nonlinear functions $\tilde{f}_{31}(\mathbf{z}(t))$, $\tilde{f}_{32}(\mathbf{z}(t))$. Consequently were necessary $n_r = 2^2 = 4$ local models for exact representation of the system through TS fuzzy models.

In the next section, it will be presented a design procedure for the controller's gains through the stabilization conditions by Lyapunov functions and complemented by performance indexes, such as: decay rate, input and output constraints.

4.4 TS fuzzy control design

4.4.1 TS fuzzy controller

The Parallel Distributed Compensation (PDC) will be used in the design of fuzzy regulators to stabilize the nonlinear systems described by TS fuzzy models. The idea is to design a compensator for each rule of the fuzzy model. For each rule, using linear local models, linear control design techniques are used. The designed fuzzy controller shares the same sets of rules with the fuzzy model in the premise parts.

Considering the model fuzzy (13), the regulators via PDC have the following structure:

$$\begin{gathered} \mathrm{R}^{\varphi} : \text{IF } z_1(t) \text{ is } M_1^{\varphi} \text{ AND } \cdots \text{ AND } z_{n_z}(t) \text{ is } M_{n_z}^{\varphi}, \\ \text{THEN } \mathbf{u}(t) = -\mathbf{F}_{\varphi}\mathbf{x}(t), \quad \varphi \in \mathbb{I}_{n_r}. \end{gathered}$$

Similarly as (14), it can be concluded that:

$$\mathbf{u}(t) = -\sum_{\varphi=1}^{n_r} \alpha_\varphi(\mathbf{z}(t))\mathbf{F}_\varphi\mathbf{x}(t) = -\mathbf{F}(\alpha)\mathbf{x}(t). \tag{102}$$

The aim of the fuzzy regulator design is to determine the local feedback gains $\mathbf{F}_\varphi$ in the consequent parts (TANAKA; IKEDA; WANG, 1998).

Therefore, replacing equation (102) in (14), considering (30) one obtains:

$$\dot{\mathbf{x}}(t) = \sum_{i=1}^{n_r} \alpha_i(\mathbf{z}) \left[\mathbf{A}_i\mathbf{x}(t) - \mathbf{B}_i\left(\sum_{j=1}^{n_r} \alpha_j(\mathbf{z})\mathbf{F}_j\mathbf{x}(t)\right)\right]$$

$$\dot{\mathbf{x}}(t) = \sum_{i=1}^{n_r} \alpha_i(\mathbf{z}) \left[\sum_{j=1}^{n_r} \alpha_j(\mathbf{z})\mathbf{A}_i\mathbf{x}(t) - \sum_{j=1}^{n_r} \alpha_j(\mathbf{z})\mathbf{B}_i\mathbf{F}_j\mathbf{x}(t)\right],$$

$$\dot{\mathbf{x}}(t) = [\mathbf{A}(\alpha) - \mathbf{B}(\alpha)\mathbf{F}(\alpha)]\mathbf{x}(t). \tag{103}$$

Defining $\mathbf{G}_{ij} = \left[\mathbf{A}_i - \mathbf{B}_i\mathbf{F}_j\right]$, then (103) can be rewritten

$$\dot{\mathbf{x}}(t) = \sum_{i=1}^{n_r}\sum_{j=1}^{n_r} \alpha_i(\mathbf{z}(t))\alpha_j(\mathbf{z}(t))\left[\mathbf{A}_i - \mathbf{B}_i\mathbf{F}_j\right]\mathbf{x}(t), \tag{104}$$

$$\dot{\mathbf{x}}(t) = \sum_{i=1}^{n_r}\sum_{j=1}^{n_r} \alpha_i(\mathbf{z}(t))\alpha_j(\mathbf{z}(t))\mathbf{G}_{ij}x(t),$$

$$\dot{\mathbf{x}}(t) = \sum_{i=1}^{n_r} \alpha_i^2(\mathbf{z}(t))\mathbf{G}_{ii}\mathbf{x}(t) + 2\sum_{i<j}^{n_r} \alpha_i(\mathbf{z}(t))\alpha_j(\mathbf{z}(t))\left[\frac{\mathbf{G}_{ij}+\mathbf{G}_{ji}}{2}\right]\mathbf{x}(t),$$

where

$$\sum_{i<j}^{n_r} \alpha_{ij} = \sum_{i=1}^{n_r-1}\sum_{j=i+1}^{n_r} \alpha_{ij}.$$

4.4.2 Stabilization and constraints in the control design

Stabilization and constraints in controller design for nonlinear systems using TS fuzzy models via LMIs are presented in this Subsection.

As a performance index for system analysis, the decay rate, input constraint, and operation region will also be considered in LMIs.

4.4.2.1 Decay rate

Theorem 3. *(TANAKA; WANG, 2001) The equilibrium point $\mathbf{x} = \mathbf{0}$ of the continuous-time fuzzy control system given in* (14) *is globally asymptotically stable with a decay rate greater than* *or equal to β, if there is a positive definite symmetric matrix $\mathbf{X} \in \mathbb{R}^{n_x \times n_x}(\mathbf{X} > \mathbf{0})$ and matrices $\mathbf{M}_i \in \mathbb{R}^{n_x \times n_u}$ such that for all $i, j \in \mathbb{I}_{n_r}$, the following LMIs are feasible:*

$$-\mathbf{X}\mathbf{A}_i^T - \mathbf{A}_i\mathbf{X} + \mathbf{B}_i\mathbf{M}_i + \mathbf{M}_i^T\mathbf{B}_i^T - 2\beta\mathbf{X} > \mathbf{0}, i = 1, 2, \cdots, r, \tag{105}$$

$$-\left(\mathbf{A}_i + \mathbf{A}_j\right)\mathbf{X} - \mathbf{X}\left(\mathbf{A}_i + \mathbf{A}_j\right)^T + \mathbf{B}_i\mathbf{M}_j + \mathbf{B}_j\mathbf{M}_i + \mathbf{M}_i^T\mathbf{B}_j^T + \mathbf{M}_j^T\mathbf{B}_i^T - 4\beta\mathbf{X} \geq \mathbf{0}, \quad i < j, \tag{106}$$

if (105) *and* (106) *the gains are given by $\mathbf{F}_i = \mathbf{M}_i\mathbf{X}^{-1}$, $i \in \mathbb{I}_{n_r}$, guaranteed the global asymptotic stability of the system.*

Proof. The proof is detailed in Tanaka and Wang (2001). □

4.4.2.2 Input constraint

The electrical stimulators have a practical limitation on the control signal, the pulse width or amplitude can reach a maximum value to be applied on the muscle. For this reason, input constraint must be considered in control design.

Theorem 4. *(TANAKA; WANG, 2001) Assume a known initial condition $\mathbf{x}(0)$. The constraint $\|\mathbf{u}(t)\|_2 \leq \mu$ is complied for all time $t \geq 0$ if the following LMIs are feasible:*

$$\begin{bmatrix} 1 & \star \\ \mathbf{x}(0) & \mathbf{X} \end{bmatrix} \geq \mathbf{0}, \tag{107}$$

$$\begin{bmatrix} \mathbf{X} & \star \\ \mathbf{M}_i & \mu^2\mathbf{I} \end{bmatrix} \geq \mathbf{0}. \tag{108}$$

If this conditions are feasible the controller gains are given by $\mathbf{F}_i = \mathbf{M}_i\mathbf{X}^{-1}$, $i \in \mathbb{I}_{n_r}$.

Proof. The proof is detailed in Tanaka and Wang (2001).

□

4.4.2.3 Operation region

The fuzzy TS representation of a nonlinear system is adequate in a bounded domain of validity (KLUG et al., 2015). A low performance or system instability may occur when the state trajectories do not belong to the validity domain of the model. The domain of validity can be represented by a polyhedral set

$$\mathscr{O} \triangleq \left\{\mathbf{x}(t) \in \mathbb{R}^{n_x} : \left|\mathbf{N}_{(h)}\mathbf{x}(t)\right| \leqslant \phi_{(h)},\, h \in \mathbb{I}_p\right\}, \tag{109}$$

Figure 11 - State space trajectories $\bar{\mathbf{x}}_n(t)$ delimited by a region of operation $\mathscr{O}$, a positively invariant region $\mathscr{E}(\mathbf{P},1)$, and a set of initial conditions $\mathscr{X}$.

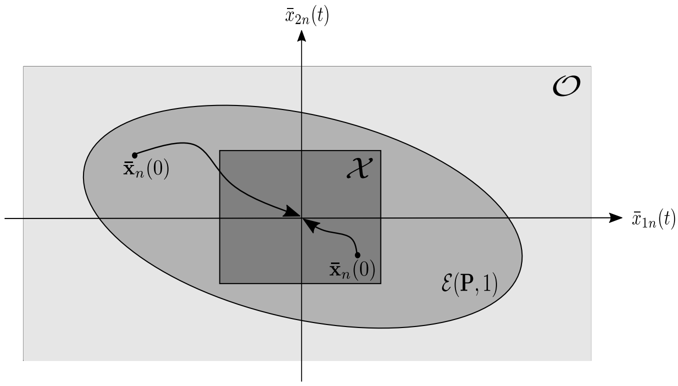

Source: From author.

where $\mathbf{N} = \begin{bmatrix} N_{(1)}^T & N_{(2)}^T \cdots N_{(p)}^T \end{bmatrix}^T \in \mathbb{R}^{p \times n_x}$ and $\phi = \begin{bmatrix} \phi_{(1)} & \phi_{(2)} \cdots \phi_{(p)} \end{bmatrix}^T \in \mathbb{R}^p$ are known.

Consider $\mathscr{E}(\mathbf{P},\delta)$ and $\mathscr{O}$ be the following sets:

$$\mathscr{E}(\mathbf{P},\delta) = \{\mathbf{x}(t) \in \mathbb{R}^{n_x} : \mathbf{x}(t)^T \mathbf{P}\mathbf{x}(t) \leqslant \delta\}. \tag{110}$$

An invariant region for the operation of the system is considered. Then the system state an initial condition in a suitable region within an operating region, will remain in this region for all $t \geqslant 0$. In other words, determining an invariant region, say $\mathscr{E}(\mathbf{P},\delta) \subset \mathscr{O}$, such that, for all $\mathbf{x}(0) \in \mathscr{E}(\mathbf{P},\delta)$, the state vector $\mathbf{x}(t)$ of (15) remains in the operating region $\mathscr{O}$ for all $t \geqslant 0$. Consequently, (14) exactly represents the system (15) for $t \geqslant 0$ and all $\mathbf{x}(0) \in \mathscr{E}(\mathbf{P},\delta)$.

For example, the Figure 11 illustrates possible state trajectories for a closed-loop system, where $\bar{\mathbf{x}}_n(t) = [\bar{x}_{1n}(t) \quad \bar{x}_{2n}(t)]^T \in \mathbb{R}^2$. Note that the desired initial conditions $\mathscr{X}$ are contained in the positively invariant set $\mathscr{E}(\mathbf{P},1)$, which in turn is a subset of the operating region $\mathscr{O}$ stipulated for the system. In other words, $\mathscr{X} \subset \mathscr{E}(\mathbf{P},1) \subset \mathscr{O}$. Then, for all trajectory in $\mathscr{X}$, or even $\mathscr{E}(\mathbf{P},1)$, the state trajectory is asymptotically stable.

Theorem 5. *Consider a nonlinear system described by* (15) *and an operation region* $\mathbf{x}(t) \in \mathscr{O}$, *for* $t \geqslant 0$, *given in* (109). *Assume that there exist a symmetric positive definite matrix* $\mathbf{X} \in \mathbb{R}^{n_x \times n_x}$, *such that*

$$\begin{bmatrix} \phi_{(h)}^2 & \mathbf{N}_{(h)}\mathbf{X} \\ \star & \mathbf{X} \end{bmatrix} \geqslant \mathbf{0}, \tag{111}$$

hold for all $h \in \mathbb{I}_p$. *Therefore, if* $\mathbf{x}(0) \in \mathscr{E}(\mathbf{P},1)$, *given in* (110), *where* $\mathbf{P} = \mathbf{X}^{-1}$, *then* $\mathbf{x}(t) \in \mathscr{O}$, $t \geqslant 0$.

Proof. More details are in Alves et al. (2016). □

A guarantee that a convex hull is contained in the invariant region $\mathscr{E}(\mathbf{P},1)$ is described in Remark 6.

Remark 6. *The constraint $\bar{\omega}\,\mathscr{W} \subset \mathscr{E}(\mathbf{P},1)$, where $\mathscr{W} = co\left\{w_1,\, w_2, \cdots,\, w_q\right\}$ and $\bar{\omega}$ is a positive constant, $\mathbf{w}_{i_w} \in \mathbb{R}^{n_x}$ for all $i_w \in \mathbb{I}_q$, is the convex hull of known vectors w_1, w_2, $\cdots$, w_q, is enforced if*

$$\begin{bmatrix} \bar{\omega}^{-2} & \star \\ \mathbf{w}_{i_w} & \mathbf{X} \end{bmatrix} \geqslant \mathbf{0}, \tag{112}$$

holds for all $i_w \in \mathbb{I}_q$. Thus, $\bar{\omega}$ can be used as a variable to obtain a less conservative estimate of the domain of attraction and to search the 'largest' ellipsoid $\mathscr{E}(\mathbf{P},1)$.

Observation 1. *The LMIs that specify input and norm constraints, and operating region must be considered together with the LMIs that guarantee the stability and decay rate, when specified.*

4.4.3 Controller for acceleration-based knee joint model

The LMIs were solved through the YALMIP language (EFBERG; LÖFBERG, 2004), MATLAB® software and SeDuMi solver (STURM, 1999).

Controller gains were based on LMIs that ensure decay rate (105)-(106), input constraint (107)-(108), an operating region (111), and a set of initial conditions (112). The following parameters were adopted for the healthy and paraplegic subjects: $\beta = 1.6$; $\bar{\omega}^{-2} = 1$; $\mathbf{N} = \mathbf{I}_3$; $\phi = [1.2 \quad 4 \quad 10]^T$; $\mathbf{w}_1 = [30\pi/180 \quad 0 \quad 0]^T$; $\mathbf{w}_2 = [-20\pi/180 \quad 0 \quad 0]^T$; $\mu = 0.001$.

In this study, it was considered control signal based on pulse width. These results can be obtained for other modulation techniques, such as voltage or current amplitude modulation.

The feedback gains and matrix $\mathbf{P}$ for healthy and paraplegic subjects are in the Tables 13 and 14. The following initial conditions $\mathbf{x}(0) = [0 \quad 0 \quad 0 \quad 0]^T$, $\theta_0 = 30^\circ$ for $0 \leqslant t < 10$ s, $\theta_0 = 47^\circ$ for $10 \leqslant t < 20$ s, $\theta_0 = 60^\circ$ for $20 \leqslant t < 30$ s, $\theta_0 = 40^\circ$ for $30 \leqslant t < 40$ s, $\theta_0 = 20^\circ$ for $40 \leqslant t < 50$ s, and $\theta_0 = 50^\circ$ for $50 \leqslant t < 60$ s, were adopted.

Knee joint control results are shown in Figures 12 and 14. The proposed controller was able to maintain the joint angle in the desired position when the reference changed. The regulation results were satisfactory for both groups. Besides that, the states variables were constrained to an operating region and positively invariant set, $\mathbf{x}(t) \in \mathscr{X} \subset \mathscr{E}(\mathbf{P},1)$, as shown in the Figures 13 and 15.

The root mean square error value in the transient (TRMSE), steady-state (SSRMSE), and over the total time (SSRMSE) were analyzed. The TRMSE values were obtained during initial 5 s of the transient response. Meanwhile, the SSRMSE corresponds the last 5 s of regulation in the reference position.

Figure 12 - Results from healthy individuals (H1-H5). Simulation of the controlled knee joint system using the acceleration-based model, whose state variables are angular position $\check{x}_1(t)$, angular velocity $\check{x}_2(t)$ and angular acceleration $\check{x}_3(t)$. The fuzzy control system presents the following performance index: decay rate β = 1.6, input constraint μ = 0.001.

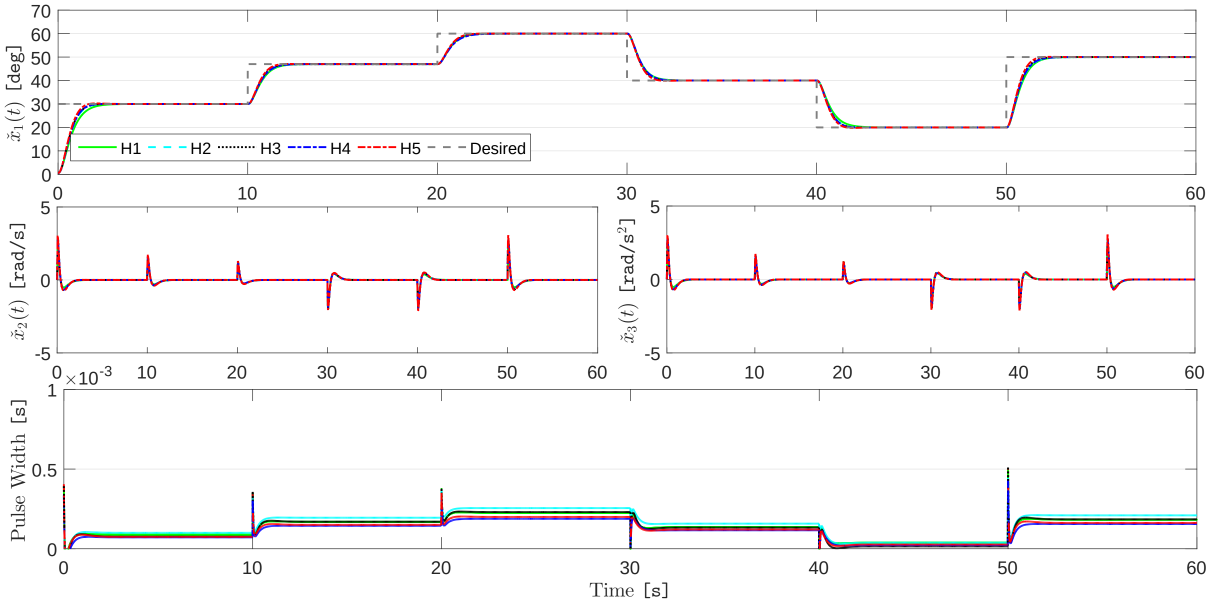

Source: From author.

The independent samples t-test was also performed to confirm the statistical significance of the mean values of RMS error for each time interval of both groups (healthy and paraplegic). The t-test assumes data samples belonging to a normal distribution population and homogeneous variances. Thus, the Shapiro-Wilk normality test was employed for data analysis. The results indicated that all data present normal distribution ($p > 0.05$). And regarding the homogeneity of the variance, the Levene test shows homogeneity for transient period (p-value of 0.278), steady-state (p-value of 0.919) and entire trial (p-value of 0.327).

At a significance level of 0.05, one cannot concluded that there is a significant difference of RMS errors for transient period (p-value of 0.180), steady-state (p-value of 0.215) and entire trial (p-value of 0.169) between healthy and paraplegic individuals. Although the performance for paraplegic individuals was satisfied, the pulse width reached a level higher than for healthy individuals.

Observation 2. *The controller gains and matrices of the Lyapunov function obtained for healthy and paraplegic individuals are listed in the Tables 13 and 14, respectively.*

Figure 13 - Lyapunov function $V(\mathbf{x}) = \mathbf{x}^T \mathbf{P} \mathbf{x}$ obtained from healthy individuals.

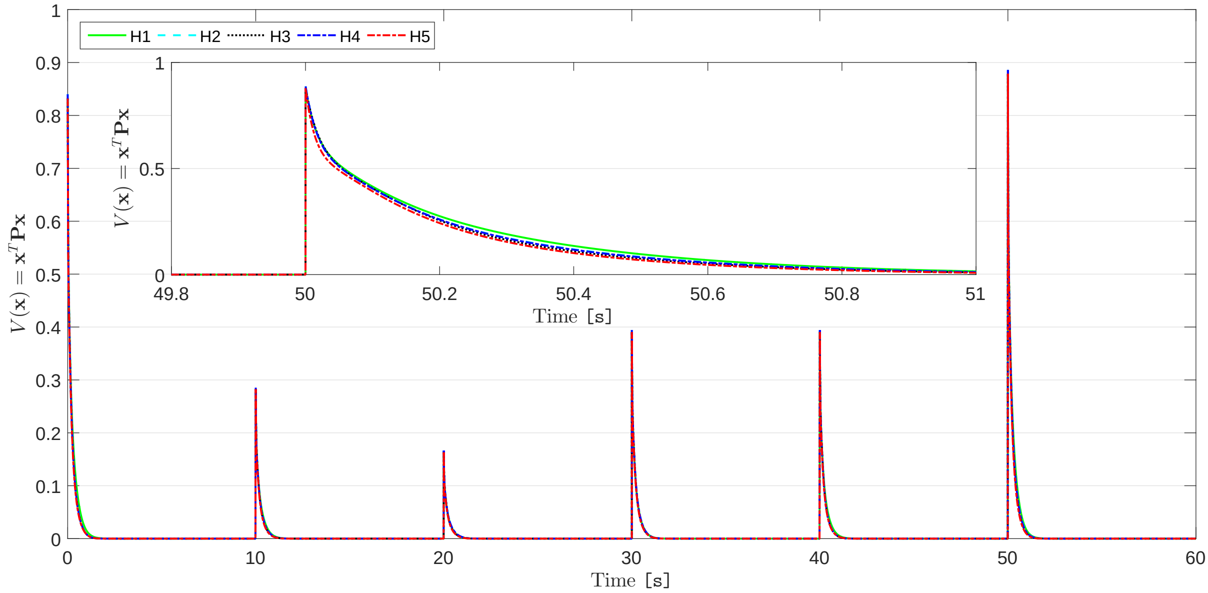

Source: From author.

Figure 14 - Results from paraplegic individuals (P1-P3). Simulation of the controlled knee joint system using the acceleration-based model, whose state variables are angular position $\check{x}_1(t)$, angular velocity $\check{x}_2(t)$ and angular acceleration $\check{x}_3(t)$. The fuzzy control system presents the following performance index: decay rate $\beta = 1.6$, input constraint $\mu = 0.001$.

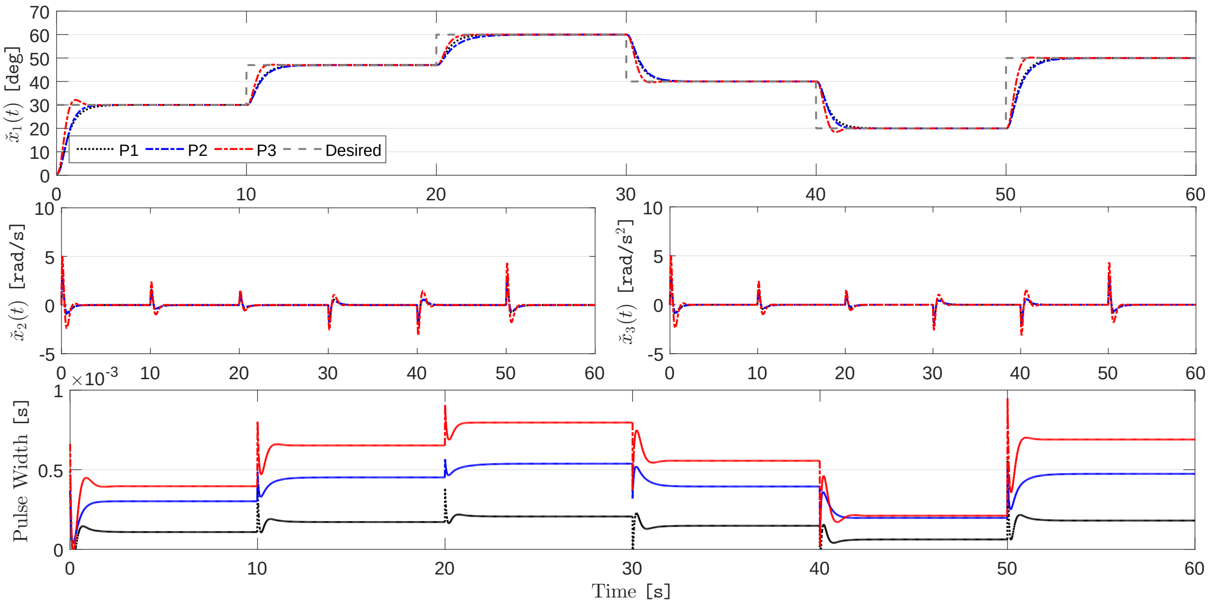

Source: From author.

Figure 15 - Lyapunov function $V(\mathbf{x}) = \mathbf{x}^T\mathbf{P}\mathbf{x}$ obtained from paraplegic individuals.

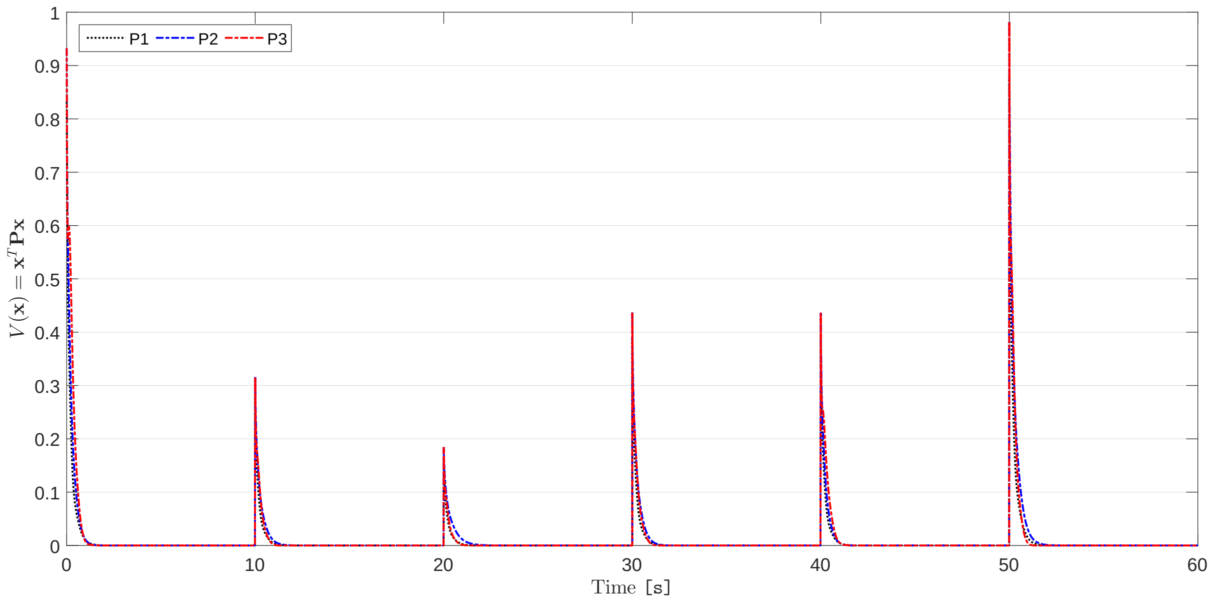

Source: From author.

4.5 Conclusion

By our knowledge, a new model based on acceleration was proposed and validated for healthy and paraplegic individuals. The nonlinear model was described by TS fuzzy models, and a state feedback regulator was applied. Results indicate that the proposed technique is suitable for lower limb joint control by electrical stimulation. An important contribution of this chapter is that the proposed model allows to replace torque estimate in the nonlinear model by angular acceleration measurement, which can be performed from accelerometer. In this study no uncertainties were considered in the plant. In future works, others closed-loop controllers, besides the presented PDC, for other joints such as the ankle, or even for upper limp joints, may be obtained based in the proposed model.

5 STATE-SPACE MODEL IDENTIFICATION FOR ELECTRICALLY STIMULATED LOWER LIMB USING GRAY-BOX APPROACH

"They were really 'Good Samaritans' - willing to give of themselves for the benefit of others. So this kind of attitude influenced me deeply."
Lotfi A. Zadeh

Functional electrical stimulation (FES) has been used for a wide range of rehabilitation applications. The modalities for spinal cord injured apply to both gait training using muscle strengthening as well as restoring vital body functions. The muscular behavior is nonlinear and uncertain, which causes difficulties in neuroprosthesis applications. One challenge is to obtain greater time of muscular activation evoked by electrical stimuli and simultaneously minimize fatigue, spasticity, tremors, disturbances, and other uncertainties. Closed-loop control systems deal satisfactorily with disturbances and uncertainties. The model-based control design approach allows understanding physical and/or biochemical principles and identifying phenomena involved. This chapter proposes an experimental apparatus for tests to identify state-space of the knee joint evoked by electrical stimuli. Model parameters from 24 individuals (20 healthy and 4 paraplegics) are presented. In addition, the system is evaluated under conditions of load disturbance, stimuli repetition, and parametric variation between days after repetitive tests. The results presented may spark ideas for developers of FES control systems.

5.1 Introduction

Functional electrical stimulation (FES) is an important technique to restore movement in people with paralyzed limbs. The system's mathematical model is fundamental to the control design. Particularly in the FES, the relationship between voltage or current applied on muscle and the joint position must be well understood. However, this process involves biomechanical interactions and several complex physiological phenomena, which are dynamic, nonlinear and uncertain.

Ferrarin and Pedotti (2000) presented experimental results from second order nonlinear model of the dynamic lower limb movement. Another important study was proposed by Previdi (2002), who used NARX models through polynomial structures and neural networks. Schauer et al. (2005) used an online approach to identify parameters. The muscle model was represented by a product between nonlinear activation dynamics and a nonlinear static contraction function, described by a neural network. In addition, an extended Kalman filter was implemented to estimate model parameters. By varying the parameter of muscle strength (in simulation mode), the obtained results showed robustness in position control for closed loop response. Although the proposed technique is valid, the implementation is a challenge for embedded systems. Teixeira et al. (2006) showed that the nonlinear dynamics of a electrically stimulated lower limb can be represented by Takagi-Sugeno fuzzy models. Although the description is adequate, the experimental validation it is difficult, because the system is uncertain.

Most models consider angular position, angular velocity and muscle torque as state variables. However, it is a challenge to measure the dynamics of muscle torque. Thus, validation of control techniques becomes difficult.

To overcome this problem, we propose a data-driven identification procedure, where position, velocity and acceleration are considered as state variables. In this chapter, the dynamic model adopted represents the lower limb kinematics and muscular activation. Through an experimental procedure, we show the parameters identification considering the linearized model. We propose three tests to analyze the muscle behavior. An analysis on statistical variation of the model parameters is presented.

This chapter is organized as follows. Section 5.2 presents the nonlinear and linearized dynamic model of electrically stimulated lower limb. Section 5.3 describes the test platform, and specifies the research methodology. Section 5.4 presents the results and discussion. Section 5.5 concludes and indicates a perspective for future works.

5.2 Dynamic Model of the Lower Limb Motion Evoked by Electrical Stimulation

Consider the nonlinear system $\dot{\check{x}}_{1n} = f(\check{x}_{1n}, \check{u})$ expressed as:

$$\begin{cases} \dot{\check{x}}_{1n} = \check{x}_{2n} \\ \dot{\check{x}}_{2n} = \check{x}_{3n} \\ \dot{\check{x}}_{3n} = \dfrac{1}{\tau J}\left[-mgl\sin(\check{x}_{1n}) - \lambda e^{-E\left(\check{x}_{1n}+\frac{\pi}{2}\right)}\left(\check{x}_{1n}+\dfrac{\pi}{2}-\omega\right)\right] \\ \qquad +\dfrac{1}{J}\left[-mgl\cos(\check{x}_{1n}) - \lambda e^{-E\left(\check{x}_{1n}+\frac{\pi}{2}\right)} + \lambda E e^{-E\left(\check{x}_{1n}+\frac{\pi}{2}\right)}\left(\check{x}_{1n}+\dfrac{\pi}{2}-\omega\right) - \dfrac{B}{\tau}\right]\check{x}_{2n} \\ \qquad\qquad + \left[-\dfrac{B}{J}-\dfrac{1}{\tau}\right]\check{x}_{3n} + \dfrac{G}{\tau J}\check{u}. \end{cases} \tag{113}$$

where $\check{x}_{1n}$ is the angular position, $\check{x}_{2n}$ is the angular velocity, $\check{x}_{3n}$ is the angular acceleration, and $\check{u}$ is the control signal.

5.2.1 Linearized State-Space System

The linearized state-space system can be computed using Jacobian linearization on (113) and considering the desired states and control signals, as

$$\mathbf{A} = \frac{\partial f(\breve{x}_n, \breve{u})}{\partial \breve{x}_n}\bigg|_{\breve{x}_n=\breve{x}_n^d,\, \breve{u}=\breve{u}^d} = \begin{bmatrix} 0 & 1 & 0 \\ 0 & 0 & 1 \\ A_{31} & A_{32} & A_{33} \end{bmatrix}, \tag{114}$$

$$\mathbf{B} = \frac{\partial f(\breve{x}_n, \breve{u})}{\partial \breve{u}}\bigg|_{\breve{x}_n=\breve{x}_n^d,\, \breve{u}=\breve{u}^d} = \begin{bmatrix} 0 \\ 0 \\ B_{31} \end{bmatrix}. \tag{115}$$

The matrix elements in (114) and (115) are

$$\begin{aligned} A_{31} = \frac{\partial f(\breve{x}_n,\, \breve{u})}{\partial \breve{x}_{1n}}\bigg|_{\breve{x}_n=\breve{x}_{1n}^d,\, \breve{u}=\breve{u}^d} &= \frac{1}{\tau J}\left[-mgl\cos(\breve{x}_{1n}^d) + \lambda E e^{-E\left(\breve{x}_{1n}^d+\frac{\pi}{2}\right)}\left(\breve{x}_{1n}^d + \frac{\pi}{2} - \omega\right)\right. \\ &\quad \left. -\lambda e^{-E\left(\breve{x}_{1n}^d+\frac{\pi}{2}\right)}\right] + \frac{1}{J}\left[mgl\sin(\breve{x}_{1n}^d) + 2\lambda E e^{-E\left(\breve{x}_{1n}^d+\frac{\pi}{2}\right)}\right. \\ &\quad \left. -\lambda E^2 e^{-E\left(\breve{x}_{1n}^d+\frac{\pi}{2}\right)}\left(\breve{x}_{1n}^d + \frac{\pi}{2} - \omega\right)\right], \end{aligned} \tag{116}$$

$$\begin{aligned} A_{32} = \frac{\partial f(\breve{x}_n,\, \breve{u})}{\partial \breve{x}_{2n}}\bigg|_{\breve{x}_n=\breve{x}_{2n}^d,\, \breve{u}=\breve{u}^d} &= \frac{1}{J}\left[-mgl\cos(\breve{x}_{1n}^d) - \lambda e^{-E\left(\breve{x}_{1n}+\frac{\pi}{2}\right)}\right. \\ &\quad \left. +\lambda E e^{-E\left(\breve{x}_{1n}^d+\frac{\pi}{2}\right)}\left(\breve{x}_{1n}^d + \frac{\pi}{2} - \omega\right) - \frac{B}{J}\right], \end{aligned} \tag{117}$$

$$A_{33} = \frac{\partial f(\breve{x}_n,\, \breve{u})}{\partial \breve{x}_{3n}}\bigg|_{\breve{x}_n=\breve{x}_{3n}^d,\, \breve{u}=\breve{u}^d} = -\frac{B}{J} - \frac{1}{\tau}, \tag{118}$$

$$B_{31} = \frac{\partial f(\breve{x}_n,\, \breve{u})}{\partial \breve{u}}\bigg|_{\breve{x}_n=\breve{x}_n^d,\, \breve{u}=\breve{u}^d} = \frac{G}{\tau J}. \tag{119}$$

5.3 Materials and Methods

5.3.1 Subjects

This study was authorized through a research ethics committee involving human beings (CAAE: 79219317.2.1001.5402) in the São Paulo State University (UNESP), being 24 healthy volunteers (age 21 ± 3 years, 16 male and 4 female), and 4 paraplegics (age 35 ± 9 years, all male). Table 12 details some informations on the paraplegics volunteers.

5.3.1.1 Inclusion criteria

Healthy and paraplegics individuals older than or equal to 18 years old were adopted, male or female. The healthy were chosen the subjects without lesion or congenital disease, which compromise the lower limbs movements partially or totally. And the paraplegis were considered individuals with spinal cord injury.

5.3.1.2 Exclusion criteria

Individuals under the age of 18 years, pregnant women and those with cardiovascular disease were considered unfit for the tests. We also excluded healthy individuals who showed fear behavior, discomfort and voluntary movements, as opposed to electrical stimulation. In this study only spinal cord injury was evaluated, other types of injuries limiting motor mobility were disregarded.

Table 12 - Specific informations on the paraplegics volunteers considered in this study.

Subject	**Mass**[kg]	**Height**[m]	**Age**[yrs]	**Time after injury**[yrs]	**Level of SCI**	**FES training** [mth]
P1	75	1.87	31	2	C4-C5	0
P2	48	1.68	25	7	T5	0
P3	68	1.80	30	10	T3-T4	0
P4	65	1.65	52	31	C7-C8	0

Source: From author.

5.3.2 Plataform

Experiments were performed on a test platform equipped with sensors and devices, as shown in Figure 16. The platform is instrumented by sensors as one electrogoniometer (Lynx®), one LPR510AL gyroscope (ST Microelectronics®), two MMA7341 triaxial accelerometers (Freescale®), one NI myRIO controller (National Instruments®) accompanied by software LabVIEW Student Edition, installed on a computer with a processor Intel Core™ i7-4780, 3.6 GHz, 16GB RAM.

The electrical stimulator consists of four independent channels. Each channel has a wave generator circuit, consisting of a bandpass filter (10 – 3000Hz), a differential amplifier and two voltage-to-current converters (VI converter). The power stage is formed by Wilson current mirrors.

The stimulation intensity is controlled by setting the pulse amplitude to the quadriceps and controlling the pulse width. The muscular electrostimulator delivers rectangular, biphasic, symmetrical pulse to the individual's muscle, and allows an adjustment of the pulse width in a range of $0-400\mu$s. The stimulus frequency were fixed in 50 Hz. The channel current amplitude was predefined at values 70, 80, 100, 120 mA, and this value is fixed. The channel for each individual was determined from pre-assessment, in order to establish which channel of lower electric-current intensity obtains muscle contraction in the range from 0 to 60°.

Anti-aliasing filter is applied to signals captured from sensors. After analog-to-digital conversion, the data is adjusted and filtered digitally. The angular position signal $\check{x}_{1n}$ from the electrogoniometer $v_e(t)$ is preprocessed as

$$\check{x}_{1n} = LPF(\tilde{x}_{1n}), \tag{120}$$

$$\tilde{x}_{1n} = \frac{2\pi}{360}\left(K_e v_e(t) - v_{off}(t)\right), \tag{121}$$

where the operator LPF denotes low-pass filter, v_{off} is the offset voltage, and the parameter $K_e = 650.8$. Similarly, the gyro signal $v_g(t)$ is obtained as

$$\check{x}_{2n} = LPF(\tilde{x}_{2n}), \tag{122}$$

$$\tilde{x}_{2n} = \frac{2\pi}{360}\left(K_{1g}^{-1} v_g(t) - K_{2g}\right), \tag{123}$$

where the gyroscope parameters are $K_{1g} = 0.0025$ and $K_{2g} = 1.22$. The LPF is an elliptic digital filter (also known as Cauer filter) considering passaband ripple 0.1 dB, sampling frequency $f_s = 50$ Hz, high cutoff frequency $f_h = 10$, stopband attenutation 80 dB, and order 10.

5.3.3 Experimental Setup

The safety and comfort indicator is a stop button that deactivates the stimulation pulses. The chair backrest and the knee joint position are adjustable for each volunteer. A procedure determines the motor activaction point for proper positioning of the surface electrodes in the quadriceps. More informations about this technique are in (GOBBO et al., 2014). Once the motor point is defined, then the surface is scraped and cleaned. The electrodes used are rectangular self-adhesive size 50×90 mm.

After the motor-point identification, open-loop experiments are performed. These tests consist to a constant pulse width signal $\check{u}_n^d$ applied during a known time interval. The stimulation frequency adopted is 50 Hz. The pulse width, position, velocity and angular acceleration data are recorded at the end of each test.

Figure 16 - The leg extension plataform for electrical stimulation tests located in the Instrumentation and Biomedical Engineering Laboratory - UNESP, FEIS.

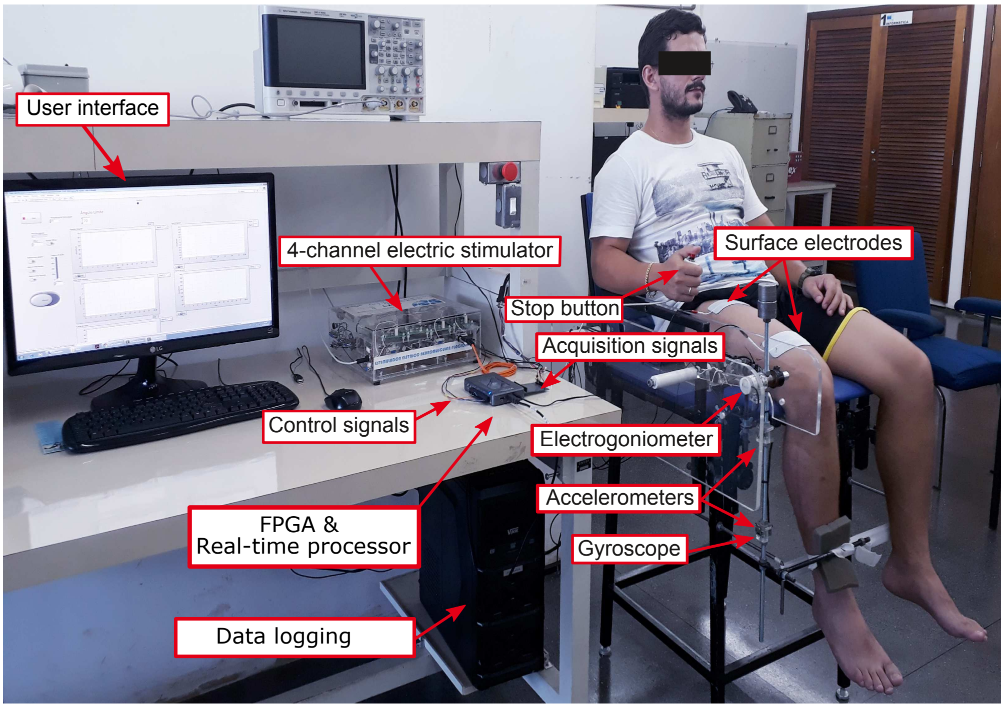

Source: From author.

5.3.4 *Assay A: identification based on step signal*

It consisted of applying a pulse-width step and monitoring the system response. The test duration is about four seconds. Approximately 2-minutes time interval is timed to muscle rest. Next, a step signal is applied again during the interval of four seconds. It was established the maximum number of 10 tests. The initial pulse width was adjusted to approximate the angular position of 40°.

5.3.5 *Assay B: load disturbance*

It consisted of 30 step-signal of electrical stimuli considering the same pulse width and ensuring rest time in all attempts. The procedure consists of three phases: i) pre-evaluation of step-signal response; ii) load disturbance inserted in the lower limb; and iii) removal of load disturbance. The step signal response is performed 10 times in each phase, maintaining the same pulse width.

After 10 pre-assessment tests, a load (1 kg) was inserted close to the ankle joint. The procedure was repeated maintaining the same pulse width defined in the previous phase. After this load disturbance, another 10 tests were performed without load.

5.3.6 Assay C: one-day interval after repetitive tests

The first session consisted of step signal applied in 30 repetitions. The volunteer was asked not to carry out physical efforts until the next experimental session. After 24 hours, the identification procedure based on the step signal was repeated. The pulse width applied was the same as the first session.

5.3.7 System identification procedure

From a state space representation, the system transfer function can be obtained. Consider $\Delta\dot{\mathbf{x}} = \mathbf{A}\Delta\mathbf{x} + \mathbf{B}\Delta\mathbf{u}$, where $\Delta\mathbf{x} = \check{\mathbf{x}}_n - \check{\mathbf{x}}_n^d$, $\Delta\mathbf{u} = \check{\mathbf{u}}_n - \check{\mathbf{u}}_n^d$, the matrices $\mathbf{A}$ and $\mathbf{B}$ expressed in (115) and (115), respectively. Then, the transfer function $H(s) = \dfrac{Y(s)}{U(s)}$, where $Y(s)$ is the system output (angular position) and $U(s)$ is the system input (pulse width), can be written as

$$H(s) = \mathbf{C}\left(s\mathbf{I} - \mathbf{A}\right)^{-1}\mathbf{B} + \mathbf{D}, \tag{124}$$

$$= \mathbf{C}\frac{1}{\det(\Lambda)}\mathrm{adj}\left(\Lambda\right)^T\mathbf{B} + \mathbf{D}, \tag{125}$$

where $\Lambda = (s\mathbf{I} - \mathbf{A})$, and

$$\det(\Lambda) = \left(s^3 - A_{33}s^2 - A_{32}s - A_{31}\right), \tag{126}$$

$$\mathrm{adj}\left(\Lambda\right)^T = \begin{bmatrix} s^2 - A_{33}s - A_{32} & s - A_{33} & 1 \\ A_{31} & s^2 - A_{33}s & s \\ A_{31}s & A_{32}s + A_{31} & s^2 \end{bmatrix}. \tag{127}$$

Therefore, taking the equations (114)-(115), (126)-(127), $\mathbf{C} = [1 \quad 0 \quad 0]$, $\mathbf{D} = 0$, and replacing in (125), one obtains

$$H(s) = \frac{B_{31}}{s^3 - A_{33}s^2 - A_{32}s - A_{31}}. \tag{128}$$

The system excitation is performed by step signal. The identification procedure considers single-input and single output system (SISO), being the input (pulse width), and the output (angular position). The system data were obtained in a period of 4 seconds. The experimental data were recorded from 20μs before the step change. The identification of the parameters is performed estimating the third-order transfer function through the MatLab® function "tfest".

Figure 17 - Identification based on step signal.

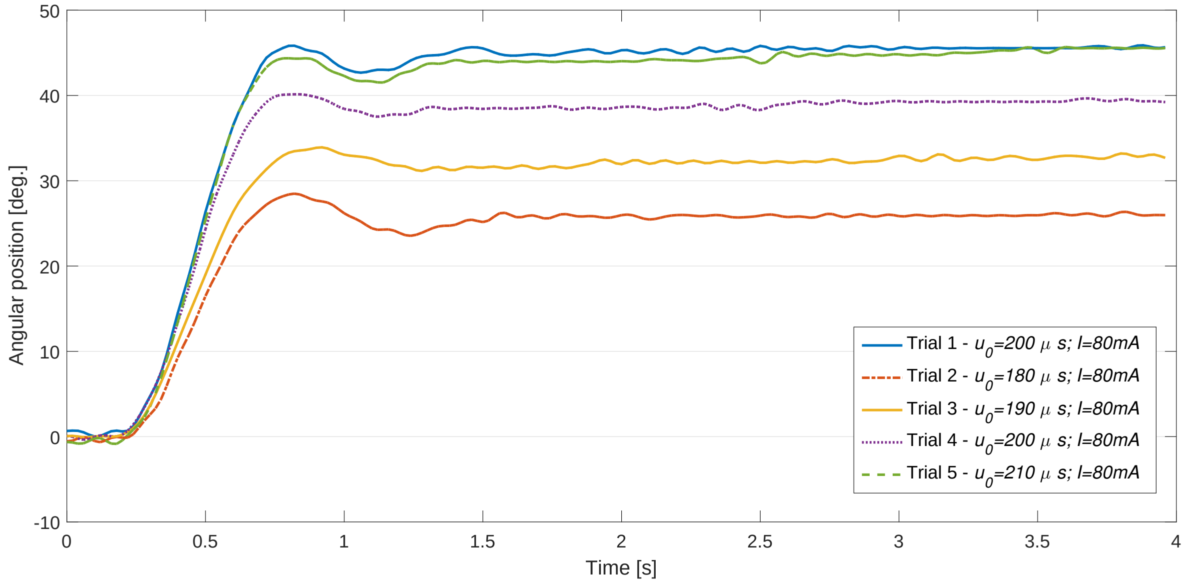

Source: From author.

5.4 Results and Discussion

5.4.1 Identification based on step signal

At each step signal applied, it is desired to obtain the system response closest to the operating point, Figure 17. The results show an interesting behavior. In the first test, by applying 200μs the angular position reached steady state about 45°. In the second test, the pulse width was reduced to 180μs, and the angular position was approximately 26°. By increasing 10μs, the angular position approached of 33° in the third test. The fourth test shows the uncertain control signal, where again applying the pulse width of the first test (200μs), the angular position is different (about 39°). The fifth test indicates that the pulse width is uncertain to operate at a given operating point. The angular position obtained resembles that of the first test, but the pulse width differs by 10μs.

Using the procedure detailed in subsection 5.3.7, the model parameters can be determined. The values of each individual are listed in Table 15. The superscript 1 and 2 indicates the maximum and minimum values, respectively. The subscript i, j refers to the matrix indices of the elements.

5.4.2 Load disturbance

The data obtained in the thirty tests are shown in Figure 18. In the pre-evaluation phase, the first system response tended to 50°. Note that although there is a rest time, after a large

Figure 18 - System behaviour in (a) pre-assessment (solid line), (b) load disturbance (dotted line), and (c) post-assessment (dashed line).

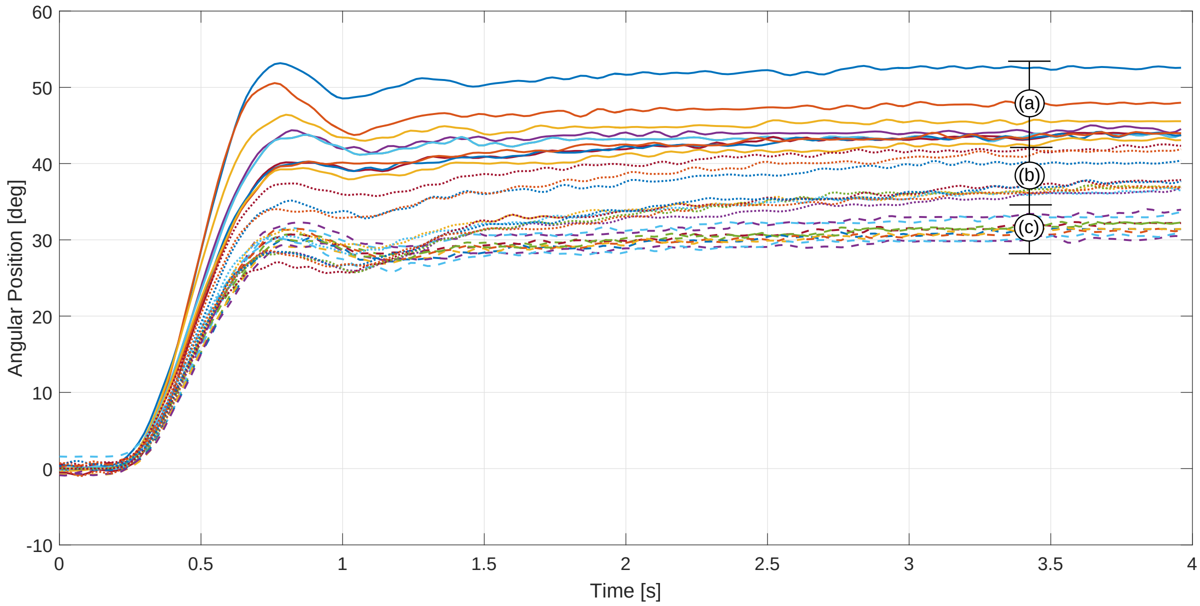

Source: From author.

number of trials, the angular difference increases significantly. Our hypothesis is that muscle fibers recruited locally by fatigue surface electrodes more quickly and consequently degrades the muscle activation performance.

When inserting load, the angular position declines, because the system operates in an open loop. Considering the system without load disturbance, it is noted that the angular position is close to 20°.

This behavior is an indicative of muscle fatigue both by the load disturbance as well as the electrical stimulation. The statistical variation of the parameters in each test phase is shown in Figure 19. On each box, the central mark is the median, the edges of the box are the 25th and 75th percentiles, the whiskers extend to the most extreme data points not considered outliers, and outliers are plotted individually. The average of the parameters A_{31}, A_{32}, A_{33} tends to increase, whereas the trend of B_{31} is to reduce as the repetitions increases. The effect intensifies after the load disturbance, which shows lower muscle activation.

5.4.3 One-day interval after repetitive tests using step signal

After a series of repetitions the fatigue condition on motor point becomes evident (GORGEY et al., 2009; WESTERBLAD et al., 2000). In the next day, when applying the same pulse width and electrode position in the quadriceps, the system response obtained is different as shown in Figure 20.

Figure 19 - Parametric variation derived from pre-assessment (PRE), load disturbance (LD), and post-assessment (POST).

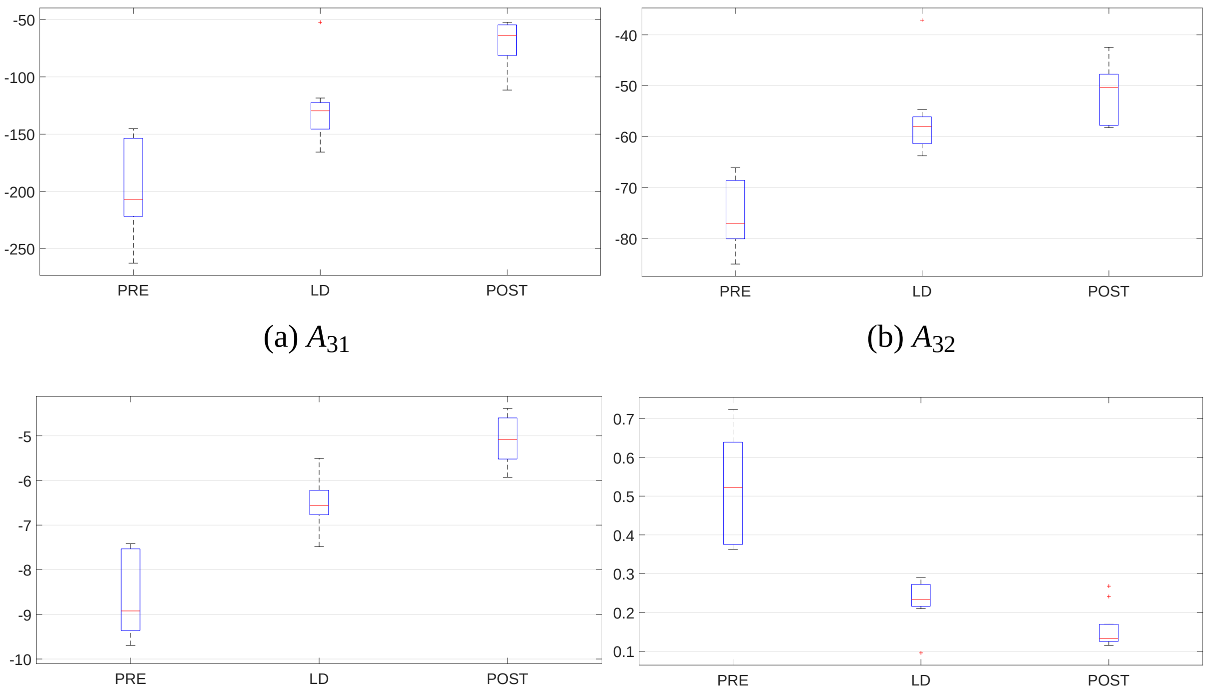

(a) A_{31} (b) A_{32}

(c) A_{33} (d) B_{31}

Source: From author.

Figure 20 - Identification performed in one-day interval: session 1 (solid line), and session 2 - after one day (dashed line).

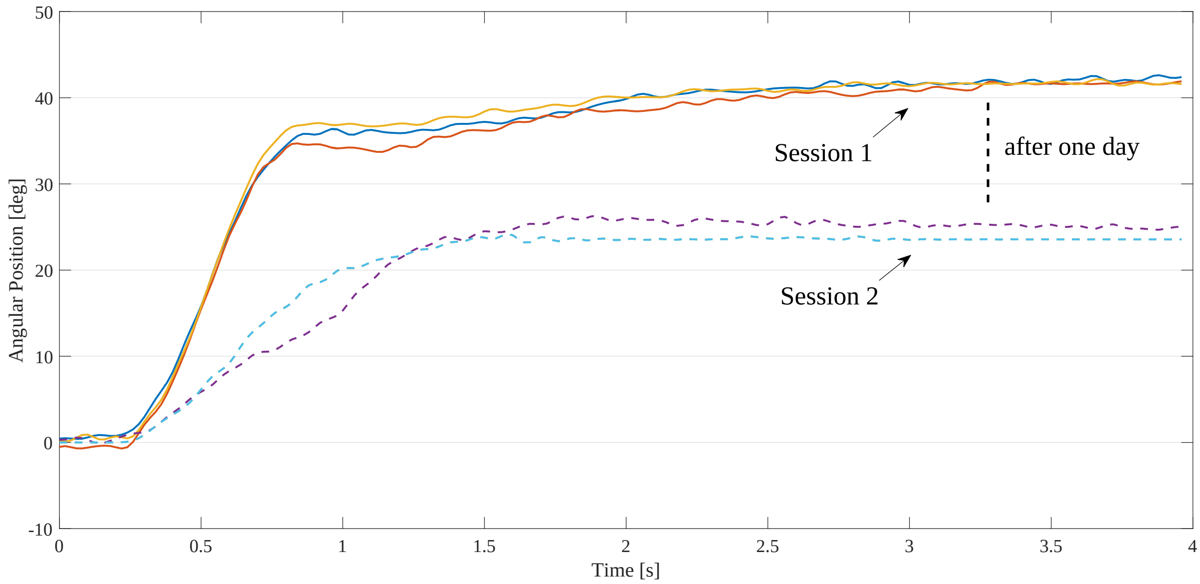

Source: From author.

The frequency of stimulation used in this study was 50 Hz, which possibly accelerated the fatigue process. Minor frequencies are suggested to minimize the effect of fatigue (WEST-

ERBLAD et al., 2000). Higher frequencies reduce the concentration of Na^+ ions and increase K^+ ions, consequently impairing motor nerve conduction.

5.4.4 Limitations

Although the gray-box technique allows to know the muscular behavior, the non-guarantee of convexity is a limitation. Consequently its application is restricted and not suitable for control design based on convex models.

5.5 Conclusion

This chapter proposes a test methodology for gray-box identification. Experimental tests were conducted to collect parameters of healthy and paraplegic individuals. The identification tests demonstrated that the technique is a good strategy to evaluate muscle behavior.

A load disturbance accentuated the muscular fatigue process, attested by the analysis of the presented model parameters. It was evident from the results that the electrical stimulation system deals with uncertain parameters, with intra- and intra-individual variation.

The data set provided is a contribution to control system design. Future works may use different closed-loop control techniques to evaluate the system behavior in relation to parametric uncertainties.

6 GENERAL CONCLUSION

In this thesis, the state-of-the-art on closed-loop control systems applied to knee joint rehabilitation using superficial electrical stimulation were presented.

The knee joint control system using electrical stimulation was treated as an uncertain nonlinear system. In the control design, LMIs conditions constrained the TS fuzzy modeling to a state-space operation region was performed. The switched control subject to actuator saturation was compared to Gaino et al. (2017). The performance of these were evaluated under non ideal conditions of the muscle (fatigue, spasms and tremor) and fault in the actuator. Remembering that the fuzzy control law is dependent on the membership functions. When the system has uncertainties, the fuzzy controller is inadequate for this problem. On the other hand, the switched-control law has proved to be an interesting approach because it does not depend on the membership functions. Using the switched control law, we obtained better results than the combination of the control gains by the membership functions, because it chooses a state-feedback controller gain belonging to a given set of gains, that minimizes the time derivative of Lyapunov function, and reduces the control signal. However, an unwanted effect is that the control signal is susceptible to a high frequency switching of the controller gains. This problem can be overcome by using the soft minimum, proposed in (ALVES et al., 2016).

In addition, a new dynamic model of electrically stimulated lower limbs was proposed. The advantage of this model is to obtain the kinematics and muscular dynamics represented in state space through the variables angular position, angular velocity and acceleration. Therefore, in this new representation the torque variable has been replaced by acceleration. A TS fuzzy modeling of this plant was shown, as well as the parallel distributed compensation control design considering an operating region.

Finally, an experimental arrangement was set up to identify parameters of the linearized model. The gray-box identification approach was performed from third-order transfer function. The muscular behavior was investigated in three tests of the system response to the step signal, load disturbance and analysis on different days. A well-defined behavior of parametric variation was observed in the presence of muscle fatigue.

6.1 Future works

The research field is broad and promising, it is possible and interesting to investigate: LMIs conditions for switched control design considering actuator subject to saturation and delay;

LMIs conditions for asymmetric saturation and/or null constraint (e.g. PWM control signal); data-driven TS fuzzy local models; real-time system to monitor muscle fatigue in isotonic and isometric contractions; an electrical stimulator based on amplitude modulation and isolated channels; a electrical stimulator that monitors the current flow into or out of the electrode, and adjusts the voltage output of the power supply to maintain a constant current; and a new hybrid system for lower and upper limb rehabilitation.

6.2 Scientific publications

In this study, the following contributions are proposed to journals:

1) NUNES, W. R. B. M.; ALVES, U. N. L. T.; SANCHES, M. A. A.; MACHADO, E. R. M. D.; CARDIM, R.; TEIXEIRA, M. C. M.; CARVALHO, A. A. *A New Acceleration-Based Model Applied to Electrically Stimulated Lower Limbs*. Submission to Journal of Biomechanics.

2) NUNES, W. R. B. M.; ALVES, U. N. L. T.; SANCHES, M. A. A.; TEIXEIRA, M. C. M.; CARVALHO, A. A. *Isometric Contraction Improvement of Electrically Stimulated Lower Limb under Non-Ideal Conditions Using Switched Controller Subject to Saturation*. Submission to IET Control Theory.

3) NUNES, W. R. B. M.; SANCHES, M. A. A.; TEIXEIRA, M. C. M.; CARVALHO, A. A. *Closed-Loop Control Techniques Applied to Motor Rehabilitation of the Knee Joint Using Electrical Stimulation: A Survey of the State-of-the-Art And Future Perspectives*. Submission to Medical Engineering & Physics.

4) TEODORO, R. G.; NUNES, W. R. B. M.; ARAUJO, R. A.; SANCHES, M. A. A.; TEIXEIRA, M. C. M.; CARVALHO, A. A. *Robust and Switched Control Design for Electrically Stimulated Lower Limbs: a Linear Model Analysis in Healthy and Spinal Cord Injured Subjects*. Submission to Control Engineering Practice.

5) NUNES, W. R. B. M.; KRUEGER, E.; BRONIERA JR, P.; SANCHES, M. A. A.; TEIXEIRA, M. C. M.; CARVALHO, A. A. *EEG-Based Brain-Controlled Functional Electrical Stimulation for Lower Limbs Rehabilitation: Advances and Perspectives*. Submission to Annals of Biomedical Engineering.

And the following contributions were accepted in conferences:

6) ARCOLEZI, H. H.; NUNES, W. R. B. M.; NAHUIS, S. L. C.; SANCHES, M. A. A.; TEIXEIRA, M. C. M.; CARVALHO, A. A. *A RISE-based Controller Fine-tuned by an Improved Genetic Algorithm for Human Lower Limb Rehabilitation via Neuromuscular Electrical Stimulation*. In: INTERNATIONAL CONFERENCE ON CONTROL, DECISION AND INFORMATION TECHNOLOGIES - CODIT, 6th., 2019, Paris, France. **Proceedings [...]**. Paris: IEEE, 2019.

7) BRONIERA JUNIOR, P.; NUNES, W. R. B. M.; LAZZARETTI, A. E.; NOHAMA, P.; CARVALHO, A. A. de; KRUEGER, E.; TEIXEIRA, M. C. M. *Classifier for motor imagery during parametric functional electrical stimulation frequencies on the quadriceps muscle*. In: INTERNATIONAL IEEE/EMBS CONFERENCE ON NEURAL ENGINEERING (NER), 9th., 2019, San Francisco, CA, USA. **Proceedings [...]**. San Francisco: IEEE EMBS, 2019. pp. 526-529.

8) NUNES, W. R. B. M.; TEODORO, R. G.; de ARAUJO, R. A.; SANCHES, M. A. A.; TEIXEIRA, M. C. M.; CARVALHO, A. A. *Switched Controller Applied to Functional Electrical Stimulation of Lower Limbs under Fatigue Conditions: a Linear Analysis*. In: XXVI BRAZILIAN CONGRESS ON BIOMEDICAL ENGINEERING. IFMBE Proceedings, vol 70/1. Springer, Singapore, 2019. **Proceedings [...]**. Heidelberg: IFMBE, 2019. pp 383-390.

9) TEODORO, R. G.; NUNES, W. R. B. M.; ARAUJO, R. A.; SANCHES, M. A. A.; TEIXEIRA, M. C. M.; CARVALHO, A. A. *Polytopic Uncertainties Identification for Electrically Stimulated Lower Limbs*. In: BRAZILIAN CONGRESS ON BIOMEDICAL ENGINEERING. IFMBE Proceedings, vol 70/1. Springer, Singapore, 2019. **Proceedings [...]**. Heidelberg: IFMBE, 2019. pp 337-342.

10) NUNES, W. R. B. M.; TEODORO, R. G.; ARAUJO, R. A.; SANCHES, M. A. A.; TEIXEIRA, M. C. M.; CARVALHO, A. A. *Robust and Switched Control Design for Electrical Stimulation of Lower Limbs: a linear analysis*. In: CONGRESSO BRASILEIRO DE AUTOMÁTICA - CBA, 2018, Natal. **Anais [...]**. Natal: SBA, 2018.

11) NUNES, W. R. B. M.; BRONIERA JR, P.; KRUEGER, E.; CARVALHO, A. A. *Common Spatial Pattern apresenta 18% a mais de acurácia que o Laplaciano em Imagética Motora de membros superiores*. In: CONGRESSO BRASILEIRO DE ELETROMIOGRAFIA E CINESIOLOGIA-COBEC E SIMPÓSIO DE ENGENHARIA BIOMÉDICA-SEB, 2017, Uberlândia. **Anais [...]**. Uberlândia: SBEB, 2017.

12) BRONIERA JR, P.; NUNES, W. R. B. M.; KRUEGER, E.; GAINO, R.; COVACIC, M. R.; TEIXEIRA, M. C. M.; CARVALHO, A. A. *Análise Comparativa da Classificação de Sinais de Eletroencefalografia no Domínio do Tempo Utilizando Redes PMC e RBF*. In: CONGRESSO BRASILEIRO DE ELETROMIOGRAFIA E CINESIOLOGIA-COBEC E SIMPÓSIO DE ENGENHARIA BIOMÉDICA-SEB, 2017, Uberlândia. **Anais [...]**. Uberlândia: SBEB, 2017.

13) NUNES, W. R. B. M.; BEBETO, M. A. L.; ASSUNÇÃO, E.; TEIXEIRA, M. C. M.; CARVALHO, A. A. *Síntese de Controlador Robusto via LMI para o Helicóptero 3-DOF*. In: CONFERÊNCIA BRASILEIRA DE DINÂMICA, CONTROLE E APLICAÇÕES-DINCON, 2017, São José do Rio Preto. **Anais [...]**. IBILCE: SBMAC, 2017.

14) NUNES, W. R. B. M.; GAINO, R.; COVACIC, M.R.; BRONIERA JR, P.; TEIXEIRA,

M. C. M.; CARVALHO, A. A. *Predição via Redes Neurais Artificiais da Curva de Recrutamento Muscular com Estimulação Elétrica Funcional dos Membros Inferiores*. In: CONFERÊNCIA BRASILEIRA DE DINÂMICA, CONTROLE E APLICAÇÕES-DINCON, 2017, São José do Rio Preto. **Anais [...]**. IBILCE: SBMAC, 2017.

15) BRONIERA JR, P.; NUNES, W. R. B. M.; KRUEGER, E.; GAINO, R.; COVACIC, M. R.; TEIXEIRA, M. C. M.; CARVALHO, A. A. Estudo Comparativo entre Redes Perceptron Multicamadas (PMC) e Redes de Funções de Base Radial (RBF) para a Classificação de Sinais Eletroencefalográficos no Domínio do Tempo. In: SIMPÓSIO DE NEUROENGENHARIA, IV, 2017, Macaíba. **Anais [...]**. CEPS Anita Garibaldi: ISD, 2017.

BIBLIOGRAPHY

ABBAS, J. J.; TRIOLO, R. J.; JJ, A.; RJ, T. Experimental evaluation of an adaptive feedforward controller for use in functional neuromuscular stimulation systems. **IEEE Transactions on Rehabilitation Engineering**, Pistacaway, v. 5, n. 1, p. 12–22, 1997.

AJOUDANI, A.; ERFANIAN, A. Neuro-Sliding Mode Control of Knee-Joint Angle with Quadriceps Electrical Stimulation. In: ANNUAL CONFERENCE OF THE INTERNATIONAL FES SOCIETY, 11th., 2006, Senday. **Proceedings [...]**. Sendai: Tohoku University Graduate School of Medicine, 2006. p. 26–28.

AJOUDANI, A.; ERFANIAN, A. A Neuro-Sliding Mode Control With Adaptive Modeling of Uncertainty for Control of Movement in Paralyzed Limbs Using Functional Electrical Stimulation. **IEEE Transactions on Biomedical Engineering**, Pistacaway, v. 56, n. 7, p. 1771–1780, 2009.

ALIBEJI, N.; KIRSCH, N.; DICIANNO, B. E.; SHARMA, N. A Modified Dynamic Surface Controller for Delayed Neuromuscular Electrical Stimulation. **IEEE/ASME Transactions on Mechatronics**, Pistacaway, v. 22, n. 4, p. 1755–1764, 2017.

ALVES, U. N. L. T. **Controle chaveado e chaveado suave de sistemas não lineares incertos via modelos fuzzy T-S**. 2017. 107 p. Tese (Doutorado em Engenharia Elétrica) — Faculdade de Engenharia, Universidade Estadual Paulista, 2017.

ALVES, U. N. L. T.; TEIXEIRA, M. C. M.; OLIVEIRA, D. R.; CARDIM, R.; ASSUNÇÃO, E.; SOUZA, W. A. Smoothing switched control laws for uncertain nonlinear systems subject to actuator saturation. **International Journal of Adaptive Control and Signal Processing**, Oxford, v. 30, n. 8-10, p. 1408–1433, 2016.

ANDREWS, B.; GIBBONS, R.; WHEELER, G. Development of Functional Electrical Stimulation Rowing: The Rowstim Series. **Artificial Organs**, Hoboken, v. 41, n. 11, p. E203–E212, 2017.

BELLMAN, M. J.; CHENG, T. H.; DOWNEY, R. J.; HASS, C. J.; DIXON, W. E. Switched Control of Cadence during Stationary Cycling Induced by Functional Electrical Stimulation. **IEEE Transactions on Neural Systems and Rehabilitation Engineering**, Pistacaway, v. 24, n. 12, p. 1373–1383, 2016.

BENAHMED, S.; KERMIA, O.; TADJINE, M. The use of the principle of feedback scheduling for enhancing the real-time paraplegic knee response. In: INTERNATIONAL CONFERENCE ON SYSTEMS AND CONTROL, 3rd., 2013, Algiers. **Proceedings [...]**. Algiers: IEEE, 2013. p. 995–1000.

BENAHMED, S.; TADJINE, M.; KERMIA, O. Adaptive super twisting controller: In search of a universal controller for the paraplegic knee movement using FES. In: INTERNATIONAL

CONFERENCE ON ELECTRICAL ENGINEERING (ICEE), 5th., 2017, Boumerdes. **Proceedings [...]**. Boumerdes: IEEE, 2017. p. 1–6.

BENZAOUIA, A.; MESQUINE, F.; BENHAYOUN, M.; SCHULTE, H.; GEORG, S. Stabilization of positive constrained T-S fuzzy systems: Application to a Buck converter. **Journal of the Franklin Institute**, Oxford, v. 351, n. 8, p. 4111–4123, 2014.

BO, A. P. L.; FONSECA, L. O. da; GUIMARAES, J. A.; FACHIN-MARTINS, E.; PAREDES, M. E. G.; BRINDEIRO, G. A.; SOUSA, A. C. C. de; DORADO, M. C. N.; RAMOS, F. M. Cycling with Spinal Cord Injury: A Novel System for Cycling Using Electrical Stimulation for Individuals with Paraplegia, and Preparation for Cybathlon 2016. **IEEE Robotics & Automation Magazine**, Pistacaway, v. 24, n. 4, p. 58–65, 2017.

BO, A. P. L.; LOPES, A. C. G.; FONSECA, L. O. da; OCHOA-DIAZ, C.; AZEVEDO-COSTE, C.; FACHIN-MARTINS, E. **Experimental Results and Design Considerations for FES-Assisted Transfer for People with Spinal Cord Injury**. Heidelberg: Springer, 2019. 939–943 p.

BOYD, S. P.; El Ghaoui, L.; FERON, E.; BALAKRISHNAN, V. **Linear matrix inequalities in system and control theory**. Philadelphia: SIAM, 1994. 193 p.

CAO, Y.-Y.; LIN, Z. Robust stability analysis and fuzzy-scheduling control for nonlinear systems subject to actuator saturation. **IEEE Transactions on Fuzzy Systems**, Pistacaway, v. 11, n. 1, p. 57–67, 2003.

CHANG, G.-C.; LUH, J.-J.; LIAO, G.-D.; LAI, J.-S.; CHENG, C.-K.; KUO, B.-L.; KUO, T.-S. K. A neuro-control system for the knee joint position control with quadriceps stimulation. **IEEE Transactions on Rehabilitation Engineering**, Pistacaway, v. 5, n. 1, p. 2–11, 1997.

CHEN, Y.-J.; TANAKA, M.; TANAKA, K.; WANG, H. O. Nonconvex stabilization criterion for polynomial fuzzy systems. In: IEEE. **Decision and Control (CDC), 2013 IEEE 52nd Annual Conference on**. [S.l.], 2013. p. 7415–7419.

CHENG, T. H.; WANG, Q.; KAMALAPURKAR, R.; DINH, H. T.; BELLMAN, M.; DIXON, W. E. Identification-Based Closed-Loop NMES Limb Tracking with Amplitude-Modulated Control Input. **IEEE Transactions on Cybernetics**, Pistacaway, v. 46, n. 7, p. 1679–1690, 2016.

CHENGWEI, G.; QIAN, J. Optimized Proportional-Integral-Derivative Control Strategies and Simulation for Lower Limb Functional Electrical Stimulation. In: INTERNATIONAL CONFERENCE ON INFORMATION AND COMPUTING, 4th., 2011, Phuket Island. **Proceedings [...]**. Phuket Island: IEEE, 2011. p. 420–423.

COOPER, E. B.; BUNCH, W. H.; CAMPA, J. F. Effects of chronic human neuromuscular stimulation. **Surgical forum**, Philadelphia, v. 24, p. 477–9, 1973.

COOPER, G.; SHERET, I.; MCMILLIAN, L.; SILIVERDIS, K.; SHA, N.; HODGINS, D.; KENNEY, L.; HOWARD, D. **Journal of Biomechanics**, Oxford, v. 42, n. 16, p. 2678–2685, 2009.

COVACIC, M.; TEIXEIRA, M. C. M.; ASSUNÇÃO, E.; GAINO, R. LMI-based algorithm for strictly positive real systems with static output feedback. **Systems & Control Letters**, Amsterdam, v. 61, n. 4, p. 521–527, 2012.

DEJNABADI, H.; JOLLES, B. M.; CASANOVA, E.; FUA, P.; AMINIAN, K. Estimation and visualization of sagittal kinematics of lower limbs orientation using body-fixed sensors. **IEEE Transactions on Biomedical Engineering**, Pistacaway, v. 53, n. 7, p. 1385–1393, 2006.

DING, J.; WEXLER, A. S.; BINDER-MACLEOD, S. A. A mathematical model that predicts the force-frequency relationship of human skeletal muscle. **Muscle and Nerve**, Hoboken, v. 26, n. 4, p. 477–485, 2002.

DING, J.; WEXLER, A. S.; BINDER-MACLEOD, S. A. Mathematical models for fatigue minimization during functional electrical stimulation. **Journal of Electromyography and Kinesiology**, London, v. 13, n. 6, p. 575–588, 2003.

DORGAN, S.; O'MALLEY, M. A nonlinear mathematical model of electrically stimulated skeletal muscle. **IEEE Transactions on Rehabilitation Engineering**, Pistacaway, v. 5, n. 2, p. 179–194, 1997.

DOWNEY, R. J.; BELLMAN, M. J.; KAWAI, H.; GREGORY, C. M.; DIXON, W. E. Comparing the Induced Muscle Fatigue Between Asynchronous and Synchronous Electrical Stimulation in Able-Bodied and Spinal Cord Injured Populations. **IEEE Transactions on Neural Systems and Rehabilitation Engineering**, Pistacaway, v. 23, n. 6, p. 964–972, 2015.

DOWNEY, R. J.; CHENG, T. H.; BELLMAN, M. J.; DIXON, W. E. Closed-Loop Asynchronous Neuromuscular Electrical Stimulation Prolongs Functional Movements in the Lower Body. **IEEE Transactions on Neural Systems and Rehabilitation Engineering**, Pistacaway, v. 23, n. 6, p. 1117–1127, 2015.

DOWNEY, R. J.; CHENG, T.-H.; BELLMAN, M. J.; DIXON, W. E. Switched Tracking Control of the Lower Limb During Asynchronous Neuromuscular Electrical Stimulation: Theory and Experiments. **IEEE Transactions on Cybernetics**, Pistacaway, v. 47, n. 5, p. 1251–1262, 2017.

EFBERG, J.; LÖFBERG, J. Yalmip: A toolbox for modeling and optimization in matlab. In: IEEE INTERNATIONAL SYMPOSIUM ON COMPUTER AIDED CONTROL SYSTEMS DESIGN, 2004., Taipei. **Proceedings [...]**. Taipei: IEEE, 2004. p. 284–289.

ERAIFEJ, J.; CLARK, W.; FRANCE, B.; DESANDO, S.; MOORE, D. Effectiveness of upper limb functional electrical stimulation after stroke for the improvement of activities of daily living and motor function: a systematic review and meta-analysis. **Systematic reviews**, London, v. 6, n. 1, p. 40, 2017.

FARIA, U. d. C. **Implementação de um sistema de geração de marcha para pacientes com lesões medulares**. 2006. 222 p. Tese (Doutorado em Engenharia Elétrica) — Faculdade de Engenharia, Universidade Estadual Paulista, 2006.

FAVRE, J.; JOLLES, B. M.; AISSAOUI, R.; AMINIAN, K. Ambulatory measurement of 3D knee joint angle. **Journal of Biomechanics**, Oxford, v. 41, n. 5, p. 1029–1035, 2008.

FERRANTE, S.; PEDROCCHI, A.; IANNÒ, M.; De Momi, E.; FERRARIN, M.; FERRIGNO,

G. Functional electrical stimulation controlled by artificial neural networks: Pilot experiments with simple movements are promising for rehabilitation applications. **Functional Neurology**, Rome, v. 19, n. 4, p. 243–252, 2004.

FERRARIN, M.; PALAZZO, F.; RIENER, R.; QUINTERN, J. Model-based control of FES induced single joint movements. **IEEE Transactions on Neural Systems and Rehabilitation Engineering**, Pistacaway, v. 9, n. 3, p. 245–257, 2001.

FERRARIN, M.; PEDOTTI, A. The relationship between electrical stimulus and joint torque: a dynamic model. **IEEE Transactions on Rehabilitation Engineering**, Pistacaway, v. 8, n. 3, p. 342–352, 2000.

FRANKEN, H.; VELTINK, P.; TIJSMANS, R.; NIJMEIJER, H.; BOOM, H. Identification of passive knee joint and shank dynamics in paraplegics using quadriceps stimulation. **IEEE Transactions on Rehabilitation Engineering**, Pistacaway, v. 1, n. 3, p. 154–164, 1993.

FRANKLIN, B. An account of the effects of electricity in paralytic cases. **Philosophical Transactions**, London, v. 50, p. 481–483, 1757.

FREY LAW, L.; SHIELDS, R. Mathematical models of human paralyzed muscle after long-term training. **Journal of Biomechanics**, Oxford, v. 40, n. 12, p. 2587–2595, 2007.

GAHINET, P.; NEMIROVSKII, A.; LAUB, A. J.; CHILALI, M. The LMI control toolbox. In: IEEE CONFERENCE ON DECISION AND CONTROL, 33, 1994, Lake Buena Vista. **Proceedings [...]**. Lake Buena Vista: IEEE, 1994. v. 3, p. 2038–2041.

GAINO, R. **Controle de Movimentos de Pacientes Paraplégicos Utilizando Modelos Fuzzy T-S**. 2009. 180 p. Tese (Doutorado em Engenharia Elétrica) — Faculdade de Engenharia, Universidade Estadual Paulista, 2009.

GAINO, R.; COVACIC, M. R.; TEIXEIRA, M. C. M.; CARDIM, R.; ASSUNÇÃO, E.; CARVALHO, A. A. de; SANCHES, M. A. A. Electrical stimulation tracking control for paraplegic patients using T-S fuzzy models. **Fuzzy Sets and Systems**, Amsterdam, v. 314, p. 1–23, 2017.

GOBBO, M.; MAFFIULETTI, N. A.; ORIZIO, C.; MINETTO, M. A. Muscle motor point identification is essential for optimizing neuromuscular electrical stimulation use. **Journal of NeuroEngineering and Rehabilitation**, London, v. 11, n. 1, p. 17, 2014.

GORGEY, A. S.; BLACK, C. D.; ELDER, C. P.; DUDLEY, G. A. Effects of Electrical Stimulation Parameters on Fatigue in Skeletal Muscle. **Journal of Orthopaedic & Sports Physical Therapy**, Alexandria, v. 39, n. 9, p. 684–692, 2009.

HA, K. H.; MURRAY, S. A.; GOLDFARB, M. An Approach for the Cooperative Control of FES with a Powered Exoskeleton during Level Walking for Persons with Paraplegia. **IEEE Transactions on Neural Systems and Rehabilitation Engineering**, Pistacaway, v. 24, n. 4, p. 455–466, 2016.

HATWELL, M.; ODERKERK, B.; SACHER, C.; INBAR, G. The development of a model reference adaptive controller to control the knee joint of paraplegics. **IEEE Transactions on Automatic Control**, Pistacaway, v. 36, n. 6, p. 683–691, 1991.

HU, T.; LIN, Z.; CHEN, B. M. An Analysis and Design Method for Linear Systems Subject to Actuator Saturation and Disturbance. **Automatica**, Oxford, v. 38, p. 351–359, 2002.

IANNÒ, M.; FERRARIN, M.; PEDROCCHI, A.; FERRIGNO, G. A neuro-adaptive control system for knee joint movements during quadriceps electrical stimulation. In: ANNUAL CONFERENCE OF THE INTERNATIONAL FUNCTIONAL ELECTRICAL STIMULATION SOCIETY (IFESS2002), 7th., 2002, Ljubljana. **Proceedings [...]**. Ljubljana: IFESS, 2002.

IBRAHIM, B. K. K.; TOKHI, M.; HUQ, M.; GHAROONI, S. Fuzzy logic based cycle-to-cycle control of FES-induced swinging motion. In: INTERNATIONAL CONFERENCE ON ELECTRICAL, CONTROL AND COMPUTER ENGINEERING (INECCE), 1st., 2011, Pahang. **Proceedings [...]**. Pahang: IEEE, 2011. p. 60–64.

IBRAHIM, B. S. K. K.; TOKHI, M. O.; HUQ, M. S.; GHAROONI, S. C. Natural trajectory based FES-induced swinging motion control. In: INTERNATIONAL CONFERENCE ON MECHATRONICS (ICOM), 4th., 2011, Kuala Lumpur. **Proceedings [...]**. Kuala Lumpur: IEEE, 2011. p. 1–5.

IBRAHIM, B. S. K. K.; TOKHI, M. O.; HUQ, M. S.; GHAROONI, S. C. Optimized Fuzzy Control For Natural Trajectory Based Fes- Swinging Motion. **International Journal of Integrated Engineering**, Batu Pahat, v. 3, n. 1, p. 17–23, 2011.

JEZERNIK, S.; INDERBITZIN, P.; KELLER, T.; RIENER, R. A novel sliding mode controller for functional electrical stimulation. In: IFAC WORLD CONGRESS ON AUTOMATIC CONTROL, 15th., 2002, Barcelona. **Proceedings [...]**. Barcelona: IFAC, 2002. v. 5, p. 2–6.

JEZERNIK, S.; RIENER, R. A computer simulation of tuned PID and continuous sliding mode FES control. In: INTERNATIONAL BIOMECHATRONICS WORKSHOP, 1999, 1999, Twente. **Proceedings [...]**. Twente: IBW, 1999. p. 37–41.

JEZERNIK, S.; WASSINK, R. G. V.; KELLER, T. Sliding mode closed-loop control of FES: controlling the shank movement. **IEEE Transactions on Biomedical Engineering**, Pistacaway, v. 51, n. 2, p. 263–272, 2004.

JOVIC, J.; Azevedo Coste, C.; FRAISSE, P.; HENKOUS, S.; FATTAL, C. Coordinating Upper and Lower Body During FES-Assisted Transfers in Persons With Spinal Cord Injury in Order to Reduce Arm Support. **Neuromodulation: Technology at the Neural Interface**, Hoboken, v. 18, n. 8, p. 736–743, 2015.

JOVIC, J.; LENGAGNE, S.; FRAISSE, P.; AZEVEDO-COSTE, C. Impact of functional electrical stimulation of lower limbs during sitting pivot transfer motion for paraplegic people. **International Journal of Advanced Robotic Systems**, London, v. 10, 2013.

JUNQUEIRA, M. V. N. **Eletroestimulador funcional de oito canais com malha de realimentação utilizando Controlador Digital**. 2013. 105 p. Dissertação (Mestrado em Engenharia Elétrica) — Faculdade de Engenharia, Universidade Estadual Paulista, 2013.

KANTROWITZ, A. **Electronic physiologic aids**. New York, USA, 1960. 4–5 p.

KARAFYLLIS, I.; MALISOFF, M.; QUEIROZ, M. de; KRSTIC, M.; YANG, R. A new tracking controller for neuromuscular electrical stimulation under input delays: Case study in prediction. In: AMERICAN CONTROL CONFERENCE, 2014, 2014, Portland. **Proceedings [...]**. Portland: IEEE, 2014. p. 4186–4191.

KIRSCH, N.; ALIBEJI, N.; SHARMA, N. Nonlinear model predictive control of functional electrical stimulation. **Control Engineering Practice**, Oxford, v. 58, p. 319–331, 2017.

KLUG, M.; CASTELAN, E. B.; LEITE, V. J.; SILVA, L. F. Fuzzy dynamic output feedback control through nonlinear Takagi-Sugeno models. **Fuzzy Sets and Systems**, Amsterdam, v. 263, p. 92–111, 2015.

KOBRAVI, H. R.; ERFANIAN, A. A decentralized adaptive fuzzy robust strategy for control of upright standing posture in paraplegia using functional electrical stimulation. **Medical Engineering and Physics**, London, v. 34, n. 1, p. 28–37, 2012.

KOIKE, Y.; GONZALEZ, J.; GOMEZ, J.; YU, W. Implementing Feedback Error Learning for FES control. In: INTERNATIONAL CONFERENCE ON BIOMEDICAL ENGINEERING AND INFORMATICS (BMEI), 4th., 2011, Shanghai. **Proceedings [...]**. Shanghai: IEEE, 2011. p. 1324–1328.

KOZAN, R. F. **Controle da Posição da Perna de Pessoas Hígidas Utilizando um Controlador PID**. 2012. 96 p. Dissertação (Mestrado em Engenharia Elétrica) — Faculdade de Engenharia, Universidade Estadual Paulista, 2012.

KOZAN, R. F. **Sistema de Estimulação Elétrica Funcional para Controle da Posição da Perna Utilizando Controlador LQG/LTR**. 2016. 144 p. Tese (Doutorado em Engenharia Elétrica) — Faculdade de Engenharia, Universidade Estadual Paulista, 2016.

KRUEGER, E.; POPOVIĆ-MANESKI, L.; NOHAMA, P. Mechanomyography-Based Wearable Monitor of Quasi-Isometric Muscle Fatigue for Motor Neural Prostheses. **Artificial Organs**, Hoboken, v. 42, n. 2, p. 208–218, 2018.

LI, M.; MENG, W.; HU, J.; LUO, Q. Adaptive Sliding Mode Control of Functional Electrical Stimulation (FES) for Tracking Knee Joint Movement. In: INTERNATIONAL SYMPOSIUM ON COMPUTATIONAL INTELLIGENCE AND DESIGN (ISCID), 10th., 2017, Hangzhou. **Proceedings [...]**. Hangzhou: IEEE, 2017. p. 346–349.

LONGLONG, C.; GUANGJU, Z.; BAIKUN, W.; LINLIN, H.; HONGZHI, Q.; DONG, M. Radial basis function neural network-based PID model for functional electrical stimulation system control. In: ANNUAL INTERNATIONAL CONFERENCE OF THE IEEE EMBS, 31st., 2009, Minneapolis. **Proceedings [...]**. Minneapolis: IEEE, 2009. p. 3481–3484.

LUINGE, H. J.; VELTINK, P. H. Measuring orientation of human body segments using miniature gyroscopes and accelerometers. **Medical and Biological Engineering and Computing**, Heidelberg, v. 43, n. 2, p. 273–282, 2005.

LYNCH, C. L. **Closed-Loop Control of Electrically Stimulated Skeletal Muscle Contractions**. 2011. 131 p. Tese (Doutorado em Engenharia Elétrica) — University of Toronto, 2011.

LYNCH, C. L.; GRAHAM, G. M.; POPOVIC, M. R. A generic model of real-world non-ideal behaviour of FES-induced muscle contractions: Simulation tool. **Journal of Neural Engineering**, Bristol, v. 8, n. 4, 2011.

LYNCH, C. L.; GRAHAM, G. M.; POPOVIC, M. R. Including Nonideal Behavior in Simulations of Functional Electrical Stimulation Applications. v. 35, n. 3, p. 267–269, 2011.

LYNCH, C. L.; POPOVIC, M. R. Functional Electrical Stimulation. **IEEE Control Systems**, v. 28, n. 2, p. 40–50, 2008.

LYNCH, C. L.; POPOVIC, M. R. A comparison of closed-loop control algorithms for regulating electrically stimulated knee movements in individuals with spinal cord injury. **IEEE Transactions on Neural Systems and Rehabilitation Engineering**, Pistacaway, v. 20, n. 4, p. 539–548, 2012.

MARION, M. S.; WEXLER, A. S.; HULL, M. L. Predicting fatigue during electrically stimulated non-isometric contractions. **Muscle & Nerve**, Hoboken, v. 41, n. 6, p. 857–867, 2010.

MCDANIEL, J.; LOMBARDO, L. M.; FOGLYANO, K. M.; MARASCO, P. D.; TRIOLO, R. J. Setting the pace: Insights and advancements gained while preparing for an FES bike race. **Journal of NeuroEngineering and Rehabilitation**, London, v. 14, n. 1, p. 1–8, 2017.

MILLER, L.; MCFADYEN, A.; LORD, A. C.; HUNTER, R.; PAUL, L.; RAFFERTY, D.; BOWERS, R.; MATTISON, P. Functional Electrical Stimulation for Foot Drop in Multiple Sclerosis: A Systematic Review and Meta-Analysis of the Effect on Gait Speed. **Archives of Physical Medicine and Rehabilitation**, Maryland Heights, v. 98, n. 7, p. 1435–1452, 2017.

MIURA, N.; WATANABE, T.; SUGIMOTO, S.; SEKI, K.; KANAI, H. Fuzzy FES controller using cycle-to-cycle control for repetitive movement training in motor rehabilitation. Experimental tests with wireless system. **Journal of Medical Engineering & Technology**, Abingdon, v. 35, n. 6-7, p. 314–321, 2011.

MOHAMMED, S.; FRAISSE, P.; GUIRAUD, D.; POIGNET, P.; El Makssoud, H. Robust control law strategy based on high order sliding mode: towards a muscle control. In: IEEE/RSJ INTERNATIONAL CONFERENCE ON INTELLIGENT ROBOTS AND SYSTEMS, 2005, Edmonton. **Proceedings [...]**. Edmonton: IEEE, 2005. p. 2644–2649.

MOHAMMED, S.; POIGNET, P.; FRAISSE, P.; GUIRAUD, D. Lower limbs movement restoration using input-output feedback linearization and model predictive control. In: IEEE/RSJ INTERNATIONAL CONFERENCE ON INTELLIGENT ROBOTS AND SYSTEMS, 2007, San Diego. **Proceedings [...]**. San Diego: IEEE, 2007. p. 1945–1950.

MOHAMMED, S.; POIGNET, P.; FRAISSE, P.; GUIRAUD, D. Toward lower limbs movement restoration with input-output feedback linearization and model predictive control through functional electrical stimulation. **Control Engineering Practice**, Oxford, v. 20, n. 2, p. 182–195, 2012.

MOHAMMED, S.; POIGNET, P.; GUIRAUD, D. Closed Loop Nonlinear Model Predictive Control Applied On Paralyzed Muscles To Restore Lower Limbs Functions. In: IEEE/RSJ INTERNATIONAL CONFERENCE ON INTELLIGENT ROBOTS AND SYSTEMS, 2006, Beijing. **Proceedings [...]**. Beijing: IEEE, 2006. p. 259–264.

OBUZ, S.; DOWNEY, R. J.; KLOTZ, J. R.; DIXON, W. E. Unknown time-varying input delay compensation for neuromuscular electrical stimulation. In: IEEE CONFERENCE ON CONTROL APPLICATIONS (CCA), 2015, Sydney. **Proceedings [...]**. Sydney: IEEE, 2015. p. 365–370.

OLIVEIRA, D. R. de; TEIXEIRA, M. C. M.; ALVES, U. N. L. T.; SOUZA, W. A. de; ASSUNÇÃO, E.; CARDIM, R. On local Hoo switched controller design for uncertain T-S fuzzy systems subject to actuator saturation with unknown membership functions. **Fuzzy Sets and Systems**, Amsterdam, v. 1, p. 1–26, 2017.

PEDROCCHI, A.; FERRANTE, S.; De Momi, E.; FERRIGNO, G. Error mapping controller: a closed loop neuroprosthesis controlled by artificial neural networks. **Journal of NeuroEngineering and Rehabilitation**, London, v. 3, n. 1, p. 25, 2006.

PERUMAL, R.; WEXLER, A. S.; BINDER-MACLEOD, S. A. Mathematical model that predicts lower leg motion in response to electrical stimulation. **Journal of Biomechanics**, Oxford, v. 39, n. 15, p. 2826–2836, 2006.

PRADO, T. A. **Implementação de um controlador PID embarcado para o controle em malha fechada de um estimulador neuromuscular funcional**. 2009. 77 p. Dissertação (Mestrado em Engenharia Elétrica) — Faculdade de Engenharia, Universidade Estadual Paulista, 2009.

PREVIDI, F. Identification of black-box nonlinear models for lower limb movement control using functional electrical stimulation. **Control Engineering Practice**, Oxford, v. 10, n. 1, p. 91–99, 2002.

PREVIDI, F.; CARPANZANO, E. Design of a gain scheduling controller for knee-joint angle control by using functional electrical stimulation. **IEEE Transactions on Control Systems Technology**, Pistacaway, v. 11, n. 3, p. 310–324, 2003.

PREVIDI, F.; CARPANZANO, E.; CIRILLO, C. Application of a gain scheduling control strategy to artificial stimulation of the quadriceps muscle. In: IEEE. **Control Conference (ECC), 1999 European**. [S.l.], 1999. p. 2000–2005.

RAGNARSSON, K. T. Functional electrical stimulation after spinal cord injury: current use, therapeutic effects and future directions. **Spinal cord**, London, v. 46, n. 4, p. 255–274, 2008.

RIENER, R.; FUHR, T. Patient-driven control of FES-supported standing up: a simulation study. **IEEE Transactions on Rehabilitation Engineering**, Pistacaway, v. 6, n. 2, p. 113–124, 1998.

RIENER, R.; QUINTERN, J.; SCHMIDT, G. Biomechanical model of the human knee evaluated by neuromuscular stimulation. **Journal of Biomechanics**, Oxford, v. 29, n. 9, p. 1157–1167, 1996.

RIESS, J.; ABBAS, J. Adaptive neural network control of cyclic movements using functional neuromuscular stimulation. **IEEE Transactions on Rehabilitation Engineering**, Pistacaway, v. 8, n. 1, p. 42–52, 2000.

SANCHES, M. A. A. **Sistema Eletrônico para Geração e Avaliação de Movimentos**

em Paraplégicos. 2013. 186 p. Tese (Doutorado em Engenharia Elétrica) — Faculdade de Engenharia, Universidade Estadual Paulista, 2013.

SANCHES, M. A. A.; GAINO, R.; KOZAN, R. F.; TEIXEIRA, M. C. M.; CARVALHO, A. A. de; COVACIC, M. R.; ALVES, C. A.; URBAN, M. F. R.; JUNQUEIRA, M. V. N.; CARDIM, R.; ASSUNÇÃO, E.; Gentilho Junior, E. Digital controller design considering hardware constraints: application in a paraplegic patient. **Revista Brasileira de Engenharia Biomédica**, Rio de Janeiro, v. 30, n. 3, p. 232–241, 2014.

SANTOS, E. d. L. dos; GELAIN, M. C.; KRUEGER, E.; NOGUEIRA-NETO, G. N.; NOHAMA, P. Artificial motor control for electrically stimulated upper limbs of plegic or paretic people. **Research on Biomedical Engineering**, Rio de Janeiro, v. 32, n. 2, p. 199–211, 2016.

SANTOS, N. M. dos; GAINO, R.; COVACIC, M. R.; TEIXEIRA, M. C. M.; CARVALHO, A. A. de; ASSUNÇÃO, E.; CARDIM, R.; SANCHES, M. A. A. Robust Control of the Knee Joint Angle of Paraplegic Patients considering Norm-Bounded Uncertainties. **Mathematical Problems in Engineering**, New York, v. 2015, p. 1–8, 2015.

SCHAUER, T.; HOLDERBAUM, W.; HUNT, K. J. Sliding-mode control of knee-joint angle: experimental results. In: ANNUAL CONFERENCE OF THE INTERNATIONAL FUNCTIONAL ELECTRICAL STIMULATION SOCIETY (IFESS 2002), 7th., 2002, Ljubljana. **Proceedings [...]**. Ljubljana: [s.n.], 2002. p. 316–318.

SCHAUER, T.; HUNT, K. J. Linear Controller Design for the Single Limb Movement of Paraplegics. **IFAC Proceedings Volumes**, Elsevier, v. 33, n. 3, p. 7–12, 2000.

SCHAUER, T.; NEGÅRD, N. O.; PREVIDI, F.; HUNT, K. J.; FRASER, M. H.; FERCHLAND, E.; RAISCH, J. Online identification and nonlinear control of the electrically stimulated quadriceps muscle. **Control Engineering Practice**, Oxford, v. 13, n. 9, p. 1207–1219, 2005.

SEEL, T.; RAISCH, J.; SCHAUER, T. IMU-Based Joint Angle Measurement for Gait Analysis. **Sensors**, Basel, v. 14, n. 4, p. 6891–6909, 2014.

SHARMA, N.; GREGORY, C. M.; DIXON, W. E. Predictor-Based Compensation for Electromechanical Delay During Neuromuscular Electrical Stimulation. **IEEE Transactions on Neural Systems and Rehabilitation Engineering**, Pistacaway, v. 19, n. 6, p. 601–611, 2011.

SHARMA, N.; GREGORY, C. M.; JOHNSON, M.; DIXON, W. E. Closed-loop neural network-based NMES control for human limb tracking. **IEEE Transactions on Control Systems Technology**, Pistacaway, v. 20, n. 3, p. 712–725, 2012.

SHARMA, N.; KIRSCH, N. A.; ALIBEJI, N. A.; DIXON, W. E. A Non-Linear Control Method to Compensate for Muscle Fatigue during Neuromuscular Electrical Stimulation. **Frontiers in Robotics and AI**, Laussane, v. 4, p. 68, 2017.

SHARMA, N.; MUSHAHWAR, V.; STEIN, R. Dynamic optimization of FES and orthosis-based walking using simple models. **IEEE Transactions on Neural Systems and Rehabilitation Engineering**, Pistacaway, v. 22, n. 1, p. 114–126, 2014.

SHARMA, N.; PATRE, P. M.; GREGORY, C. M.; DIXON, W. E. Nonlinear Control of NMES: Incorporating Fatigue and Calcium Dynamics. In: ASME 2009 DYNAMIC SYSTEMS AND CONTROL CONFERENCE, 2009, Hollywood. **Proceedings [...]**. Hollywood: ASME, 2009. p. 705–712.

SHARMA, N.; STEGATH, K.; GREGORY, C.; DIXON, W. Nonlinear Neuromuscular Electrical Stimulation Tracking Control of a Human Limb. **IEEE Transactions on Neural Systems and Rehabilitation Engineering**, Pistacaway, v. 17, n. 6, p. 576–584, 2009.

SILVA, T. I. da. **Implementação de um Sistema para Geração e Avaliação de Movimentos em Pacientes Hemiplégicos**. 2007. 197 p. Tese (Doutorado em Engenharia Elétrica) — Faculdade de Engenharia, Universidade Estadual Paulista, 2007.

SOUZA, D. C. de; GAIOTTO, M. d. C.; Nogueira Neto, G. N.; CASTRO, M. C. F. de; NOHAMA, P.; SOUZA, D. C. de; GAIOTTO, M. d. C.; Nogueira Neto, G. N.; CASTRO, M. C. F. de; NOHAMA, P. Power amplifier circuits for functional electrical stimulation systems. **Research on Biomedical Engineering**, Rio de Janeiro, v. 33, n. 2, p. 144–155, 2017.

SOUZA, W. A. D.; TEIXEIRA, M.; SANTIM, M.; CARDIM, R.; ASSUNÇÃO, E. On switched control design of linear time-invariant systems with polytopic uncertainties. **Mathematical Problems in Engineering**, New York, v. 2013, 2013.

SOUZA, W. A. D.; TEIXEIRA, M. C. M.; CARDIM, R.; ASSUNÇÃO, E. On Switched Regulator Design of Uncertain Nonlinear Systems Using Takagi-Sugeno Fuzzy Models. **IEEE Transactions on Fuzzy Systems**, Pistacaway, v. 22, n. 6, p. 1720–1727, 2014.

STEGATH, K.; SHARMA, N.; GREGORY, C. M.; DIXON, W. E. Nonlinear tracking control of a human limb via neuromuscular electrical stimulation. In: AMERICAN CONTROL CONFERENCEE, 2008, Seattle. **Proceedings [...]**. Seattle: IEEE, 2008. p. 1941–1946.

STEIN, R.; ZEHR, E.; LEBIEDOWSKA, M.; POPOVIC, D.; SCHEINER, A.; CHIZECK, H. Estimating mechanical parameters of leg segments in individuals with and without physical disabilities. **IEEE Transactions on Rehabilitation Engineering**, Pistacaway, v. 4, n. 3, p. 201–211, 1996.

STURM, J. F. Using sedumi 1.02, a matlab toolbox for optimization over symmetric cones. **Optimization methods and software**, Abingdon, v. 11, n. 1-4, p. 625–653, 1999.

SUN, Z.; BAO, X.; SHARMA, N. Lyapunov-based Model Predictive Control of an Input Delayed Functional Electrical Simulation. **IFAC-PapersOnLine**, Elsevier, v. 51, n. 34, p. 290–295, 2019.

TANAKA, K.; IKEDA, T.; WANG, H. O. Fuzzy regulators and fuzzy observers: relaxed stability conditions and lmi-based designs. **IEEE Transactions on Fuzzy Systems**, Pistacaway, v. 6, n. 2, p. 250–265, 1998.

TANAKA, K.; WANG, H. O. **Fuzzy Control Systems Design and Analysis:A Linear Matrix Inequality Approach**. New York: John Wiley & Sons, 2001.

TANIGUCHI, T.; TANAKA, K.; OHTAKE, H.; WANG, H. O. Model construction, rule reduction, and robust compensation for generalized form of takagi-sugeno fuzzy systems.

IEEE Transactions on Fuzzy Systems, Pistacaway, v. 9, n. 4, p. 525–538, 2001.

TEIXEIRA, M. C. M.; DEAECTO, G. S.; GAINO, R.; ASSUNÇÃO, E.; CARVALHO, A. A.; FARIAS, U. C. Design of a Fuzzy Takagi-Sugeno Controller to Vary the Joint Knee Angle of Paraplegic Patients. In: Neural Information Processing (ICONIP). Lecture Notes in Computer Science, 13th., 2006, Hong Kong. **Proceedings [...]**. Heidelberg: Springer, 2006. v. 4234, p. 118–126.

TEODORO, R. G. **Controle da posição angular da perna de voluntários hígidos e com lesão medular utilizando estimulação elétrica funcional e técnicas de controle robusto e chaveado**. 2018. 198 p. Tese (Doutorado em Engenharia Elétrica) — Faculdade de Engenharia, Universidade Estadual Paulista, 2018.

WAGNER, F. B.; MIGNARDOT, J.-B.; LE GOFF-MIGNARDOT, C. G.; DEMESMAEKER, R.; KOMI, S.; CAPOGROSSO, M.; ROWALD, A.; SEÁÑEZ, I.; CABAN, M.; PIRONDINI, E.; VAT, M.; MCCRACKEN, L. A.; HEIMGARTNER, R.; FODOR, I.; WATRIN, A.; SEGUIN, P.; PAOLES, E.; VAN DEN KEYBUS, K.; EBERLE, G.; SCHURCH, B.; PRALONG, E.; BECCE, F.; PRIOR, J.; BUSE, N.; BUSCHMAN, R.; NEUFELD, E.; KUSTER, N.; CARDA, S.; ZITZEWITZ, J. von; DELATTRE, V.; DENISON, T.; LAMBERT, H.; MINASSIAN, K.; BLOCH, J.; COURTINE, G. Targeted neurotechnology restores walking in humans with spinal cord injury. **Nature**, London, v. 563, n. 7729, p. 65–71, 2018.

WANG, L.-X.; MENDEL, J. M. Fuzzy basis functions, universal approximation, and orthogonal least-squares learning. **IEEE Transactions on Neural Networks**, Pistacaway, v. 3, n. 5, p. 807–814, 1992.

WANG, Q.; SHARMA, N.; JOHNSON, M.; DIXON, W. E. Adaptive inverse optimal Neuromuscular Electrical Stimulation. In: IEEE INTERNATIONAL SYMPOSIUM ON INTELLIGENT CONTROL, 2010, Yokohama. **Proceedings [...]**. Yokohama: IEEE, 2010. p. 1287–1292.

WANG, Q.; SHARMA, N.; JOHNSON, M.; DIXON, W. E. Asymptotic optimal control of neuromuscular electrical stimulation. In: IEEE CONFERENCE ON DECISION AND CONTROL (CDC), 49th., 2010, Atlanta. **Proceedings [...]**. Atlanta: IEEE, 2010. p. 839–844.

WANG, Q.; SHARMA, N.; JOHNSON, M.; GREGORY, C. M.; DIXON, W. E. Adaptive Inverse Optimal Neuromuscular Electrical Stimulation. **IEEE Transactions on Cybernetics**, Pistacaway, v. 43, n. 6, p. 1710–1718, 2013.

WATERS, R. L.; MCNEAL, D. R.; PERRY, J. Experimental correction of footdrop by electrical stimulation of the peroneal nerve. **Journal of Bone and Joint Surgery**, Needham, v. 57, n. 8, p. 1047–1054, 1975.

WESTERBLAD, H.; BRUTON, J. D.; ALLEN, D. G.; LÄNNERGREN, J. Functional significance of Ca 2+ in long-lasting fatigue of skeletal muscle. **European Journal of Applied Physiology**, Heidelberg, v. 83, n. 2-3, p. 166–174, 2000.

WIESENER, C.; AXELGAARD, J.; HORTON, R.; NIEDEGGEN, A.; SCHAUER, T. Functional electrical stimulation assisted swimming for paraplegics. In: ANNUAL CONFERENCE OF THE INTERNATIONAL FUNCTIONAL ELECTRICAL STIMULATION SOCIETY, 22nd., 2018, Nottwil. **Proceedings [...]**. Nottwil: IFESS, 2018. p. 1–4.

WU, L.; WU, Q.; ZHANG, Q.; XIONG, C. Electrically induced joint movement control with iterative learning algorithm. In: INTERNATIONAL CONFERENCE ON ADVANCED ROBOTICS AND MECHATRONICS (ICARM), 2nd., 2017, Hefei. **Proceedings [...]**. Hefei: IEEE, 2017. p. 426–430.

YANG, R.; QUEIROZ, M. de. Adaptive control of the nonlinearly parameterized limb dynamics with application to neuromuscular electrical stimulation. In: AMERICAN CONTROL CONFERENCE (ACC), 2016, Boston. **Proceedings [...]**. Boston: IEEE, 2016. p. 4883–4888.

YANG, R.; QUEIROZ, M. de. Robust Adaptive Control of the Nonlinearly Parameterized Human Shank Dynamics for Electrical Stimulation Applications. **Journal of Dynamic Systems, Measurement, and Control**, New York, v. 140, n. 8, p. 081019, 2018.

ZHOU, B. Analysis and design of discrete-time linear systems with nested actuator saturations. **Systems & Control Letters**, Amsterdam, v. 62, n. 10, p. 871–879, 2013.

APPENDIX A - GAINS AND POSITIVE DEFINITE SYMMETRIC MATRIX FOR ACCELERATION-BASED MODEL

Table 13 - Gains F_i and positive definite symmetric matrix P for healthy individuals.

Subject	Gains F_i and Matrix P
H1	$\mathbf{F}_1 = 10^{-4} \times [9.0209 \quad 3.5518 \quad 0.5237 \quad 7.7498]$
	$\mathbf{F}_2 = 10^{-4} \times [9.3899 \quad 3.1200 \quad 0.5234 \quad 8.0343]$
	$\mathbf{F}_3 = 10^{-4} \times [0.9353 \quad 1.8415 \quad 0.2492 \quad 4.6685]$
	$\mathbf{F}_4 = 10^{-4} \times [2.6891 \quad 2.0179 \quad 0.3347 \quad 6.0963]$
	$\mathbf{P} = \begin{bmatrix} 10.3971 & 2.9199 & 0.2259 & 9.5720 \\ 2.9199 & 1.1569 & 0.0900 & 2.4257 \\ 0.2259 & 0.0900 & 0.0174 & 0.1834 \\ 9.5720 & 2.4257 & 0.1834 & 10.6226 \end{bmatrix}$
H2	$\mathbf{F}_1 = 10^{-4} \times [9.1088 \quad 3.9388 \quad 0.5132 \quad 8.4391]$
	$\mathbf{F}_2 = 10^{-4} \times [10.0667 \quad 2.6240 \quad 0.5266 \quad 9.4213]$
	$\mathbf{F}_3 = 10^{-4} \times [0.7726 \quad 2.3724 \quad 0.2991 \quad 5.3228]$
	$\mathbf{F}_4 = 10^{-4} \times [4.0725 \quad 2.0271 \quad 0.4540 \quad 5.5159]$
	$\mathbf{P} = \begin{bmatrix} 15.9184 & 3.8450 & 0.3725 & 16.3964 \\ 3.8450 & 1.3207 & 0.1327 & 3.7165 \\ 0.3725 & 0.1327 & 0.0237 & 0.3459 \\ 16.3964 & 3.7165 & 0.3459 & 22.0041 \end{bmatrix}$
H3	$\mathbf{F}_1 = 10^{-4} \times [7.6939 \quad 4.1346 \quad 0.5422 \quad 7.8072]$
	$\mathbf{F}_2 = 10^{-4} \times [9.8349 \quad 3.0977 \quad 0.5957 \quad 9.7553]$
	$\mathbf{F}_3 = 10^{-4} \times [1.4290 \quad 2.7174 \quad 0.3440 \quad 5.1198]$
	$\mathbf{F}_4 = 10^{-4} \times [5.5850 \quad 2.5735 \quad 0.5265 \quad 8.8893]$
	$\mathbf{P} = \begin{bmatrix} 13.0601 & 3.4774 & 0.3279 & 12.8984 \\ 3.4774 & 1.3015 & 0.1274 & 3.1843 \\ 0.3279 & 0.1274 & 0.0229 & 0.2903 \\ 12.8984 & 3.1843 & 0.2903 & 16.0667 \end{bmatrix}$
H4	$\mathbf{F}_1 = 10^{-4} \times [6.9823 \quad 3.7967 \quad 0.4584 \quad 5.9000]$
	$\mathbf{F}_2 = 10^{-4} \times [8.8415 \quad 2.8763 \quad 0.4979 \quad 7.3841]$
	$\mathbf{F}_3 = 10^{-4} \times [1.1120 \quad 2.3429 \quad 0.2546 \quad 3.3184]$
	$\mathbf{F}_4 = 10^{-4} \times [5.6234 \quad 2.5887 \quad 0.4600 \quad 6.9751]$
	$\mathbf{P} = \begin{bmatrix} 10.9661 & 3.1937 & 0.2719 & 10.0889 \\ 3.1937 & 1.2886 & 0.1129 & 2.6791 \\ 0.2719 & 0.1129 & 0.0204 & 0.2209 \\ 10.0889 & 2.6791 & 0.2209 & 11.2078 \end{bmatrix}$
H5	$\mathbf{F}_1 = 10^{-4} \times [7.4336 \quad 3.5307 \quad 0.4768 \quad 6.9769]$
	$\mathbf{F}_2 = 10^{-4} \times [8.5100 \quad 2.6771 \quad 0.5050 \quad 7.9008]$
	$\mathbf{F}_3 = 10^{-4} \times [3.8992 \quad 1.9783 \quad 0.2349 \quad 4.0101]$
	$\mathbf{F}_4 = 10^{-4} \times [3.5395 \quad 2.0389 \quad 0.3992 \quad 6.7444]$
	$\mathbf{P} = \begin{bmatrix} 11.4204 & 3.0557 & 0.2622 & 11.0618 \\ 3.0557 & 1.1554 & 0.1002 & 2.7229 \\ 0.2622 & 0.1002 & 0.0191 & 0.2248 \\ 11.0618 & 2.7229 & 0.2248 & 13.2890 \end{bmatrix}$

Source: From author.

Table 14 - Gains F_i and positive definite symmetric matrix P for paraplegic individuals.

Subject	Gains $\mathbf{F}_i$ and Matrix $\mathbf{P}$
P1	$\mathbf{F}_1 = 10^{-3} \times [2.8453 \quad 1.3618 \quad 0.1368 \quad 2.2129]$
	$\mathbf{F}_2 = 10^{-3} \times [2.7093 \quad -0.0611 \quad 0.0666 \quad 1.9508]$
	$\mathbf{F}_3 = 10^{-3} \times [2.0908 \quad 1.2589 \quad 0.1218 \quad 2.0390]$
	$\mathbf{F}_4 = 10^{-3} \times [2.7625 \quad 0.1157 \quad 0.1069 \quad 2.4242]$
	$\mathbf{P} = \begin{bmatrix} 17.2221 & 4.1228 & 0.1957 & 15.2875 \\ 4.1228 & 1.6459 & 0.0747 & 3.1002 \\ 0.1957 & 0.0747 & 0.0136 & 0.1511 \\ 15.2875 & 3.1002 & 0.1511 & 15.9950 \end{bmatrix}$
P2	$\mathbf{F}_1 = 10^{-3} \times [1.6418 \quad 0.8764 \quad 0.0687 \quad 1.4259]$
	$\mathbf{F}_2 = 10^{-3} \times [1.6490 \quad 0.6193 \quad 0.0689 \quad 1.4315]$
	$\mathbf{F}_3 = 10^{-3} \times [1.0667 \quad 0.8762 \quad 0.0686 \quad 1.4258]$
	$\mathbf{F}_4 = 10^{-3} \times [1.0743 \quad 0.6192 \quad 0.0689 \quad 1.4317]$
	$\mathbf{P} = \begin{bmatrix} 11.1800 & 3.4527 & 0.2441 & 9.8420 \\ 3.4527 & 1.4156 & 0.1032 & 2.7673 \\ 0.2441 & 0.1032 & 0.0179 & 0.1891 \\ 9.8420 & 2.7673 & 0.1891 & 10.1228 \end{bmatrix}$
P3	$\mathbf{F}_1 = 10^{-3} \times [3.2295 \quad 1.2034 \quad 0.1532 \quad 2.7914]$
	$\mathbf{F}_2 = 10^{-3} \times [2.9733 \quad 0.3930 \quad 0.1260 \quad 2.5824]$
	$\mathbf{F}_3 = 10^{-3} \times [-0.0900 \quad 0.6483 \quad 0.0654 \quad 1.5710]$
	$\mathbf{F}_4 = 10^{-3} \times [1.0998 \quad 0.3704 \quad 0.1287 \quad 2.7369]$
	$\mathbf{P} = \begin{bmatrix} 14.7978 & 3.4543 & 0.3242 & 15.5100 \\ 3.4543 & 1.1550 & 0.1073 & 3.4334 \\ 0.3242 & 0.1073 & 0.0203 & 0.3012 \\ 15.5100 & 3.4334 & 0.3012 & 21.4222 \end{bmatrix}$

Source: From author.

APPENDIX B - STATE-SPACE MODEL IDENTIFICATION FOR ELECTRICALLY STIMULATED LOWER LIMB

Table 15 - Model's parameters from healthy and paraplegic individuals.

Subject	Session	N_T	a_{31}^2	a_{31}^1	a_{32}^2	a_{32}^1	a_{33}^2	a_{33}^1	b_{31}^2	b_{31}^1	I [mA]	u_{min} [μs]	u_{max} [μs]
H1	1	10	-208.3518	-107.329	-78.4714	-55.3666	-9.4785	-6.6546	0.2228	0.4393	70	340	340
	2	10	-262.6347	-145.2338	-85.0702	-66.0235	-9.6953	-7.4066	0.3631	0.7235	70	300	300
H2	1	10	-366.2919	-106.0237	-134.7143	-37.7548	-26.6076	-2.8082	0.1774	0.4770	70	390	390
	2	10	-380.5041	-137.8383	-81.1869	-41.5447	-10.1800	-4.2611	0.2091	0.6068	70	390	390
H3	1	10	-291.5581	-62.6548	-75.3536	-41.5937	-9.0396	-3.8922	0.1645	0.7199	70	290	290
	2	10	-222.8938	-97.1484	-77.7864	-47.8532	-10.7384	-5.3193	0.2055	0.5292	70	290	310
H4	1	10	-107.9921	-13.6093	-160.2695	-17.4008	-14.0896	-4.0638	0.0349	0.3120	70	265	265
	2	10	-146.3542	-17.1347	-65.3395	-16.4418	-19.6807	-5.5236	0.0582	0.2878	70	265	265
H5	1	10	-28.5538	-0.0001	-54.8781	-31.0824	-5.8112	-3.4596	0.0132	0.0715	100	310	310
	2	10	-216.0328	-3.4153	-92.956	-27.4802	-8.6471	-4.5313	0.0201	0.5412	100	230	300
H6	1	10	-314.1281	-2.8144	-104.2689	-11.3976	-14.6985	-1.3206	0.0169	0.6189	70	205	210
	2	10	-172.1663	-18.2726	-115.7653	-27.8994	-14.4875	-3.9954	0.0716	0.7178	70	210	210
H7	1	10	-33.9763	-3.2647	-28.7298	-12.3878	-6.3673	-3.9455	0.0133	0.1087	80	250	250
	2	10	-112.2274	-1.4620	-56.6962	-16.3206	-8.7886	-3.7917	0.0121	0.3101	80	250	300
H8	1	10	-311.5347	-234.5072	-90.0313	-80.9556	-10.7240	-9.5933	0.6789	0.9240	70	223	223
	2	10	-229.9216	-140.9376	-78.1216	-62.8343	-9.7505	-8.5312	0.4659	0.8008	70	220	220
H9	1	10	-126.6589	-10.4113	-55.6474	-18.1725	-8.5560	-4.2891	0.0101	0.2579	80	320	390
	2	10	-14.5575	-2.6509	-21.3817	-9.0361	-8.0816	-2.4738	0.0115	0.0379	100	275	282
H10	1	10	-230.2553	-47.3409	-87.3230	-38.4507	-11.1278	-6.6213	0.1330	0.5498	70	250	250
	2	10	-282.9698	-167.5383	-130.1712	-71.6617	-14.2140	-6.6257	0.6077	1.0586	70	190	190
	3	10	-187.0645	-3.5156	-85.8503	-16.1093	-10.9313	-4.1479	0.0126	0.3661	70	310	320
H11	1	10	-39.0603	-5.2241	-31.2847	-9.5072	-4.8772	-2.6318	0.02641	0.1857	100	140	140
	2	10	-229.0225	-29.6343	-109.7201	-28.4365	-20.4394	-4.7356	0.1176	0.9546	100	155	170
H12	1	10	-415.3087	-131.0427	-99.7279	-48.9604	-16.7668	-6.6893	0.1440	0.4409	70	400	400
	2	4	-9.3420	-0.0003	-23.4866	-20.7240	-7.0869	-3.8388	0.0105	0.0249	100	310	310

Continued on next page

Table 15 – *Continued from previous page*

Subject	**Session**	$\mathbf{N_T}$	a_{31}^2	a_{31}^1	a_{32}^2	a_{32}^1	a_{33}^2	a_{33}^1	b_{31}^2	b_{31}^1	I [mA]	u_{min} [μs]	u_{max} [μs]
H13	1	4	-54.9791	-2.2707	-36.8982	-20.8832	-5.8894	-3.0236	0.0158	0.1390	70	300	300
H14	1	7	-495.6669	-0.0001	-95.6153	-1.1372	-17.5206	-1.1148	-0.0001	0.3301	80	230	300
	2	10	-133.9872	-1.6529	-64.3092	-18.6579	-8.0623	-2.4499	0.0155	0.2325	80	230	247
H15	1	10	-61.9333	-2.3748	-91.9681	-5.9837	-8.6658	-2.9013	0.0089	0.1586	70	295	295
	2	10	-189.6134	-6.4645	-119.2415	-21.3261	-16.7554	-2.6522	0.0225	0.5500	70	295	295
H16	1	10	-176.6017	-39.1472	-84.7384	-34.7689	-9.3832	-5.292	0.0763	0.3800	70	330	370
	2	10	-415.5939	-3.5187	-122.0402	-33.3080	-10.2373	-6.1786	0.0062	0.4651	70	340	360
H17	1	10	-122.0760	-15.8112	-59.5658	-22.1080	-7.5859	-3.9295	0.0324	0.3236	70	315	350
	2	10	-127.8641	-6.0191	-72.4038	-21.0464	-10.6838	-2.5670	0.0276	0.3336	70	315	330
H18	1	8	-539.8027	-0.8040	-160.6109	-4.9047	-188.9384	-0.5066	0.0072	0.5978	70	160	165
H19	1	10	-67.1334	-1.0414	-58.2693	-15.3464	-8.4179	-3.2185	0.0103	0.2111	70	220	240
	2	10	-58.8651	-5.6363	-48.7529	-7.5680	-13.6385	-2.1563	0.0196	0.2419	70	190	220
H20	1	10	-175.6832	-0.0001	-91.5647	-4.5114	-10.7701	-1.4052	0.0039	0.4424	70	250	250
	2	10	-337.8324	-13.7402	-226.4101	-18.2836	-35.2319	-4.9105	0.0340	0.7966	70	287	287
P1	1	10	-154.0400	-93.6318	-68.3566	-51.1396	-7.2553	-5.6350	0.1876	0.3110	70	350	380
	2	5	-110.3978	-49.4599	-52.4159	-31.1436	-7.0402	-6.2417	0.1140	0.2809	80	280	300
	3	5	-88.9525	-29.9835	-46.7651	-24.6258	-6.2290	-3.9167	0.0740	0.2306	80	290	300
	4	5	-152.6574	-83.5007	-61.2818	-44.8905	-7.3111	-3.7473	0.1973	0.3710	80	280	300
	5	5	-116.7021	-82.9055	-52.0386	-44.3848	-5.3108	-3.6805	0.22311	0.34176	100	230	240
P2	1	5	-14.6319	-6.9517	-15.2461	-10.1326	-3.6238	-2.5659	0.0139	0.0279	80	350	370
	2	5	-212.5456	-183.8859	-75.7601	-63.9973	-11.5934	-9.2428	0.2992	0.3754	80	310	370
	3	5	-127.7830	-35.1559	-58.1002	-31.5816	-8.1616	-7.0172	0.0626	0.2263	80	300	350
P3	1	3	-337.0047	-237.2122	-85.7010	-79.3645	-12.2678	-8.7924	0.7363	0.9050	140	250	260
P4	1	5	-288.9254	-119.0084	-72.7393	-58.6385	-11.4148	-6.4664	0.3515	0.5333	120	280	300
Total	**50**	**426**											

Legend: N_T Number of trials in each session.

Source: From author.